# From Wishart to Jacobi ensembles: statistical properties and applications


Pierpaolo Vivo

Department of Mathematical Sciences

Brunel University

In partial fulfillment of the requirements for the degree of

*Doctor of Philosophy*

July 2008

A well-known scientist (some say it was Bertrand Russell) once gave a public lecture on astronomy. He described how the earth orbits around the sun and how the sun, in turn, orbits around the center of a vast collection of stars called our galaxy. At the end of the lecture, a little old lady at the back of the room got up and said: "What you have told us is rubbish. The world is really a flat plate supported on the back of a giant tortoise." The scientist gave a superior smile before replying, "What is the tortoise standing on?" "You're very clever, young man, very clever," said the old lady. "But it's turtles all the way down!"

# Abstract

Sixty years after the works of Wigner and Dyson, Random Matrix Theory still remains a very active and challenging area of research, with countless applications in mathematical physics, statistical mechanics and beyond. In this thesis, we focus on rotationally invariant models where the requirement of independence of matrix elements is dropped. Some classical examples are the Jacobi and Wishart-Laguerre (or chiral) ensembles, which constitute the core of the present work. The Wishart-Laguerre ensemble contains covariance matrices of random data, and represents a very important tool in multivariate data analysis, with recent applications to finance and telecommunications. We will first consider large deviations of the maximum eigenvalue, providing new analytical results for its large $N$ behavior, and then a power-law deformation of the classical Wishart-Laguerre ensemble, with possible applications to covariance matrices of financial data. For the Jacobi matrices, which arise naturally in the quantum conductance problem, we provide analytical formulas for quantities of interest for the experiments.

# Acknowledgements

First and foremost, I am grateful and indebted with my supervisor Gernot Akemann for his constant advice, encouragement and manifestation of friendship throughout these intense years. Even in the gloomiest moments of my PhD (which are probably commonplace among research students!), I've always known I could count on him. That's why his support and friendship are acknowledged with thanks.

Many thanks to my family and friends in Italy, who were always with me when I needed them. I hug them all affectionately.

A special thank goes to Satya and Oriol in Paris. I owe them so much in terms of mentoring and friendship, that any word here would be inappropriate to express. I'm looking forward for many more years of intense and fruitful collaboration.

After this long and tiring journey (I can't believe it's all going to be over so soon!), I can't help remembering and thanking all the wonderful people I shared my time in London with: Elisa and Sergio above all, to whom I wish an exciting life, full of joy and satisfaction. Bernard and Marta, hoping that we'll keep in touch wherever you'll be in the years to come. Leonid and Michael, wishing to both of you a great time. And all my friends in London, who have raised my mood up so many times.

But mostly my thoughts are for my dear Kate, who always had a good word and a smile for me: without her, this time here would have been completely void.

Financial support from a Marie Curie Early Stage Training Fellowship (NET-ACE project) is also gratefully acknowledged.

# Previously published work

1. P. Vivo, S.N. Majumdar and O. Bohigas
   Large deviations of the maximum eigenvalue in Wishart random matrices
   *J. Phys. A: Math. Theor.* **40**(16), 4317 (2007).

2. P. Vivo, S.N. Majumdar and O. Bohigas
   Large deviations and Random Matrices
   proceedings of ESF Workshop in Krakow, 2-6 May 2007.
   *Acta Physica Polonica* **38**, 4139 (2007).

3. G. Akemann and P. Vivo
   Power-law deformation of Wishart-Laguerre ensembles of random matrices
   to appear in *JSTAT*, online at `http://arxiv.org/abs/0806.1861`

4. P. Vivo and E. Vivo
   Transmission Eigenvalue Densities and Moments in Chaotic Cavities from Random Matrix Theory
   *J. Phys. A: Math. Theor.* **41**(12), 122004 (2008).

5. P. Vivo and S.N. Majumdar
   On invariant $2 \times 2$ $\beta$-ensembles of random matrices
   *Physica A* **387**(19-20), 4839 (2008).

6. P. Vivo, M. Casartelli, L. Dall'Asta and A. Vezzani
   On a class of rational matrices and interpolating polynomials related to the discrete Laplace operator
   to appear in *Note di Matematica*, online at `http://arxiv.org/abs/0705.1294`

7. M. Casartelli, L. Dall'Asta, A. Vezzani and P. Vivo
   Dynamical Invariants in the Deterministic Fixed-Energy Sandpile
   *Eur. Phys. J. B* **52**, 91 (2006).

The papers 1. and 2. cover the content of Chapter 3, paper 3. of Chapter 4 and paper 4. of part of Chapter 5. The remaining papers have not been included in the present thesis. Section 5.4 includes results not yet published.

# Contents

# List of Figures

*Things should be made as simple as possible, but not any simpler.*

ALBERT EINSTEIN

# Chapter 1

# Overview of Random Matrix Theory

Ensembles of matrices with random entries have been systematically studied since the pioneering works of Wigner [1] and Dyson [2; 3] since the 1950s, although earlier studies by Wishart [4] and Hsu [5] need to be recalled. The purpose was to develop a statistical theory of energy levels of heavy nuclei, such that the unknown Hamiltonian (representing the complicated interactions among nucleons) is replaced by a statistical ensemble of random Hamiltonians satisfying minimal symmetry requirements.

In the words of Dyson [2]:

> In ordinary statistical mechanics a comparable renunciation of exact knowledge is made. By assuming all states of a very large ensemble to be equally probable, one obtains useful information about the overall behaviour of a complex system, when the observation of the state of the system in all its detail is impossible. This type of statistical mechanics is clearly inadequate for the discussion of nuclear energy levels. We wish to make statements about the fine detail of the level structure, and such statements cannot be made in terms of an ensemble of states. What is here required is a new kind of statistical mechanics, in which we renounce exact knowledge not of the state of a system but of the nature of the system itself. We picture a complex

> nucleus as a black box in which a large number of particles are interacting according to unknown laws. The problem is then to define in a mathematically precise way an ensemble of systems in which all possible laws of interaction are equally probable.

After the initial successes in Nuclear Physics, the field of random matrices has developed immensely with countless applications in physics, mathematics and beyond. Just to mention few of them:

- Number theory, in connection with Riemann's hypothesis [6];
- Algebraic and enumerative combinatorics [7; 8; 9];
- Effective theories of strong interactions [10];
- Electronic transport in mesoscopic systems [11];
- Random graphs theory [12; 13];
- Numerical analysis [14; 15];
- Disordered materials [16];
- Computational biology and genomics [17];
- Entanglement in quantum systems [18];
- Quantum gravity [19];
- Quantum chaos [20];
- Multivariate data analysis and financial applications [21; 22; 23];
- Wireless communication [24; 25];

Comprehensive reviews, with emphasis on different aspects, also abound (see e.g. [6; 26; 27]).

As a first, gross classification of random matrix models one can consider whether some of the following features are present:

1. the entries are sampled independently from each other;

2. there is a group of invariance for the probability density of entries;

3. there are other symmetry requirements (hermiticity, positive definiteness etc.)

Many classifications of random matrix ensembles have been provided in the literature: for real eigenvalue models by Dyson, Altland-Zirnbauer and Caselle [3; 28]. Extensions to complex eigenvalue models (non-hermitian) have been given first in [29] and later refined in [30], where explicit matrix representations for each class were exhibited. Dyson's taxonomy, the one relevant for the present work, will be reviewed in the next Chapter.

Given a $N \times N$ matrix $\mathcal{X}$, the relevant object is the joint probability density function (jpdf) of the entries $P[\mathcal{X}] := P(X_{11}, \ldots, X_{NN})$, where $X_{ij}$ may be real, complex or quaternion numbers. In the case of independent entries, the distribution factorizes as:

$$P(X_{11}, ..., X_{NN}) := \prod_j f_j(X_{\alpha\beta}) \tag{1.0.1}$$

On the other hand, the group invariance requirement *à la* Dyson implies:

$$P[\mathcal{X}] = P[\mathcal{G}^{-1}\mathcal{X}\mathcal{G}] \tag{1.0.2}$$

where $\mathcal{G}$ is a member of the orthogonal, unitary or symplectic group (depending on whether $\mathcal{X}$ has real, complex or quaternion entries, see next chapter). The three cases will be labelled by Dyson's index $\beta = 1, 2, 4$ respectively.

In figure 1.1, we provide a schematic grouping of many known random matrix models according to the three features described above. At the core of the diagram lies the Gaussian ensemble, the only one endowed with all three features (see next chapter for details). Dropping one of the features may lead for instance to the following ensembles:

- Lévy: introduced by Cizeau and Bouchaud [31] in 1994, this ensemble contains symmetric matrices with independent entries, whose individual distribution decays as a power law. Thus, the group invariance is abandoned, but the symmetry of matrices ensures that a real spectrum is obtained.

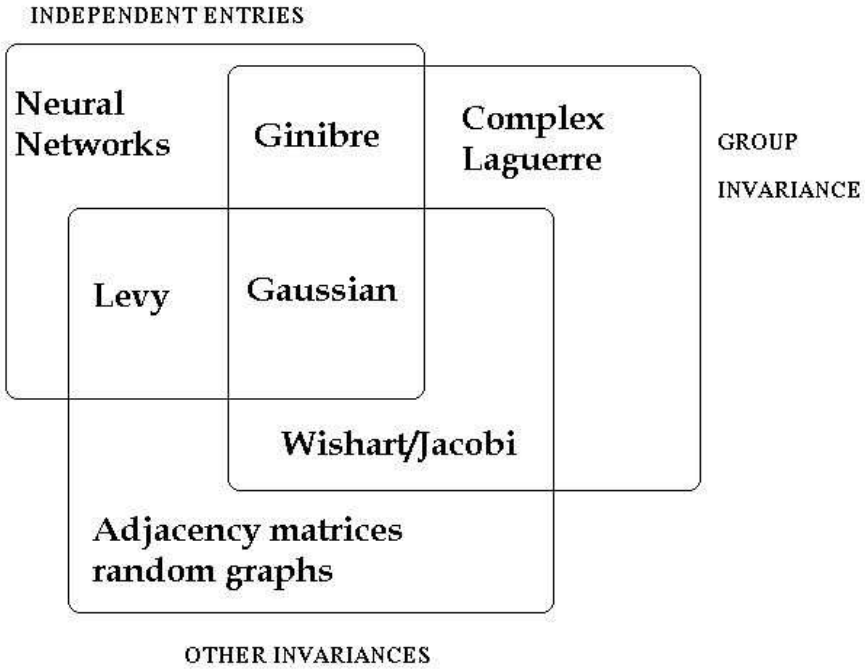


Figure 1.1: Examples of random matrix models, grouped according to three possible features: independent entries, group invariance and other invariances.

- Ginibre: introduced by J. Ginibre [32] in 1965, these ensembles are formed by matrices with independent entries. The invariance under the orthogonal, unitary and symplectic group is preserved, but the symmetry of individual matrices is dropped. As a consequence, the spectrum invades the complex plane.

- Wishart or Jacobi: these ensembles constitute the core of this thesis and will be reviewed in detail in the next chapters. They have non-independent entries, but all other symmetries.

In the outer layer of the diagram, we lodge examples of ensembles where two out of the three features above are dropped:

- Synaptic matrix for neural networks: in a recent publication [33], a model for a synaptic matrix of neural networks was introduced, where the entries are drawn independently from two distributions (with different means and variances). No other symmetries are present and the spectrum lies in the complex plane.

- Complex Laguerre: extensions of the chiral-Laguerre ensemble were proposed in [34] as effective models for QCD with non-vanishing chemical potential. All the group symmetries can be implemented, but the model has a complex spectrum and non-independent entries.

- Adjacency matrix of random graphs: given a random undirected graph, the adjacency matrix $\mathcal{A}$ has entries $A_{ij} = 1$ if there is an edge connecting nodes $i$ and $j$, and $A_{ij} = 0$ otherwise. It is obviously symmetric, but has no group symmetry and the entries are generally not independent, since their distribution is determined by the topology and degree distributions of the underlying graph [13].

In a very broad sense, the aim of Random Matrix Theory (RMT) is to study the statistics of spectral properties (eigenvalues and eigenvectors), given the jpdf of entries. However, the available mathematical techniques available to accomplish this task depend strongly on whether a group invariance is present or not: in the first case, it is usually possible to perform the change of variables $\mathcal{X} \to \mathcal{G}^{-1}\mathcal{D}\mathcal{G}$

explicitly (where $\mathcal{D}$ is the diagonal matrix containing the eigenvalues). This way, the jpdf of eigenvalues $P(\lambda_1, \ldots, \lambda_N)$ (where $\{\lambda_i\}$ can be real or complex) may be obtained (see next chapter).

This procedure reduces considerably the number of degrees of freedom involved, and thanks to the works of Mehta and many others, several powerful tools are available in this case (orthogonal polynomial techniques, Dyson's Coulomb gas analogy, supersymmetric methods etc.). On the contrary, more limited insights are usually within reach if group invariance is lacking: typically, one is confined to the average spectral density $\rho(\lambda)$ in the limit of large matrix size $N \to \infty$, a quantity which is computable e.g. with Green function methods and the replica trick among others. However, in the case of independent entries general theorems about the convergence in distribution of $\rho(\lambda)$ (semicircle law, Girko's circular law [35] etc.) are available.

In this thesis, we focus on the invariant sector of fig. 1.1, whose matrices are endowed with group symmetries and a real spectrum but have correlated entries. Many models in this class have been studied for long time: for instance, we can mention fixed and restricted trace ensembles [36], models with power law tails [37; 38], critical ensembles [39]. The classical families of Wishart-Laguerre and Jacobi, having many applications in multivariate statistical theory and beyond, belong to this category and constitute the core of the present work. Loosely speaking, one can draw the following chain:

$$\mathsf{Gaussian} \to \mathsf{Wishart\text{-}Laguerre} \to \mathsf{Jacobi}$$

where the $\to$ symbol means that combining matrices with Gaussian entries one obtains Wishart-Laguerre matrices, and combining Wishart-Laguerre matrices one obtains Jacobi matrices. More details will be given in next chapter.

A survey of the current knowledge about the statistics of eigenvalues of these classical ensembles is provided in next chapter, focusing mostly on the unitary case ($\beta = 2$).

## 1.1 Outline of the thesis

The purpose of the present work is to present new analytical results regarding the following three topics:

**Large deviations of the Maximum Eigenvalue:** There is a recent, growing interest both in physics and mathematics for the statistics of unlikely events involving correlated random variables. Due to their logarithmic repulsion, the eigenvalues of invariant matrix models are an ideal object of study. The typical question is: what is the rate of decay with $N$ (the size of the matrix) for the probability that all the eigenvalues are 'smaller than expected' (in a sense to be made more precise later)? These events involve anomalous fluctuations of the largest eigenvalue to the left of its mean: to the leading order, an accurate estimate for this probability can be obtained using a transparent and powerful method devised recently by Dean and Majumdar in an insightful publication [40]. We extend their approach, originally confined to the case of Gaussian random matrices, to the slightly more complicated Wishart-Laguerre ensemble: we analyze $\mathcal{O}(N)$ fluctuations of the largest eigenvalue to the left of its mean and provide exact results for the left rate function. This work completes a related analysis by Johansson [41] in the context of shape fluctuations and growth models, where the right rate function was computed by rigorous methods. These results are included in Chapter 3 and have been published in [42].

**Power-law deformations of Wishart-Laguerre:** In Chapter 4, we consider a one-parameter deformation of the Wishart-Laguerre ensemble. The jpdf of the entries of covariance matrices in the ensemble includes a power-law weight depending on the single parameter $\gamma$. When $\gamma \to \infty$, the usual Wishart-Laguerre ensemble is recovered. Earlier studies have focused on just the macroscopic spectral density, whereas we are able to provide a complete solution for finite $N$, and in both the macroscopic and microscopic large $N$ limits. Hence, we obtain a generalized Marčenko-Pastur distribution (for both square and rectangular matrices) and a generalized Bessel law close to the origin. This work is motivated by possible applications to

financial data, and in fact we have checked that the resulting density is in reasonable agreement with covariance matrices taken from financial assets. The main technical tool is an integral identity, through which we are able to establish an exact mapping between the generalized model and the standard one, together with the identification of the correct scaling with both $N$ and $\gamma$. The issue of universality is also discussed. These results appear in a paper recently accepted for publication [43].

**Quantum conductance in mesoscopic physics:** The Jacobi ensemble appears in the theoretical treatment of current fluctuations inside chaotic cavities of sub-micron dimensions. In the scattering theory framework, the scattering matrix connecting incoming and outgoing electronic waves is assumed to be random and uniformly distributed within the unitary group. It has a block structure, where each block encodes transmission and reflection coefficients for each of the two attached leads. The statistical properties of the conductance are derived from the knowledge of the transmission eigenvalues, whose jpdf can be easily mapped onto Jacobi. In the mesoscopic literature, several quantities are of interest for comparison with experiments: among these, one can mention the average density of transmission eigenvalues, their moments and higher order cumulants. While results for those quantities are well-known in some limiting cases, a general solution for the case of *finite* and *arbitrary* number of open channels in the two attached leads was still missing. In Chapter 5, we provide the sought formulas for the spectral density for $\beta = 2, 4$ and a formula for the moments of the transmission eigenvalues for $\beta = 2$, together with some intriguing combinatorial puzzles yet to be solved. Finally, we show how the Dean-Majumdar technique mentioned earlier can be used to gain further insight into the *full* probability distributions of the experimental quantities (conductance, shot noise, moments) in the limit of large number of open channels. As a byproduct, we also obtain a new exact formula for the variance of integer moments. These results are partially contained in ref. [44], while section 5.4 has not been published yet.

In the following Chapter, we will thoroughly review the main features of classical invariant ensembles and introduce the main technical tools that we need (orthogonal polynomials method, Dyson's Coulomb gas analogy and determinantal structure of correlations). We also provide a detailed introduction to the families of Gaussian, Wishart-Laguerre and Jacobi matrices, corresponding to the classical orthogonal polynomials (Hermite, Laguerre and Jacobi). Eventually, some concluding remarks are offered in chapter 6, together with technical details in the appendices (from A to E).

*The intention of the Holy Ghost is to teach us how one goes to heaven, not how heaven goes.*

GALILEO GALILEI

# Chapter 2

# Invariant Random Matrix models

## 2.1 Joint probability density of eigenvalues

As disclosed in the Introduction, we focus on ensembles of random matrices whose jpdf of matrix entries $P[\mathcal{X}]$ satisfies

$$P[\mathcal{X}] = P[\mathcal{G}^{-1}\mathcal{X}\mathcal{G}] \tag{2.1.1}$$

(where $\mathcal{G}$ is any element of a suitable invariance group) and having a real spectrum.

It is clear that we need to answer a few questions first:

- Where does the requirement (2.1.1) come from?
- How does (2.1.1) constrain the possible forms of $P[\mathcal{X}]$?
- What are the invariance groups involved?

To answer these questions, we recall that, since the early times of RMT, a random matrix $\mathcal{X}$ stands for the Hamiltonian $\mathbf{H}$ of an unknown system, written in a given orthonormal basis. It is always possible to go from one orthonormal basis to another thanks to a linear transformation:

$$\mathbf{H}' = \mathbf{U}^{-1}\mathbf{H}\mathbf{U} \tag{2.1.2}$$

However, even if *no other symmetries are present*, in conventional quantum mechanics every Hamiltonian ($\mathbf{H}$ or $\mathbf{H}'$) must be Hermitian to ensure a real energy spectrum[1]. This can be achieved only if the transformation matrix $\mathbf{U}$ is *unitary*:

$$\mathbf{U}\mathbf{U}^\dagger = \mathbf{U}^\dagger\mathbf{U} = \mathbf{I} \tag{2.1.3}$$

Even though Hamiltonians in matrix form related by linear transformations appear different, they of course represent the very same physical system, i.e. physical observables such as energy levels cannot depend on the choice of a particular basis.

It is then clear that, for consistency with the physical world the theory aims to represent, the same 'basis independence' carries over to random matrices: on a more general ground, Dyson showed that, in order for a random matrix to be consistent with physical requirements, its entries should belong to a division algebra over the reals [2]. Thus, we classify RMT models according to their entries (real, complex or quaternions) and symmetries (symmetric, hermitian or quaternion self-dual), which are invariant respectively under the Orthogonal, Unitary or Symplectic groups.

The requirement of basis invariance for RMT has two crucial consequences:

1. Weyl's lemma holds [46], so the jpdf of the entries $P[\mathcal{X}]$ can be only a function of the first $N$ traces of $\mathcal{X}$, where $N$ is the size of $\mathcal{X}$:

$$P[\mathcal{X}] = \varphi\left(\mathrm{Tr}\mathcal{X}, \ldots, \mathrm{Tr}\mathcal{X}^N\right) \tag{2.1.4}$$

2. The information encoded in the jpdf of entries is overabundant. One can always perform a change of variables $\{\mathcal{X}_{\alpha\beta}\} \to \{\lambda_k\}$, in such a way that the $\mathcal{O}(N^2)$ variables in $P[\mathcal{X}]$ get replaced by the $N$ eigenvalues of $\mathcal{X}$.

How do we get from the jpdf of entries to the jpdf of eigenvalues? First, we recall that any $N \times N$ Hermitian matrix $\mathcal{X}$ can be diagonalized uniquely by a unitary transformation:

$$\mathcal{X} = \mathcal{U}^\dagger\mathcal{D}\mathcal{U} \tag{2.1.5}$$

[1] Less restrictive requirements have been proposed in complex extensions of quantum mechanics [45].

Instead of parametrizing $\mathcal{X}$ using its matrix entries, we can use the $N$ eigenvalues and a set of parameters $\{u_1, u_2, u_3, \ldots\}$ pertaining to the transformation matrix $\mathcal{U}$. Now, the jpdf (2.1.4) is merely a density: in order to get a distribution function, it needs to be integrated over. The differential volume element will obviously change in passing from the variables 'entries' to the variables 'eigenvalues'. How do we take this effect into account? We just need to compute the Jacobian $J$ of this change of variables:

$$\prod_{i \leq j} dX_{ij} = J\left[\{\lambda_k\}, \{u_k\}\right] \prod_{k=1}^{N} d\lambda_k \prod_j du_j \tag{2.1.6}$$

A nice step-by-step calculation of the above Jacobian can be found e.g. in [26]. The final result reads:

$$J\left[\{\lambda_k\}, \{u_k\}\right] = f(\{u_k\}) \prod_{j<k} |\lambda_j - \lambda_k|^\beta \tag{2.1.7}$$

so it factorizes in a part depending only on the eigenvectors components, and a second part depending only on the eigenvalues. The latter is readily recognized as a Vandermonde determinant, raised to the so-called Dyson index $\beta$. Classically, the allowed $\beta$ values are $1, 2$ or $4$, according to the number of real variables needed to specify a single entry[1] of $\mathcal{X}$ (1 for real, 2 for complex and 4 for quaternion numbers). This Vandermonde factor is ultimately responsible for the typical eigenvalue repulsion which is observed in invariant random matrix models, and constitutes the basis for both the orthogonal polynomial technique and the Dyson's Coulomb gas analogy, the two main technical tools we are going to introduce in the following.

Starting from (2.1.7) and upon integrating out the 'eigenvectors' degrees of freedom, one ends up with the most general jpdf of unordered eigenvalues in the form:

$$P(\lambda_1, \ldots, \lambda_N) = C_{N,\beta}\, \varphi\left(\sum_{i=1}^{N} \lambda_i, \ldots, \sum_{i=1}^{N} \lambda_i^N\right) \prod_{j<k} |\lambda_j - \lambda_k|^\beta \tag{2.1.8}$$

[1] Random matrix models having a continuous range for $\beta > 0$ have been introduced in [47] (non-invariant, independent entries) and in [48] (invariant, correlated entries).

where $P(\lambda_1, \ldots, \lambda_N)$ is a normalizable, positive definite and symmetric function of the eigenvalues.

Note that another less general (but usually correct and more manageable) alternative expression is often given:

$$P(\lambda_1, \ldots, \lambda_N) = C_{N,\beta} \prod_{j=1}^{N} \omega(\lambda_j) \prod_{j<k} |\lambda_j - \lambda_k|^\beta \tag{2.1.9}$$

However, there are cases where such a representation does not hold (see chapter 4 and [37]).

The classical ensembles (Gaussian, Wishart-Laguerre and Jacobi) all admit the representation (2.1.9) with:

$$\begin{cases} \omega_{\mathrm{G}}(x) = e^{-n\beta x^2} & \text{Gaussian} \\ \omega_{\mathrm{WL}}(x) = x^\nu e^{-n\beta x} & \text{Wishart-Laguerre} \\ \omega_{\mathrm{J}}(x) = (1-x)^\alpha (1+x)^\beta & \text{Jacobi} \end{cases} \tag{2.1.10}$$

where $n$ is a parameter we introduce to reconcile different conventions in the literature. In (2.1.10), the support of the spectral density (i.e. the range of variability for the eigenvalues) is respectively $\mathbb{R}$, $\mathbb{R}_+$ and $[-1, 1]$.

Before introducing the main technical tools that are needed, we first ask the question: what quantities can be computed from (2.1.9)? A non-exhaustive list may include (see also next section for further details):

- Density of eigenvalues $\rho_N(\lambda) = \left\langle \sum_i \delta(\lambda - \lambda_i) \right\rangle$, where the average is taken over the jpdf (2.1.9). This may be done for finite matrix size $N$ (using e.g. the orthogonal polynomial technique) or asymptotically for large $N$ (using e.g. asymptotics of orthogonal polynomials or the Coulomb gas analogy described below). For the large $N$ setting, it is customary to distinguish between a *macroscopic* limit, where the argument $\lambda$ of the density grows as $N^\kappa$ ($\kappa$ being a typical scale, unique for a given matrix model[1]). Conversely, a *microscopic* limit can also be considered, where the combination $N^\kappa(\lambda - \lambda_0)$ is kept fixed for large $N$, where $\lambda_0$ is the location within the spectrum where one wishes to zoom in (origin, bulk or edge points): this amounts to

[1] For example, in the Gaussian case $\kappa = 1/2$, while for Wishart-Laguerre $\kappa = 1$

probing correlations on the scale of the mean level spacing, and gives rise to universal laws (e.g. the sine kernel in the bulk for Gaussian matrices, and the Bessel law at the hard edge for Wishart-Laguerre; a more detailed discussion of the latter follows in Chapter 4). Universality in this context means stability with respect to polynomial deformations of the confining potential, which typically does not hold for macroscopic properties (see, however, the more detailed discussion in section 4.3.1). Ultimately, the two kinds of large-$N$ behaviors can be blamed on different asymptotic laws for orthogonal polynomials.

- $n$-point correlation functions among the eigenvalues (see next section);
- Gap distributions, i.e. probability that a region (e.g. the interval $[a, \infty)$) of the real axis is free of eigenvalues. This amounts to integrating the jpdf of eigenvalues (2.1.9) over the complementary interval $\mathbb{R} \setminus [a, \infty)$.
- Single eigenvalue distributions (of particular interest is the case of extreme eigenvalues), which follow by differentiation of the gap distribution (see also section 4.4.2).
- Variance of the number statistics and least square statistics (see chapter 16 in [46]).

In subsection 2, we introduce in full detail the orthogonal polynomial technique for $\beta = 2$ (unitary case), which allows to write all correlation functions as determinants of a suitable kernel. The cases $\beta = 1, 4$ are more complicated, but doable in the same framework and the reader is referred to [46] for details.

In subsection 3, we briefly summarize the so-called Coulomb gas analogy (due to Dyson) which is invaluable for large $N$ density calculations. A variant of this method will be used in chapter 3 to address large deviations of the maximum eigenvalue in Wishart-Laguerre matrices.

In the last section, we review in detail the classical ensembles pointing to the relevant literature on the subject.

## 2.2 Orthogonal polynomials and determinantal structure of correlations

In this section, we follow very closely the pedagogical review by Fyodorov [26] for the unitary case ($\beta = 2$). Details for the other cases can be found e.g. in [46].

The orthogonal polynomial technique allows to write down a compact expression for the $n$-point correlation function of the $N$ eigenvalues, which is defined as:

$$R(\lambda_1, \dots, \lambda_n) := \frac{N!}{(N-n)!} \int d\lambda_{n+1} \cdots d\lambda_N P(\lambda_1, \dots, \lambda_N) \tag{2.2.1}$$

First, one observes that the following holds:

$$\prod_{j<k} (\lambda_j - \lambda_k) = (-1)^{\frac{N(N-1)}{2}} \det \begin{pmatrix} 1 & \dots & 1 \\ \lambda_1 & \dots & \lambda_N \\ \vdots & \vdots & \vdots \\ \lambda_1^{N-1} & \dots & \lambda_N^{N-1} \end{pmatrix} = \Delta(\lambda_1, \dots, \lambda_N) \tag{2.2.2}$$

Now, the determinant does not change upon linearly combining its rows. In particular, the entries $\lambda_i^k$ in the $(k+1)$-th row can be replaced by a polynomial $\pi_k(\lambda_i) = a_k \lambda_i^k +$lower order terms, for any choice of the coefficients $a_\ell, \ell = 0, ..., k$.

So, we can write:

$$\prod_{j<k} (\lambda_j - \lambda_k) = \frac{(-1)^{\frac{N(N-1)}{2}}}{a_0 \cdots a_{N-1}} \det \begin{pmatrix} \pi_0(\lambda_1) & \dots & \pi_0(\lambda_N) \\ \pi_1(\lambda_1) & \dots & \pi_1(\lambda_N) \\ \vdots & \vdots & \vdots \\ \pi_{N-1}(\lambda_1) & \dots & \pi_{N-1}(\lambda_N) \end{pmatrix} \tag{2.2.3}$$

Now, if we multiply every entry in the $j$-th column of the matrix in (2.2.3) by $\sqrt{\omega(\lambda_j)}$, the jpdf of eigenvalues (2.1.9) can be written as:

$$P(\lambda_1, \dots, \lambda_N) \propto \left[ \det \left( \sqrt{\omega(\lambda_j)} \pi_{i-1}(\lambda_j) \right)_{1 \le i,j \le N} \right]^2 \tag{2.2.4}$$

Now, the square of the determinant in (2.2.4) can be rewritten using the following observation: if $\mathcal{A}$ is a matrix whose elements are $A_{ij} = \phi_{i-1}(x_j)$, the square of its determinant reads

$$(\det \mathcal{A})^2 = \det(\mathcal{A}^T \mathcal{A}) = \det \left( \sum_j A_{ji} A_{jk} \right)_{1 \le i,k \le N} \tag{2.2.5}$$

so that (2.2.4) can be written as:

$$P(\lambda_1,\ldots,\lambda_N) \propto \det\left(\sum_{j=1}^{N}\phi_{j-1}(\lambda_i)\phi_{j-1}(\lambda_k)\right)_{1\le i,k\le N} = \det(K_N(\lambda_i,\lambda_k))_{1\le i,k\le N} \tag{2.2.6}$$

where we introduced the kernel:

$$K_N(x,x') = \sum_{j=0}^{N-1}\phi_j(x)\phi_j(x') \tag{2.2.7}$$

$$\phi_{i-1}(x) = \sqrt{\omega(x)}\pi_{i-1}(x) \tag{2.2.8}$$

So far, we have left the polynomials $\pi_k(x)$ unspecified. Suppose that we now make the choice:

$$\int \omega(x)\pi_i(x)\pi_j(x)dx = \delta_{ij} \tag{2.2.9}$$

i.e. the $\pi_k(x)$ constitute an orthonormal set with respect to the weight $\omega(x)$. Then, the following 'reproducing' property for the kernel $K_N$ holds:

$$\int K_N(x,y)K_N(y,z)dy = K_N(x,z) \tag{2.2.10}$$

This property allows to invoke the following lemma by Dyson [1] [51], in the simplified form given by Fyodorov [26] for $\beta = 2$:

**Lemma 2.2.1 (Dyson)** *Let $\mathcal{J}_n(\mathbf{x}) = (J_{ij})_{1\le i,j\le n}$ be an $n\times n$ matrix whose entries depend on a real vector $\mathbf{x} = (x_1, x_2, \ldots, x_n)$ and have the form $J_{ij} = f(x_i, x_j)$, where $f$ is some complex-valued function satisfying for some measure $d\mu(x)$ the 'reproducing kernel' property:*

$$\int f(x,y)f(y,z)d\mu(y) = f(x,z) \tag{2.2.11}$$

*Then:*

$$\int \det \mathcal{J}_n(\mathbf{x})d\mu(x_n) = [q-(n-1)]\det\mathcal{J}_{n-1} \tag{2.2.12}$$

*where $q = \int f(x,x)d\mu(x)$ and the matrix $\mathcal{J}_{n-1}$ has the same functional form as $\mathcal{J}_n$ with $\mathbf{x}$ replaced by $(x_1, x_2, \ldots, x_{n-1})$.*

[1] Generalizations of this theorem have been given recently in [49] and [50].

We see that the kernel $K_N(x,y)$ satisfies exactly the property (2.2.11) (see eq. (2.2.10)), with the constant $q$ of the Lemma is readily computed as:

$$q = \int K_N(x,x)dx = \sum_{j=0}^{N-1} \int \omega(x)[\pi_j(x)]^2 dx = N \tag{2.2.13}$$

Thanks to Dyson's Lemma, we are able to compute iteratively some multiple integrals of the determinant of $K_N(\lambda_i, \lambda_j)$ over some proper subset of the sequence of eigenvalues $\{\lambda_k\}$, i.e. exactly the definition of correlation functions (2.2.1). Let us see in detail how this works. First, let us integrate the jpdf of eigenvalues (2.2.6) over one eigenvalue, using the reproducing lemma:

$$\int P(\lambda_1, \ldots, \lambda_N)d\lambda_N \propto \int \det(K_N(\lambda_i,\lambda_j))_{1\leq i,j\leq N} d\lambda_N = \det(K_N(\lambda_i,\lambda_j))_{1\leq i,j\leq N-1} \tag{2.2.14}$$

Proceeding one step further:

$$\int\int \det(K_N(\lambda_i,\lambda_j))_{1\leq i,j\leq N} d\lambda_{N-1} d\lambda_N = \int \det(K_N(\lambda_i,\lambda_j))_{1\leq i,j\leq N-1} d\lambda_{N-1} = [N-(N-2)]\det(K_N(\lambda_i,\lambda_j))_{1\leq i,j\leq N-2} \tag{2.2.15}$$

and by induction:

$$\int \ldots \int \det(K_N(\lambda_i,\lambda_j))_{1\leq i,j\leq N} d\lambda_{k+1}\ldots d\lambda_N = (N-k)!\det(K_N(\lambda_i,\lambda_j))_{1\leq i,j\leq k} \tag{2.2.16}$$

Recalling the definition (2.2.1), we can immediately write down a compact expression for the $n$-point correlation function as:

$$R(\lambda_1, \ldots, \lambda_n) = \det(K_N(\lambda_i,\lambda_j))_{1\leq i,j\leq n} \tag{2.2.17}$$

In particular, the average density of eigenvalues $R(\lambda)$ (one-point function) is given immediately by:

$$R(\lambda) = K_N(\lambda,\lambda) = \omega(\lambda)\sum_{i=1}^{N-1}[\pi_{i-1}(\lambda)]^2 \tag{2.2.18}$$

It is then clear that the classical ensembles introduced earlier (2.1.10) require the use of orthonormal polynomials with respect to the classical weights, i.e. Hermite, Laguerre and Jacobi respectively. Note also that the normalization of the spectral density (2.2.18) is $\int R(\lambda)d\lambda = N$, while it is customary to rescale it to have it normalized to 1. In the following, we will always make clear when we adopt one convention or another by using $R$ or $\rho$ for normalization to $N$ or 1 respectively.

## 2.3 Dyson's Coulomb gas analogy

The macroscopic density, in the limit of large matrix size $N \to \infty$, can be computed in principle from the finite $N$ result, exploiting known asymptotics of the classical orthogonal polynomials. Generally speaking, this is not the most convenient route: a more effective and less cumbersome method goes under the name of 'Coulomb gas analogy' and was first proposed by Dyson [2]. The eigenvalues of a given invariant ensemble (lying on the real line) are considered as point particles of a charged fluid, subject to two competing interactions: the logarithmic repulsion, originated by the Vandermonde factor, is just a 2D Coulomb interaction among the charged particles (though confined on a line), whereas a confining potential (e.g. parabolic for the Gaussian ensembles) prevents the particles from escaping to infinity (see the schematic picture in fig. 2.1). More formally, one can write the jpdf of an invariant ensemble as a Boltzmann's weight:

$$P(\lambda_1, \dots, \lambda_N) \propto e^{-\beta F[\vec{\lambda}]} \tag{2.3.1}$$

where $\vec{\lambda} = \{\lambda_1, \dots, \lambda_N\}$ and the 'free energy' incorporates the two competing contributions. In the continuum limit, where the individual eigenvalues are replaced by a smoothed macroscopic density $\rho(\lambda)$ [1], the free energy becomes a sum of integrals over the sought density. For example, in the Gaussian case ($n = 1$ for simplicity):

$$F[\vec{\lambda}] \simeq \int d\lambda\ \lambda^2 \rho(\lambda) - \int\int d\lambda d\lambda' \rho(\lambda)\rho(\lambda') \log|\lambda - \lambda'| + C\left(\int d\lambda \rho(\lambda) - 1\right) \tag{2.3.2}$$

where $C$ is a Lagrange multiplier, enforcing the normalization of the density to 1, and the range of integration depends on the matrix model ($(-\infty, \infty)$ for the Gaussian model).

The equilibrium density $\rho(\lambda)$ of the fluid particles is such that the free energy is minimized: after one functional and one ordinary differentiation of (2.3.2), we obtain a Poisson-like equation for the charge density as:

$$\lambda = \mathcal{P} \int d\lambda' \frac{\rho(\lambda')}{\lambda - \lambda'} \tag{2.3.3}$$

[1] This replacement is legitimate for $N \to \infty$.

where $\mathcal{P}$ denotes the Cauchy principal part, and on the left hand side one has more generally the derivative of the confining potential $V'(\lambda)$. We will encounter this singular integral equation many times throughout the present thesis. A general treatment, with different conditions at the boundaries of the support, was first provided by Tricomi [52]. For the Gaussian case, this leads directly to the celebrated semicircle law (see [46] and subsection 2.4.1).

## 2.4 The classical ensembles

### 2.4.1 Gaussian ensemble

The Gaussian ensemble is composed by square matrices having independent and normally distributed entries (real, complex or quaternion numbers), supplemented by an appropriate group invariance (orthogonal, unitary and symplectic respectively). The joint probability density of the entries can be written in the compact form:

$$P_{\mathrm{G}}[\mathcal{X}] \propto \exp\left(-n\beta \mathrm{Tr}\mathcal{X}^{\dagger}\mathcal{X}\right) \tag{2.4.1}$$

In fact, the jpdf (2.4.1) was proven by Rosenzweig and Porter (see e.g. [46]) to be the only one satisfying i) independence of the entries and ii) rotational invariance. The Dyson's index $\beta$ reflects the invariance group as usual.

The spectrum lies on the real line, and its properties are determined by the jpdf of $N$ eigenvalues, where $N$ is the size of the matrix:

$$P_{\mathrm{G}}(\lambda_1, \ldots, \lambda_N) = B_N \, e^{-n\beta \sum_{i=1}^{N} \lambda_i^2} \prod_{j<k} |\lambda_j - \lambda_k|^{\beta} \tag{2.4.2}$$

where $B_N$ is a normalization constant, whose value can be computed exploiting a variant of the Selberg's integral [46] or the norms of orthogonal polynomials (see section 2.2).

The macroscopic density of eigenvalues in the large $N$ limit can be computed from Tricomi's equation (see [46]), and after the scaling $x = \lambda/\sqrt{n\beta N}$ has the celebrated Wigner's semicircular form:

$$\rho_{\mathrm{G}}(x) = \frac{2}{\pi}\sqrt{1-x^2} \tag{2.4.3}$$

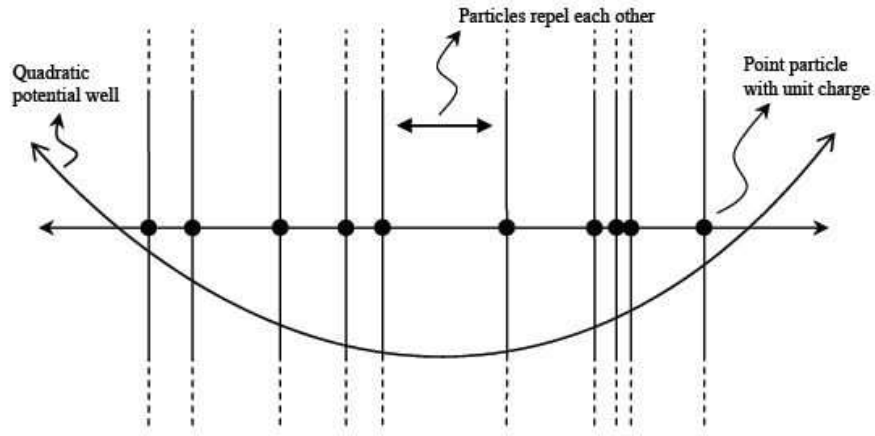


Figure 2.1: A schematic picture of eigenvalues (Coulomb fluid particles) repulsion, in presence of a quadratic potential well.

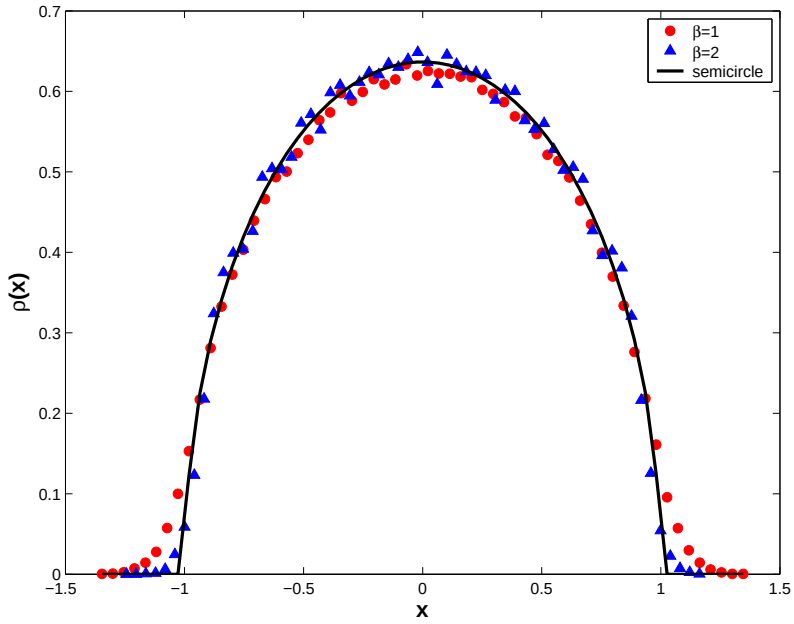


Figure 2.2: Normalized histogram of eigenvalues of Gaussian $10 \times 10$ random matrices, averaged over 10000 samples.

plotted in fig. 2.2. The agreement with the theoretical distribution (2.4.3) is excellent already for $N = 10$.

Finite $N$ results for the spectral density and higher order correlation functions are known from the general Gaudin-Mehta theory, using the orthogonal polynomial techniques (see discussion in previous section). For example, for $\beta = 2$ the density for finite $N$ can be found (see e.g. [36]) in terms of Hermite polynomials:

$$\rho_{\mathrm{G}}^{(N)}(\lambda) = \frac{1}{N}\sqrt{\frac{2n}{\pi}}e^{-2n\lambda^2}\sum_{k=0}^{N-1}\frac{H_k^2(\lambda\sqrt{2n})}{2^k\ k!} \tag{2.4.4}$$

Gap distributions for the Gaussian ensemble are known [46] in terms of infinite products. For the case of nearest-neighbor spacing, a rather accurate approximation is provided by the so-called Wigner's surmise, which is the *exact* result for $N = 2$. The general formula for the probability of having a spacing $s$ (measured in units of the mean level spacing) between the two eigenvalues reads:

$$\mathcal{P}_{\mathrm{G}}^{(\beta)}(s) = C_\beta s^\beta e^{-\alpha_\beta s^2} \tag{2.4.5}$$

where the constants $C_\beta$ and $\alpha_\beta$ ensure the following:

$$\int_0^\infty \mathcal{P}_{\mathrm{G}}^{(\beta)}(s)ds = 1 = \int_0^\infty s\mathcal{P}_{\mathrm{G}}^{(\beta)}(s)ds \tag{2.4.6}$$

The cumulative distribution of the largest eigenvalue for the GUE case has been given by Tracy and Widom [53] in terms of a Painlevé IV trascendent. For the other symmetry classes, a good reference is Dieng [54], which contains more general results for the distribution of the $m$-th eigenvalue in the large $N$ regime.

It is worth mentioning that a matrix model with independent (but not identically distributed) entries, corresponding to the jpdf (2.4.2) for real $\beta > 0$, has been found recently by Dumitriu and Edelman [47]. From the point of view of numerical sampling of random matrices, their construction is extremely efficient and will be adopted in section 3.5 for the Wishart-Laguerre case.

### 2.4.2 Wishart-Laguerre ensemble

Consider a rectangular $(M \times N)$ matrix $\mathcal{X}$ whose elements $X_{ij}$ represent some data. The $N$ entries of each of the $M$ rows constitute the components of an $N$-dimensional vector $\vec{X}_i$ (with $i = 1, 2, \ldots, M$). The vector $\vec{X}_i$ (the $i$-th row of the array) represents the $i$-th sample of the data and the matrix element $X_{ij}$ represents the $j$-th component of the vector $\vec{X}_i$. For example, suppose we are considering a population of $M$ students in a class, and for each student we have the data of their heights, their marks in an examination, their weights etc. forming a vector of $N$ elements (or traits) for each of the $M$ students. Then the product $\mathcal{W} = \mathcal{X}^T\mathcal{X}$ is a positive definite symmetric $(N \times N)$ matrix that represents the covariance matrix of the data (unnormalized). This matrix characterizes the correlations between different traits. The spectral properties of this matrix, i.e., its eigenvectors and eigenvalues, play a very important role in the so called 'principal components analysis' (PCA) of multivariate data, a technique that is used regularly in detecting hidden patterns in data and also in image processing [55; 56; 57], amongst other applications [58]. In PCA, one diagonalizes the covariance matrix $\mathcal{W}$ and identifies all the eigenvalues and eigenvectors. The data are usually maximally scattered in the direction of its principal eigenvector, corresponding to the largest eigenvalue and are least scattered in the direction of

the eigenvector corresponding to the minimum eigenvalue. One can then prune the data by successively getting rid of the components (setting them to zero) along the eigenvectors corresponding to the smaller eigenvalues, but retaining the components along the larger eigenvalues, in particular those corresponding to the maximal eigenvalue. This method thus reduces the effective dimension of the data. This technique is called 'dimensional reduction' and forms the basis of e.g, image compression in computer vision [57].

When the underlying data are random, e.g. the elements of the matrix $\mathcal{X}$ are independent and identically distributed (i.i.d) random variables, real or complex, drawn from a Gaussian distribution, the product matrices $\mathcal{W} = \mathcal{X}^\dagger\mathcal{X}$ constitute the so called Wishart ensemble, named after Wishart who first introduced them [4]. In literature one can also find the term 'Laguerre' ensemble, because the Laguerre polynomials arise in the analytical treatment of its spectral properties (e.g. spectral density and higher order correlation functions for finite $N$, see also Appendix C). It is also called 'chiral' ensemble, because in the applications to the low-energy sector of gauge theories, random matrices with chiral symmetry (modelling the Dirac operator) appear (see e.g. [10]).

The Wishart-Laguerre (hereafter WL) ensemble of random matrices has since appeared in many different contexts, such as multivariate statistical data analysis [55; 59], analysis of the capacity of channels with multiple antennae and receivers [24], low-energy QCD and other gauge theories [10], knowledge networks [60] and also in statistical physics problems, such as a class of $(1+1)$-dimensional directed polymer problems [41]. Very recent analytical results include the distribution of the matrix elements for the Anti-Wishart matrices (when $M < N$) [61; 62] and distributions related to entangled random pure states [18].

Provided that the joint distribution of the elements of the $(M \times N)$ matrix $\mathcal{X}$ (real or complex) is Gaussian, the spectral properties of the Wishart matrix $\mathcal{W} = \mathcal{X}^\dagger\mathcal{X}$ have been studied extensively for many decades. For the case when $M \geq N$ (the number of samples is larger than the dimension) it is known that all the eigenvalues are positive, a typical eigenvalue scales as $\lambda \sim N$ for large $N$ (as remarked earlier), and the joint probability density (jpdf) of the eigenvalues

is given by:

$$P_{\rm WL}(\lambda_1,\ldots,\lambda_N) = K_N e^{-\beta n\sum_{i=1}^N \lambda_i}\prod_{i=1}^N \lambda_i^{\frac{\beta}{2}(1+M-N)-1}\prod_{j<k}|\lambda_j-\lambda_k|^\beta \tag{2.4.7}$$

where $n$ is a parameter related to the variance of the entries of $\mathcal{X}$ ($n = 1/2$ for standard normal): in the next chapter, we keep $n = 1/2$ for simplicity, whereas in chapter 4 we will keep $n$ completely general (this just corresponds to a trivial rescaling of the spectrum).

From (2.4.7), the average density of eigenvalues in the large $N$ limit (with $c = N/M < 1$ fixed) has a scaling form $\rho_{\rm WL}(\lambda; c) = 2nN^{-1}f(2nN^{-1}\lambda)$, where:

$$f(x) = \frac{1}{2\pi x}\sqrt{(x-x_-)(x_+-x)} \tag{2.4.8}$$

is the Marčenko-Pastur (MP) function [63] on the compact support $x \in [x_-, x_+]$, with $x_\pm = \left(\frac{1}{\sqrt{c}} \pm 1\right)^2$. (This result was also rederived by a different method by Dyson [64] and the spectral fluctuations were numerically investigated by Bohigas *et al.* [65]). Thus, for $c \leq 1$, all the eigenvalues lie within a compact Marčenko-Pastur sea and the average eigenvalue (see also appendix B),

$$\langle\lambda\rangle = \int_0^\infty \rho_{\rm WL}(\lambda)\lambda d\lambda = \frac{N}{2nc}. \tag{2.4.9}$$

For all $c < 1$, the distribution goes to zero at the edges $x_-$ and $x_+$. For the case $c = 1$ ($x_- = 0$ and $x_+ = 4$), the distribution diverges as $x^{-1/2}$ at the origin, $f(x) = \frac{1}{2\pi}\sqrt{(4-x)/x}$ for $0 \leq x \leq 4$. For the Anti-Wishart case ($M < N$, i.e., $c > 1$) where one has $M$ positive eigenvalues (the rest of the $(N-M)$ eigenvalues are identically zero), the corresponding result can be obtained from the $M \geq N$ case simply by exchanging $M$ and $N$.

For finite $N$, results for the spectral density and higher order correlation functions are readily obtained using Laguerre polynomials. For $\beta = 2$, see (C.0.7) upon putting $\xi = \gamma = 1$. Several interesting results are also available for the distributions of individual eigenvalues. A comprehensive account of the literature on this subject, together with our generalizations, is provided in section 4.4.2.

Another interesting ensemble closely related to Wishart is the one considered e.g. in [66] and studied in [18], with applications to entangled quantum states and quantum information.

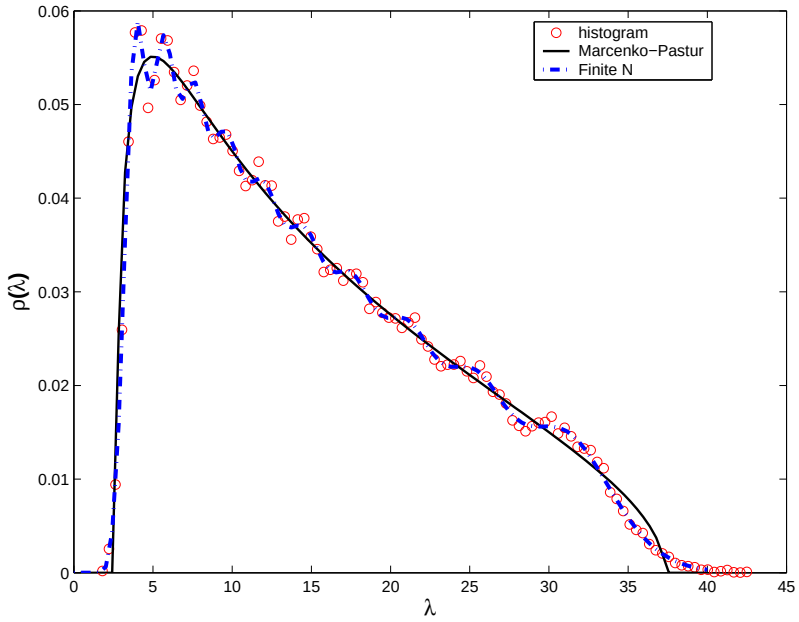


Figure 2.3: Normalized histogram of eigenvalues of Wishart matrices $N = 10, M = 30$, compared with Marčenko-Pastur and finite $N$ result.

### 2.4.3 Jacobi ensemble

The Jacobi ensemble is the third classical ensemble we consider. It bears its name from the Jacobi polynomials $P_k^{(\alpha,\beta)}(x)$, which are orthogonal on $[-1, 1]$ with respect to the weight function:

$$w_{\mathrm{J}} := (1-x)^{\alpha}(1+x)^{\beta} \tag{2.4.10}$$

The Jacobi matrices are obtained as combination of Wishart matrices, and different conventions are adopted in the literature, with rather confusing consequences. A good source of information is the Muirhead's book [23], although it must be complemented with more recent accounts.

A very clear definition of the Jacobi ensemble is given in [67; 68]: consider two normalized Wishart matrices $\mathcal{W}_1 = M_1^{-1}\mathcal{X}_1\mathcal{X}_1^{\dagger}$ and $\mathcal{W}_2 = M_2^{-1}\mathcal{X}_2\mathcal{X}_2^{\dagger}$, the first obtained from a rectangular $(N \times M_1)$ matrix $\mathcal{X}_1$ and the second from a $(N \times M_2)$ matrix $\mathcal{X}_2$ $(M_1, M_2 \geq N)$. The elements $X_{jk}$ of both matrices $\mathcal{X}_{1,2}$ are drawn independently from a real (or complex) standard normal distribution ($N(0,1)$ or

$N(0,1/\sqrt{2}+iN(0,1/\sqrt{2}))$. Then, define the matrix $\mathcal{J}=(\mathcal{W}_1+\mathcal{W}_2)^{-1}\mathcal{W}_1$. The eigenvalues of $\mathcal{J}$ are random variables between 0 and 1, whose jpdf is given by [69]:

$$P_{\mathrm{J}}(\lambda_1,\ldots,\lambda_N)\propto\prod_{j=1}^{N}\lambda_j^{M_1-N+1-2/\beta}(1-\lambda_j)^{M_2-N+1-2/\beta}\prod_{j<k}|\lambda_j-\lambda_k|^{\beta} \tag{2.4.11}$$

After the change of variables $\lambda\mapsto(1-\lambda)/2$, we recover the Jacobi weight function (2.4.10).

The limiting eigenvalue density can be obtained using a Coulomb gas analogy and reads [68]:

$$\rho_{\mathrm{J}}(\lambda)=\frac{\sqrt{(\lambda-b_-)(b_+-\lambda)}}{2\pi c_0(\lambda)} \tag{2.4.12}$$

on the support $[b_-,b_+]$, where:

$$c_0(\lambda)=\lambda^3(c_1-c_2)+\lambda^2(c_2-2c_1)+\lambda c_1 \tag{2.4.13}$$

$$b_{\pm}=\frac{(1-c_1)^2}{c_1^2-c_1+2+c_2-c_1c_2\mp2\sqrt{c_1+c_2-c_1c_2}} \tag{2.4.14}$$

$$c_1=N/M_1 \tag{2.4.15}$$

$$c_2=N/M_2 \tag{2.4.16}$$

Depending on the values of $c_1$ and $c_2$, both soft edges or hard edges in $0,1$ are allowed. The finite $N$ density is written in terms of Jacobi polynomials and will be extensively discussed in chapter 5 in connection with the quantum conductance problem. In fact, the Jacobi ensemble also arises as the distribution of certain combinations of sub-blocks of unitary distributed matrices, and this construction will be reviewed in chapter 5.

Numerous results are available in the literature for gap probabilities [67] and also distributions of the extreme eigenvalues [21]. The former results reveal interesting connection with the theory of Painlevé equations, whereas the latter have been nicely extended to the case of arbitrary $\beta$ in [69].

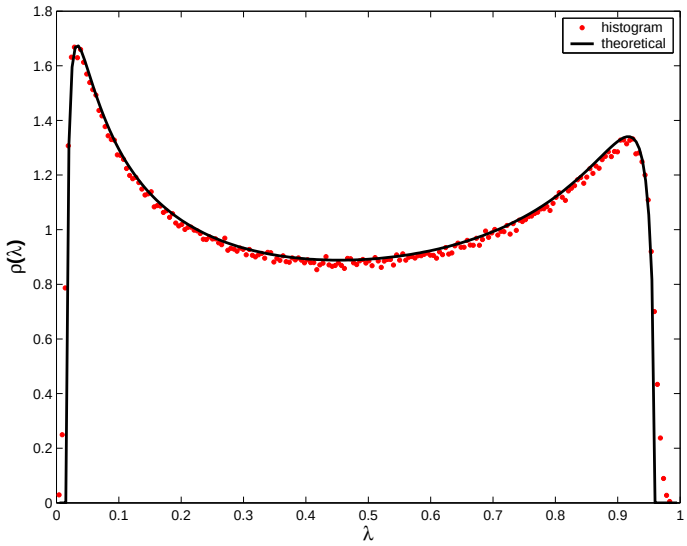


Figure 2.4: Normalized histogram of eigenvalues of a Jacobi ensemble with $N = 30, M_1 = 40$ and $M_2 = 50$ ($c_1 = 0.75$ and $c_2 = 0.6$, for $\beta = 1$ (red points), and corresponding limiting distribution (2.4.12) (solid black line).

*When people thought the Earth was flat, they were wrong. When people thought the Earth was spherical, they were wrong. But if you think that thinking the Earth is spherical is just as wrong as thinking the Earth is flat, then your view is wronger than both of them put together.*

ISAAC ASIMOV

# Chapter 3

# Large deviations of the maximum eigenvalue

## 3.1 Tracy-Widom distribution: typical fluctuations of the largest eigenvalue

The average density of states for large matrices in the Gaussian or Wishart-Laguerre ensemble has been introduced in the last chapter. It is worth remarking that such quantity is highly *non-universal* and depends strongly on the confining potential of the ensemble under consideration. Thanks to Dyson's Coulomb gas approach, it is also fairly easy to derive (at least for invariant ensembles) by solving an appropriate singular integral equation of Tricomi type (see section 2.3).

Conversely, much harder efforts are needed for *universal* quantities in the large $N$ limit, the prototype being the distribution of extreme eigenvalues. On a level of full mathematical rigor, this programme was undertaken by Tracy and Widom [53; 70] in a series of breakthroughs since 1994. Two fundamental questions have been answered there:

- What is the *typical* scale of fluctuations with $N$ of the largest eigenvalue of a $N \times N$ Gaussian matrix?

- What is the full limiting distribution ($N$ independent) of the rescaled largest eigenvalue for large $N$?

The outcome of their analysis is the following: from the semi-circle law, we know that the average of the maximum eigenvalue will lie at the upper edge point $\sqrt{2N}$. But for finite but large $N$, this eigenvalue will fluctuate around its mean. Tracy and Widom showed that such fluctuations occur over a narrow scale of $\mathcal{O}(N^{-1/6})$ around the upper edge of Wigner's sea. More precisely, the scaling variable $\xi = \sqrt{2}N^{1/6}[\lambda_{\max} - \sqrt{2N}]$ has a limiting $N$-independent distribution $\text{Prob}[\xi \leq x] = F_\beta(x)$. The function $F_\beta(x)$ depends on the Dyson's index $\beta$ of the ensemble: for example, in the $\beta = 2$ case it reads

$$F_2(x) = \exp\left(-\int_x^\infty (t-x)q(t)^2 dt\right) \tag{3.1.1}$$

where $q(s)$ satisfies the following Painlevé II equation:

$$q'' = sq + 2q^3 \tag{3.1.2}$$

with the boundary condition $q(s) \sim \text{Ai}(s)$ as $s \to \infty$ ($\text{Ai}(s)$ is the Airy function). Analogous results hold for $\beta = 1$ and $\beta = 4$:

$$F_1(x)^2 = F_2(x)\exp\left(-\int_x^\infty q(t)dt\right) \tag{3.1.3}$$

$$F_4\left(\frac{x}{2^{2/3}}\right)^2 = F_2(x)\left(\cosh\left(\int_x^\infty q(t)dt\right)\right)^2 \tag{3.1.4}$$

For an efficient numerical implementation of $F_\beta(x)$ and its density $f_\beta(x) = \frac{d}{dx}F_\beta(x)$ , see [71]. The density is depicted in fig. 3.1.

It is quite remarkable that such distribution, which generalizes in a non-trivial way the families of Weibull, Gumbel and Fréchet distributions for the maximum of independent identically distributed random variables [72], has since cropped up in a number of seemingly unrelated problems [73]. Without being exhaustive, we can mention the longest increasing subsequence problem [74], directed polymers in $(1+1)$-dimensions [41; 75], several $(1+1)$-dimensional growth models [76], a class of sequence alignment problems [77], mesoscopic fluctuations [78] and also financial applications [79].

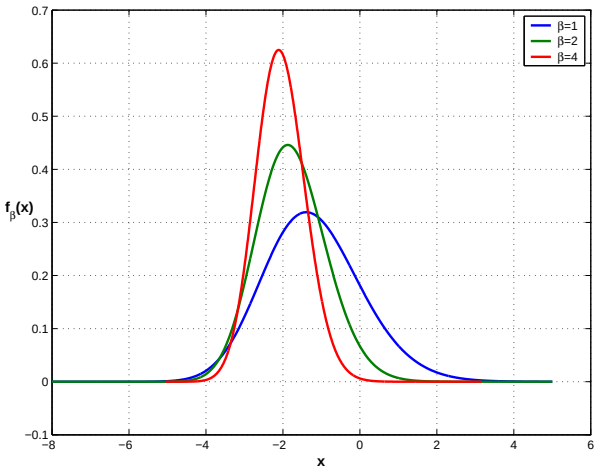


Figure 3.1: Tracy-Widom density for $\beta = 1, 2, 4$.

As another signature of universality, the same Tracy-Widom law has appeared in more recent times as the limiting distribution of the largest eigenvalue of Wishart-Laguerre matrices. More precisely, it was proven by Johannson ($\beta = 2$) and Johnstone ($\beta = 1$) that[1] for large $N$ and for $c \leq 1$ [41; 59]

$$\lambda_{\max} = \left(\frac{1}{\sqrt{c}} + 1\right)^2 N + c^{1/6}\left(\frac{1}{\sqrt{c}} + 1\right)^{4/3} N^{1/3}\chi \tag{3.1.5}$$

where the random variable $\chi$ converges in distribution to $F_\beta(x)$. Note, however, that the scale of *typical* fluctuations around the average value $x_+(c)N$ (upper edge of the Marčenko-Pastur distribution) is $\sim \mathcal{O}(N^{1/3})$ in this case: while in the Gaussian case the shape of the density of the largest eigenvalues becomes narrower as $N$ increases, in the Wishart-Laguerre case it gets broader. This prediction can be easily checked numerically.

In contrast with the *typical* and *narrow* fluctuations described by the Tracy-Widom distribution, an interest for the notion of *extreme value statistics* and atypical fluctuations arose very recently [40] in the context of Gaussian random matrices. For the general theory of large deviations in the case of uncorrelated random variables, the reader is referred to [80]. In the following section, we review motivations and results, whereas in the subsequent part of this chapter we apply

[1] No similar results appear to be rigorously known for $\beta = 4$.

the Coulomb gas approach and functional methods introduced in [40] to the case of Wishart-Laguerre random matrices.

## 3.2 Gaussian random matrices: large deviations of the maximum eigenvalue

Suppose that the following question is asked: given a $N \times N$ Gaussian random matrices, what is the probability $P_N$ that all its eigenvalues are positive (or negative)

$$P_N = \text{Prob}[\lambda_1 \geq 0, \ldots, \lambda_N \geq 0]? \tag{3.2.1}$$

Clearly, from the semicircle law one expects that on average half of the eigenvalues should be positive and half negative: hence, $P_N$ is presumably very tiny. How does $P_N$ behave for large $N$? This question came up recently in different contexts, such as string theory [81] and statistics of minima of a random polynomial [82] (for a more detailed account, see [40]).

A decay of the form $P_N \asymp \exp(-\beta\theta(0)N^2)$ had been anticipated for a number of years [83] in studies of the index (number of negative eigenvalues) of Gaussian matrices, where we use the notation $\asymp$ to mean precisely that $\lim_{N\to\infty}[-\log P_N/\beta N^2] = \theta(0)$.

However, a precise determination of $\theta(0)$ was provided only recently by Dean and Majumdar [40]. Their method is based on a combination of the standard Coulomb gas analogy (introduced in the last chapter) and functional methods. This technique has been since exploited in many other problems in statistical physics [42; 84; 85; 86].

In the following section, we are going to provide a detailed treatment of a similar but slightly more complicated problem, where the very same technique can be applied, namely the issue of large deviations of the maximum eigenvalue in Wishart random matrices [42]. In section 5.4, the same technique will be essential to provide large deviation formulas for distribution of physical quantities in the quantum transport problem.

## 3.3 Coulomb gas approach and functional methods for Wishart matrices

In the context of PCA (Principal Component Analysis) already mentioned in section 2.4.2, this *large deviation* issue arises quite naturally because one is there interested in getting rid of redundant data by the 'dimension reduction' technique and keeping only the principal part of the data in the direction of the eigenvector representing the maximum eigenvalue, as mentioned before. The 'dimension reduction' technique works efficiently only if the largest eigenvalue is much larger than the other eigenvalues. However, if the largest eigenvalue is comparable to the average eigenvalue $\langle\lambda\rangle$, the PCA technique is not very useful. Thus, the knowledge of large negative fluctuations of $\lambda_{\max}$ from its mean $\langle\lambda_{\max}\rangle \approx x_+(c)\,N$ provides useful information about the efficiency of the PCA technique.

The main purpose of this section is to provide a detailed exposition of exact analytical results for these large negative fluctuations of $\lambda_{\max}$ from its mean value [42]. Rigorous mathematical results about the asymptotics of the Airy-kernel determinant (i.e. the probability that the largest eigenvalue lies deep inside the Marčenko-Pastur sea) for the case $c = 1$ and $\beta = 2$ have been recently obtained [87]. Here we follow the Coulomb gas approach already introduced in section 2.3: the eigenvalues of a random matrix are interpreted as a fluid of charged interacting particles, for which we can use standard functional integration methods of statistical physics. This approach has been exploited in the context of the Wishart-Laguerre ensemble for the first time by Chen and Manning [88], who performed a detailed asymptotic analysis of the level spacing for general $\beta$ and determined the distribution of the two smallest eigenvalues in a certain double-scaling limit. Here we adopt this method for the maximum eigenvalue of the Wishart ensemble.

We show that for $c \leq 1$, the probability of large fluctuations to the left of the mean $\langle\lambda_{\max}\rangle \approx x_+(c)\,N$ behaves, for large $N$, as

$$\text{Prob}\left[\lambda_{\max} \leq t, N\right] \asymp \exp\left[-\frac{\beta}{2}N^2\Phi_-\left(\frac{x_+(c)\,N - t}{N};\, c\right)\right] \tag{3.3.1}$$

where $t \sim \mathcal{O}(N) \leq x_+(c)\,N$ is located deep inside the Marčenko-Pastur sea and $\Phi_-(x;c)$ is a certain *left* rate (sometimes also called large deviation) function

with $x$ being the main argument of the function and $c$ being a parameter. In this chapter, we compute the rate function $\Phi_-(x;c)$ explicitly. Knowing this function, it then follows that for large $N$

$$\text{Prob}\left[\lambda_{\max} \leq \langle\lambda\rangle = N/c, N\right] \asymp \exp(-\theta(c)N^2), \tag{3.3.2}$$

where the coefficient

$$\theta(c) = \frac{\beta}{2}\Phi_-\left(\frac{2}{\sqrt{c}}+1;\, c\right). \tag{3.3.3}$$

For example, for the case $c = 1$ ($M = N$), we show that

$$\theta(1) = \beta\left(\log 2 - \frac{33}{64}\right) = 0.177522\ldots\ \beta. \tag{3.3.4}$$

The corresponding result for the Anti-Wishart matrices ($M < N$) simply follows by exchanging $M$ and $N$. In this chapter, we focus only on the *left* large deviations of $\lambda_{\max}$. The corresponding probability of large fluctuations of $\lambda_{\max}$ to the *right* of the mean $\langle\lambda_{\max}\rangle$ was previously computed explicitly by Johansson [41].

As a byproduct of our analysis, we provide the general expression for the spectral density of a constrained Wishart ensemble of matrices whose eigenvalues are restricted to be smaller than a fixed barrier.

Our starting point is the joint distribution of eigenvalues of the Wishart ensemble in (2.4.7) with $n = 1/2$. Let $P_N(t)$ be the probability that the maximum eigenvalue $\lambda_{\max}$ is less than or equal to $t$. Clearly, this is also the probability that all the eigenvalues are less than or equal to $t$ and can be expressed as a ratio of two multiple integrals:

$$\begin{aligned} P_N(t) = \text{Prob}[\lambda_{\max} \leq t] = \frac{Z_1(t)}{Z_0} = \\ = \frac{\int_0^t \ldots \int_0^t d\lambda_1 \ldots d\lambda_N \exp(-\frac{\beta}{2}F[\vec{\lambda}])}{\int_0^\infty \ldots \int_0^\infty d\lambda_1 \ldots d\lambda_N \exp(-\frac{\beta}{2}F[\vec{\lambda}])} \end{aligned} \tag{3.3.5}$$

where:

$$F[\vec{\lambda}] = \sum_{i=1}^N \lambda_i - \left(1 + M - N - \frac{2}{\beta}\right)\sum_{i=1}^N \log\lambda_i - \sum_{j\neq k}\log|\lambda_j - \lambda_k| \tag{3.3.6}$$

Written in this form, $F$ mimics the free energy of a 2-d Coulomb gas of interacting particles confined to the positive half-line ($\lambda > 0$) and subject to an external

linear+logarithmic potential. The denominator in (3.3.5), which is simply a normalization constant, represents the partition function of a free or 'unconstrained' Coulomb gas over $\lambda \in [0, \infty)$. The numerator, on the other hand, represents the partition function of the same Coulomb gas, but with the additional constraint that the gas is confined inside the box $\lambda \in [0, t]$, i.e., there is an additional wall or infinite barrier at the position $\lambda = t$. We will refer to the numerator as the partition function of a 'constrained' Coulomb gas.

Note that in the Gaussian case, the external potential is harmonic over the whole real line ($V(\lambda) = \lambda^2/2$), while in the Wishart case, $V(\lambda) = \infty$ for $\lambda < 0$ (infinite barrier at $\lambda = 0$) and $V(\lambda) = \lambda - (1 + M - N - 2/\beta) \log \lambda$ for $\lambda > 0$ representing a linear+logarithmic potential. By comparing the external potential and the logarithmic interaction term, it is easy to see that while for Gaussian ensembles a typical eigenvalue scales as $\lambda \sim \sqrt{N}$ for large $N$, for the Wishart case it scales as $\lambda \sim N$ (as already remarked in section 2.4.2).

After defining the *constrained charge density*:

$$\hat{\varrho}_N(\lambda) := \varrho_N(\lambda; t) = \frac{1}{N} \sum_{i=1}^{N} \delta(\lambda - \lambda_i)\theta(t - \lambda) \tag{3.3.7}$$

and taking into account the following trivial identity for a generic function $h(x)$:

$$\sum_{i=1}^{N} h(\lambda_i) = N \int d\lambda \hat{\varrho}_N(\lambda) h(\lambda) \tag{3.3.8}$$

we may express, for large $N$, the partition function $Z_1(t)$ in (3.3.5) as a functional integral [40]:

$$\begin{aligned} Z_1(t) \propto \int \mathcal{D}[\hat{\varrho}_N] \exp \Bigg\{ -\frac{\beta}{2} \Bigg[ & N \int_0^t \hat{\varrho}_N(\lambda) \lambda d\lambda \\ & - N(M - N + 1 - 2/\beta) \int_0^t \hat{\varrho}_N(\lambda) \log \lambda d\lambda \\ & - N^2 \int_0^t \int_0^t \hat{\varrho}_N(\lambda) \hat{\varrho}_N(\lambda') \log |\lambda - \lambda'| d\lambda d\lambda' \\ & - N \int_0^t \hat{\varrho}_N(\lambda) \log[\hat{\varrho}_N(\lambda)] d\lambda \Bigg] \Bigg\} \end{aligned} \tag{3.3.9}$$

where the last entropic term is of order $\mathcal{O}(N)$ and arises from the change of variables in going from an ordinary multiple integral to a functional integral, $[\{\lambda_i\}] \to [\hat{\varrho}_N(\lambda)]$ [40].

The constrained charge density $\hat{\varrho}_N(\lambda)$ obviously satisfies $\hat{\varrho}_N(\lambda) = 0$ for $\lambda > t$ and $\int_0^t \hat{\varrho}_N(\lambda)d\lambda = 1$.

Since we are interested in fluctuations of $\sim \mathcal{O}(N)$, it is convenient to work with the rescaled variables $\lambda = xN$ and $\zeta = t/N$. It is also reasonable to assume that for large $N$, the charge density scales accordingly as $\hat{\varrho}_N(\lambda) = N^{-1}\hat{f}(\lambda/N)$, so that $\hat{f}(x) = 0$ for $x > \zeta$ and $\int_0^\zeta \hat{f}(x)dx = 1$.

In terms of the rescaled variables, the energy term in (3.3.9) becomes proportional to $N^2$ while the entropy term ($\sim \mathcal{O}(N)$) is subdominant in the large $N$ limit. Eventually we can write:

$$Z_1(\zeta) \propto \int \mathcal{D}[\hat{f}] \exp\left(-\frac{\beta}{2}N^2 S[\hat{f}(x);\zeta] + \mathcal{O}(N)\right) \tag{3.3.10}$$

where:

$$\begin{aligned} S[\hat{f}(x);\zeta] = &\int_0^\zeta x\hat{f}(x)dx - \alpha\int_0^\zeta \hat{f}(x)\log(x)dx + \\ &- \int_0^\zeta\int_0^\zeta \hat{f}(x)\hat{f}(x')\log|x-x'|dxdx' + \\ &+ C_1\left[\int_0^\zeta \hat{f}(x)dx - 1\right] \end{aligned} \tag{3.3.11}$$

where we have introduced the parameter $\alpha = \frac{1-c}{c}$ for later convenience. In (3.3.11), $C_1$ is a Lagrange multiplier enforcing the normalization of $\hat{f}$.

For large $N$ we can evaluate the leading contribution to the action (3.3.11) by the method of steepest descent. This gives:

$$Z_1(\zeta) \propto \exp\left[-\frac{\beta}{2}N^2 S[\hat{f}^\star(x);\zeta] + \mathcal{O}(N)\right] \tag{3.3.12}$$

where $\hat{f}^\star$ is the solution of the stationarity condition:

$$\frac{\delta S[\hat{f}(x);\zeta]}{\delta\hat{f}(x)} = 0 \tag{3.3.13}$$

This gives for $0 \leq x \leq \zeta$:

$$x - \alpha \log x + C_1 = 2 \int_0^\zeta \hat{f}(x') \log |x - x'| dx' \tag{3.3.14}$$

Differentiating (3.3.14) once with respect to $x$ gives:

$$\frac{1}{2} - \frac{\alpha}{2x} = \mathcal{P} \int_0^\zeta \frac{\hat{f}(x')}{x - x'} dx' \qquad 0 \leq x \leq \zeta \tag{3.3.15}$$

where $\mathcal{P}$ denotes the Cauchy principal part.

Finding a solution to the integral equation (3.3.15) is the main technical task. The next two subsections are devoted to the solution of (3.3.15), first for the special case $c = 1$ and then for $0 < c < 1$. We remark that the solution of (3.3.15) gives the average density of eigenvalues in the limit of large $N$ for an ensemble of Wishart matrices whose rescaled eigenvalues are restricted to be smaller than the barrier $\zeta$. We will refer to $\hat{f}(x)$ as the *constrained* spectral density.

Before proceeding to the technical points, it may be informative to first summarize the results for the constrained spectral density $\hat{f}(x)$ in the general $0 < c \leq 1$ case. The most general form is:

$$\hat{f}(x) = \frac{1}{2\pi} \frac{\sqrt{x - L_1(c, \zeta)}}{\sqrt{\zeta - x}} \left[ \frac{A(c, \zeta) - x}{x} \right] \tag{3.3.16}$$

where $L_1$ is the lower edge of the spectrum and $A$ is related to the mutual position of the barrier with respect to the lower edge. In the following table, we schematically disclose the values for $L_1$ and $A$ in the different regions of the $(c, \zeta)$ plane:

| | $c = 1$ | $0 < c < 1$ |
|---|---|---|
| $0 < \zeta < x_+$ (barrier *effective*) | $L_1 = 0$ (3.4.4) | $L_1$: see (3.4.22) |
| | $A = \frac{\zeta+4}{2}$ (3.4.4) | $A = \alpha \sqrt{\frac{\zeta}{L_1}} > \zeta$ (3.4.16) |
| $\zeta \geq x_+$ (barrier *ineffective*) | $L_1 = 0$ | $L_1 = x_-$ |
| | $A = \zeta = 4$ | $A = \zeta = x_+$ |

Table 3.1: Values of $L_1$ and $A$ in the different regions of the $(c, \zeta)$ plane.

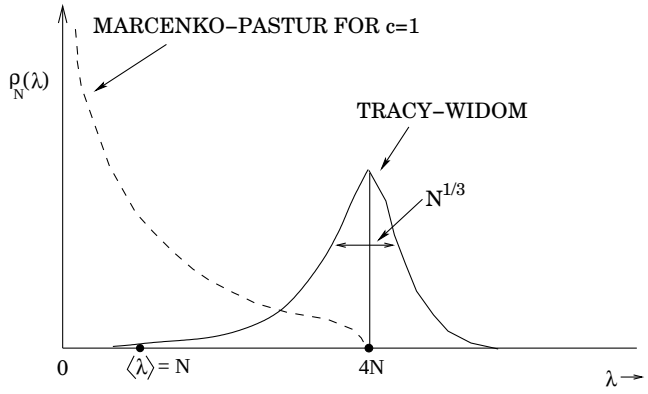


Figure 3.2: The dashed line shows schematically the Marčenko-Pastur form of the average density of states for $c = 1$. The average eigenvalue for $c = 1$ is $\langle\lambda\rangle = N$. For $c = 1$, the largest eigenvalue is centered around its mean $\langle\lambda_{\max}\rangle = 4N$ and fluctuates over a scale of width $N^{1/3}$. The probability of fluctuations on this scale is described by the Tracy-Widom distribution (shown schematically).

The support of $\hat{f}$ is:

$$L_1(c,\zeta) \leq x \leq \min[\zeta, A(c,\zeta)] \tag{3.3.17}$$

At the lower edge of the support $L_1(c,\zeta)$, the density vanishes *unless* $c = 1$, in which case it diverges as $\sim 1/\sqrt{x}$.

At the upper edge of the support, according to the value of the minimum ($\zeta$ or $A(c,\zeta)$) in (3.3.17) the density can respectively diverge as $\sim 1/\sqrt{\zeta - x}$ or vanish.

Note that the unconstrained Marčenko-Pastur law (2.4.8) is recovered from (3.3.16) when the barrier is ineffective, i.e. $\zeta \geq x_+$.

## 3.4 Gaussian decay of $\mathcal{O}(N)$ fluctuations and exact results for the rate function

### 3.4.1 The case $c = 1$

In this case, the support of the unconstrained spectral density is $(0, 4]$ and the Marčenko-Pastur law prescribes an inverse square root divergence at $x = 0$ . Furthermore, the density vanishes at $x = 4$ (see Fig. (3.2)).

In the constrained case, the barrier at $\zeta$ is only effective when $0 \leq \zeta \leq 4$. When the barrier crosses the point $\zeta = 4$ from below, the density shifts back again to the unconstrained case.

The integral equation for $\hat{f}(x)$ (3.3.15) becomes:

$$\frac{1}{2} = \mathcal{P}\int_0^\zeta \frac{\hat{f}(x')}{x - x'}dx' \qquad 0 \leq x \leq \zeta \tag{3.4.1}$$

The general solution of equations of the type:

$$\mathcal{P}\int_0^\zeta \frac{\hat{f}(x')}{x - x'}dx' = g(x) \tag{3.4.2}$$

is given by Tricomi's theorem[1] [52]:

$$\hat{f}(x) = \frac{1}{\pi^2\sqrt{x(\zeta - x)}}\left[\mathcal{P}\int_0^\zeta \sqrt{\omega(\zeta - \omega)}\frac{g(\omega)}{\omega - x}d\omega + B\right] \tag{3.4.3}$$

where $B$ is an arbitrary constant. After putting $g(\omega) = 1/2$ in (3.4.3) and determining $B$ by the normalization condition $\int_0^\zeta \hat{f}(x)dx = 1$ we finally get:

$$\hat{f}(x) = \frac{1}{2\pi\sqrt{x(\zeta - x)}}\left[\frac{\zeta}{2} + 2 - x\right] \qquad 0 \leq x \leq \zeta \tag{3.4.4}$$

A plot of this charge density for two values of the barrier $\zeta$ is given in Fig. 3.3.

In summary, the average density of states with a barrier at $\zeta$ is given by:

$$\hat{f}(x) = \begin{cases} \frac{1}{2\pi\sqrt{x(\zeta - x)}}\left[\frac{\zeta}{2} + 2 - x\right] & 0 \leq \zeta \leq 4 \\ \frac{1}{2\pi}\sqrt{\frac{4-x}{x}} & \zeta \geq 4 \end{cases} \tag{3.4.5}$$

[1] We will make an extensive use of this formula throughout this thesis.

Thus, for all $\zeta > 4$, the solution sticks to the $\zeta = 4$ case. Note that both cases in (3.4.5) can be obtained from the general formula (3.3.16).

Now we can substitute (3.4.5) back into (3.3.14) to find the value of the multiplier $C_1$ and eventually evaluate the action $S[f^\star(x);\zeta]$ (3.3.11) explicitly for $0 \leq \zeta \leq 4$:

$$S(\zeta) := S[\hat{f}^\star(x);\zeta] = 2\log 2 - \log\zeta + \frac{\zeta}{2} - \frac{\zeta^2}{32} \tag{3.4.6}$$

From (3.3.12), we get $Z_1(\zeta) \asymp \exp(-\beta N^2 S(\zeta)/2)$. For the denominator, $Z_0 = Z_1(\zeta = \infty) = Z_1(\zeta = 4) \asymp \exp(-\beta N^2 S(4)/2)$, where we have used the fact that the solution for any $\zeta > 4$ (e.g., when $\zeta = \infty$) is the same as the solution for $\zeta = 4$. Thus, eventually the probability $P_N(t)$ (3.3.5) decays for large $N$ as:

$$\begin{aligned} P_N(t) = \frac{Z_1(t)}{Z_0} &\asymp \exp\left\{-\frac{\beta}{2}N^2[S(\zeta) - S(4)]\right\} \\ &= \exp\left\{-\frac{\beta}{2}N^2\Phi_-\left(\frac{4N-t}{N};1\right)\right\} \end{aligned} \tag{3.4.7}$$

where the rate function is given by

$$\Phi_-(x;1) = \begin{cases} 2\log 2 - \log(4-x) - \frac{x}{4} - \frac{x^2}{32} & x \geq 0 \\ 0 & x \leq 0 \end{cases} \tag{3.4.8}$$

and is plotted in fig.3.4.

We now turn to the original problem of determining the probability of the following extremely rare event, i.e. that all the eigenvalues happen to lie below the mean value (see (2.4.9) for $n = 1/2$ and $c = 1$) $\langle\lambda\rangle = \int_0^{4N} \lambda\rho_N(\lambda)d\lambda = N$. Starting from (3.4.7), this is easily computed by putting the barrier at the mean value $t = N$, i.e., $\zeta = 1$. We then get for large $N$:

$$\text{Prob}\left[\lambda_{\max} \leq \langle\lambda\rangle = N, N\right] \asymp \exp[-\theta(1)N^2] \tag{3.4.9}$$

where

$$\begin{aligned} \theta(1) &= \frac{\beta}{2}\Phi_-\left(3;1\right) \\ &= \beta\left(\log 2 - \frac{33}{64}\right). \end{aligned} \tag{3.4.10}$$

Since we are calculating here the probability of negative fluctuations of $\lambda_{\max}$ of $\mathcal{O}(N)$ to the left of the mean $\langle\lambda_{\max}\rangle = x_+(c)N$, when the argument of the left

rate function $\Phi_-(x;1)$ is very small (i.e., for fluctuations $\ll \mathcal{O}(N)$), (3.4.7) should smoothly match the left tail of the Tracy-Widom distribution that describes fluctuations of order $\sim \mathcal{O}(N^{1/3})$ to the left of the mean $\langle \lambda_{\max} \rangle = x_+(c)N$. Indeed, from (3.4.8) as $x \to 0$:

$$\Phi_-(x;1) \sim \frac{x^3}{192} \tag{3.4.11}$$

and substituting (3.4.11) in (3.4.7) we get, for fluctuations $\ll \mathcal{O}(N)$ to the left of the mean,

$$\begin{aligned} P_N(t) &\asymp \exp\left[-\frac{\beta}{384} N^2 (4 - t/N)^3\right] \\ &= \exp\left[-|\chi|^3/12\right] \end{aligned} \tag{3.4.12}$$

where $\chi = (t - 4N)/(2^{4/3}N^{1/3})$. This coincides with Johansson's result [41] for the Tracy-Widom fluctuations in (3.1.5) for $c = 1$ and indeed we recover the left tail of the Tracy-Widom distribution.

### 3.4.2 The case $0 < c < 1$

Our approach is very similar to the previous case. However, some additional technical subtleties, which we emphasize, arise in this case.

As in the unconstrained case, we expect a lower bound $L_1 \equiv L_1(c, \zeta)$ to the support of the constrained $\hat{f}(x)$. The parameter $L_1$ will be determined later through the normalization condition for $\hat{f}(x)$.

It is convenient to reformulate (3.3.15) in terms of the new variable $y = x - L_1$, measuring the distance with respect to the lower edge of the support, where $\hat{f}(x)$ is assumed to vanish.

Equation (3.3.15) then reads:

$$\frac{1}{2} - \frac{\alpha}{2(y + L_1)} = \mathcal{P} \int_0^L \frac{\tilde{f}(y')}{y - y'} dx' \qquad 0 \le y \le L \tag{3.4.13}$$

where we have denoted $L = \zeta - L_1$ and $\tilde{f}(y) \equiv \hat{f}(y + L_1)$.

The general solution of (3.4.13) in this case is:

$$\tilde{f}(y) = \frac{1}{\pi\sqrt{y(L - y)}} \left[-\frac{y}{2} - \frac{\alpha}{2} \frac{\sqrt{L_1(L + L_1)}}{y + L_1} + B'\right] \tag{3.4.14}$$

and the constant $B'$ is determined by the condition $\tilde{f}(y=0)=0$. Thus we get:

$$\tilde{f}(y) = \frac{\sqrt{y}}{2\pi\sqrt{L-y}}\left[\frac{A-L_1-y}{y+L_1}\right] \tag{3.4.15}$$

where:

$$A \equiv A(c,\zeta) = \alpha\sqrt{\zeta/L_1} \tag{3.4.16}$$

Note that everything is expressed in terms of the only still unknown parameter $L_1$.

From (3.4.15) we can infer two kinds of possible behaviors for $\tilde{f}(y)$ due to the competing effects of the singularity for $y \to L$ (where the denominator vanishes) and the suppression for $y \to A - L_1$ (where the numerator vanishes).

Thus, depending on which of the following two conditions applies once we have put the barrier at $\zeta$:

$$\begin{aligned} &A(c,\zeta) - L_1(c,\zeta) > L(c,\zeta) \to \sqrt{L_1(c,\zeta)\zeta} < \alpha \qquad \text{(I)} \\ &A(c,\zeta) - L_1(c,\zeta) < L(c,\zeta) \to \sqrt{L_1(c,\zeta)\zeta} > \alpha \qquad \text{(II)} \end{aligned} \tag{3.4.17}$$

$\tilde{f}$ can diverge at $y = L$ or vanish at $A - L_1$ respectively. In (3.4.17) we have restored the functional dependence for clarity.

This is a subtle point because, given the barrier at $\zeta$, we cannot determine *a priori* which of the previous conditions holds. In fact, $L_1(c,\zeta)$ should be determined *a posteriori* separately for each case from the normalization condition:

$$\int_0^L \tilde{f}(y)dy = 1 \tag{3.4.18}$$

Once this is done, it turns out that the conditions (3.4.17) can be reformulated in terms of the position of the barrier $\zeta$ in the following much simpler way:

$$\begin{aligned} 0 < \zeta < x_+ \quad &\text{(I)} \\ \zeta \geq x_+ \quad &\text{(II)} \end{aligned} \tag{3.4.19}$$

We summarize here the final results in the two cases.

#### 3.4.2.1 Case I. $0 < \zeta < x_+$

The normalization condition (3.4.18) leads to the following cubic equation for $w \equiv w(c,\zeta) = \sqrt{L_1(c,\zeta)}$:

$$w^3 - [2(2+\alpha)+\zeta]w + 2\alpha\sqrt{\zeta} = 0 \tag{3.4.20}$$

which has always three real solutions, one negative ($w_0$) and two positive:

$$w_k(c,\zeta) = \frac{2p}{3\varrho^{1/3}} \cos\left(\frac{\theta + 2k\pi}{3}\right) \qquad k = 0,1,2 \tag{3.4.21}$$

where:

$$\begin{cases} p &= -[2(2+\alpha)+\zeta] \\ q &= 2\alpha\sqrt{\zeta} \\ B &= -\left(\frac{q^2}{4} + \frac{p^3}{27}\right) \\ \varrho &= \sqrt{-p^3/27} \\ \theta &= \arctan\left(\frac{2\sqrt{B}}{q}\right) \end{cases}$$

Note that $w_2 < w_1$. By considering the limiting behavior as $\zeta$ approaches 4, we conclude that the right root to be chosen is $w_2(c,\zeta)$. Thus:

$$L_1(c,\zeta) = w_2^2(c,\zeta) \tag{3.4.22}$$

Finally, we can write down the full constrained unshifted spectral density as:

$$\hat{f}(x) = \frac{1}{2\pi} \frac{\sqrt{x - L_1(c,\zeta)}}{\sqrt{\zeta - x}} \left[\frac{A(c,\zeta) - x}{x}\right] \tag{3.4.23}$$

valid for $L_1(c,\zeta) \le x \le \zeta$ where $L_1(c,\zeta)$ is given by (3.4.22) and $A(c,\zeta)$ by (3.4.16).

A plot of $\hat{f}(x)$ for $c = 0.1$ and $\zeta = 14$ is given in fig. 3.5. In this case, $L_1(c,\zeta) \approx 4.60084$ and $A(c,\zeta) \approx 15.6996$.

#### 3.4.2.2 Case II. $\zeta \ge x_+$

In this case, the barrier is immaterial and we should recover the unconstrained Marčenko-Pastur distribution. The support of $\tilde{f}(y)$ is $[0, A - L_1]$ and this implies that we can safely put $L = A - L_1$ in (3.4.18).

The integration can be performed and coming back to the unshifted spectral density $\hat{f}(x)$ we get:

$$\hat{f}(x) = \frac{1}{2\pi}\frac{\sqrt{x-L_1}\sqrt{L_2-x}}{x} \tag{3.4.24}$$

valid for $L_1 \leq x \leq L_2$ where:

$$\begin{cases} L_1 &= x_- \\ L_2 &= L_1 + L = x_+ \end{cases} \tag{3.4.25}$$

which is the unconstrained Marčenko-Pastur distribution, as it should.

It is interesting to evaluate the limit $c \to 1^-$ in (3.4.23) and (3.4.24) in order to recover the result (3.4.5) in subsection 3.4.1. The case of equation (3.4.24) is obvious. For the other, it is a matter of simple algebra to show that:

$$\lim_{c\to 1^-} L_1(c,\zeta) = 0 \tag{3.4.26}$$

$$\lim_{c\to 1^-} A(c,\zeta) = (\zeta+4)/2 \tag{3.4.27}$$

so that (3.4.23) matches (3.4.5).

Furthermore, Cases I and II should match smoothly as $\zeta$ hits precisely the limiting value $x_+$. This corresponds to $A(c,\zeta) \equiv \zeta \to A(c,x_+) \equiv x_+$. It is again straightforward to check that this last condition implies $L_1(c,x_+) \equiv x_-$ so that (3.4.23) recovers (3.4.24).

The interesting case for computing large fluctuations is Case I. One can insert (3.4.23) into (3.3.11) in order to evaluate (3.3.12). It turns out that the integrals involved can be analytically solved in terms of derivatives of hypergeometric functions, but a more explicit formula is derived in Appendix A. We give here a plot of the rate function $\Phi_-(x;c)$ that describes the large fluctuations of $\mathcal{O}(N)$ to the left of the mean $\langle\lambda_{\max}\rangle = x_+(c)N$:

$$\begin{aligned} P_N(t) = \frac{Z_1(t)}{Z_0} &\asymp \exp\left\{-\frac{\beta}{2}N^2[S(\zeta)-S(x_+)]\right\} \\ &= \exp\left\{-\frac{\beta}{2}N^2\Phi_-\left(x_+ - \frac{t}{N};c\right)\right\} \end{aligned} \tag{3.4.28}$$

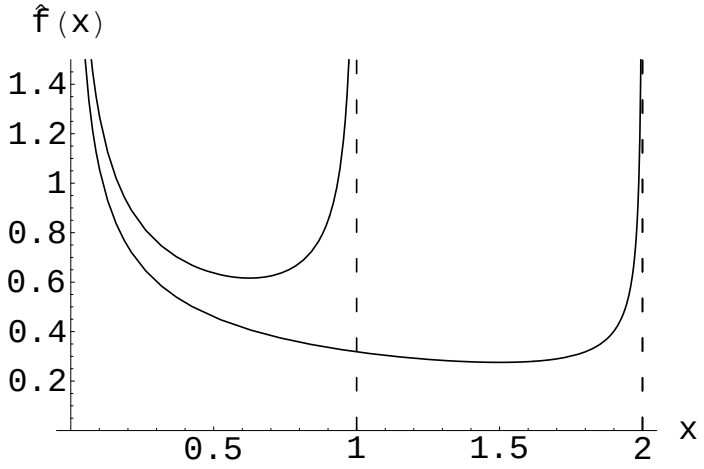


Figure 3.3: Constrained spectral density $\hat{f}(x)$ for the barrier at $\zeta = 1$ and $\zeta = 2$

The plot is given in Fig. 3.6 for several values of $c$ approaching 1. The limiting case $\Phi_-(x;1)$ (3.4.8) is also plotted.

We can now compute to leading order the probability that all the eigenvalues are less than the mean value $\langle\lambda\rangle = N/c$. This amounts to putting the barrier at $t = N/c$ in (3.4.28), which gives $\Phi_-\left(\frac{2}{\sqrt{c}}+1;c\right)$. Several numerical values are given in the following table.

| $c$ | $\Phi_-\left(\frac{2}{\sqrt{c}}+1;c\right)$ |
|---|---|
| 0.1 | 0.475802 |
| 0.2 | 0.449162 |
| 0.4 | 0.414592 |
| 0.6 | 0.390245 |
| 0.8 | 0.37104 |
| 0.95 | 0.358805 |
| 1 | 0.355044 |

Table 3.2: Some values of the rate function (see text for further explanation).

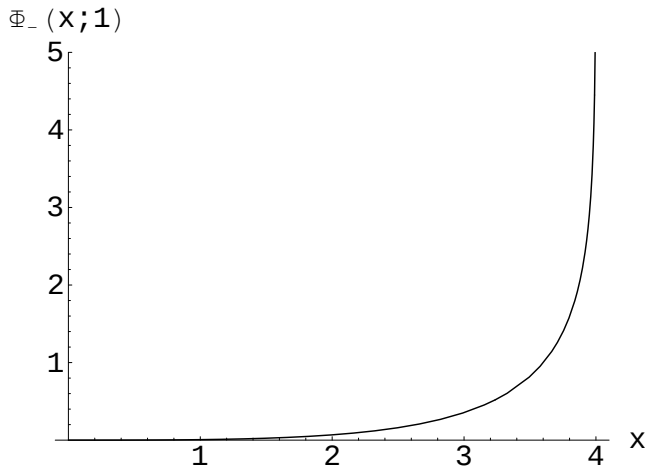


Figure 3.4: Rate function $\Phi_-(x;1)$.

## 3.5 Numerical checks

The results in the previous sections have been numerically checked on samples of hermitian matrices ($\beta = 2$) up to $N = 30$, $M = 300$ and the agreement with the analytical results is already excellent. We describe in this section the numerical methods and results.

A direct sampling of Wishart matrices up to those sizes is computationally very demanding. We applied the following much faster technique, suggested in [47].

Let $L_\beta = B_\beta B_\beta^T$ be the tridiagonal matrix corresponding to:

$$B_\beta \sim \begin{pmatrix} \chi_{2a} & & & \\ \chi_{\beta(N-1)} & \chi_{2a-\beta} & & \\ & \ddots & \ddots & \\ & & \chi_\beta & \chi_{2a-\beta(N-1)} \end{pmatrix} \tag{3.5.1}$$

$B_\beta$ is a square $N \times N$ matrix with nonzero entries on the diagonal and subdiagonal and $a = (\beta/2)M$. The nonzero entries $\chi_k$ are independent random variables obtained from the square root of a $\chi^2$-distributed variable with $k$ degrees of freedom. It has been proved in [47] that $L_\beta$ has the same joint probability distribution of eigenvalues as (2.4.7) for $n = 1/2$. Thus, as far as we are interested in eigenvalue

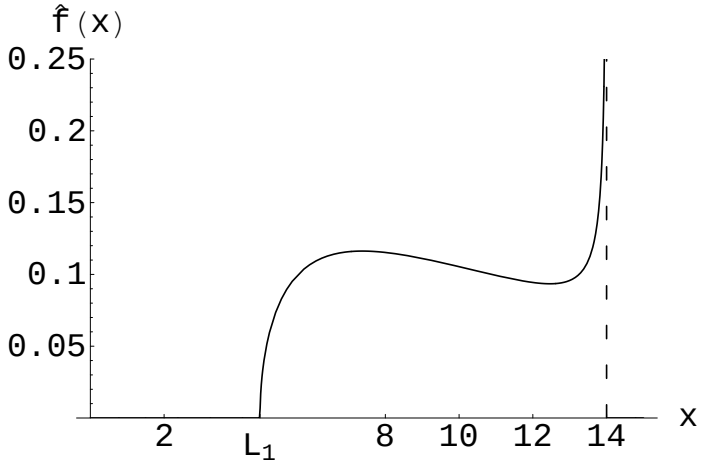


Figure 3.5: Constrained spectral density $\hat{f}(x)$ for $c = 0.1$ and $\zeta = 14$.

properties, we can use the $L_\beta$ ensemble instead of the original Wishart one. This makes the diagonalization process much faster due to the tridiagonal structure of the matrices $L_\beta$.

We report the following four plots: the first two (fig. 3.7 and 3.8) are for the case $c = 1$ and the last two (fig. 3.9 and 3.10) for the case $c = 0.1$.

In fig. 3.7, we plot the histogram of normalized eigenvalues $\lambda/2N$ for an initial sample of $3 \times 10^5$ hermitian matrices ($\beta = 2$, $N = M = 30$), such that matrices with $\lambda_{\max}/2N > \zeta$ are discarded. The barrier is located at $\zeta = 3$. On top of it we plot the theoretical distribution (3.4.5).

In fig. 3.9, we do the same but in the case $N = 10, M = 100$. The barrier is located at $\zeta = 14$. The theoretical distribution is now taken from (3.4.23).

To obtain the plots in fig. 3.8 and 3.10, we generate $\approx 5 \times 10^5$ $L_2$ matrices for different values of $N = 7 \to 30$ (or 15). The parameters $(c, \zeta)$ are kept fixed to the value $(1, 3)$ for fig. 3.8 ($x_+ = 4$) and $(0.1, 14)$ for fig. 3.10 ($x_+ \approx 17.32$). The constraining capability of those barriers can be estimated by the ratio $\kappa(c, \zeta) = (x_+ - \zeta)/(x_+ - x_-)$, corresponding to the window of forbidden values for the largest eigenvalue. We get $\kappa(1, 3) = 0.25$ and $\kappa(0.1, 14) \approx 0.26$, to be compared with the values of $\kappa(c, \zeta) = (2 + \sqrt{c})/4$ for the barrier at the mean value $\zeta = 1/c$, which would give respectively $\kappa = 0.75$ and $\kappa \approx 0.58$. This relative mildness

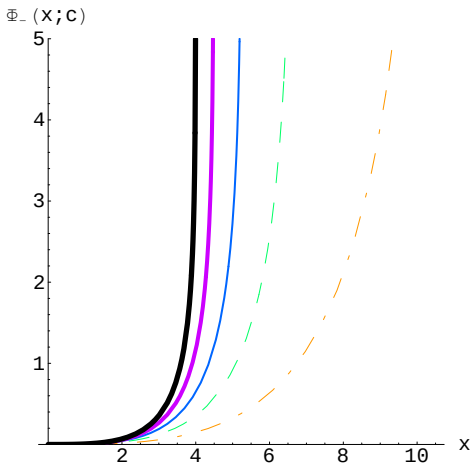


Figure 3.6: Rate function $\Phi_-(x;c)$ for the following values (from left to right) of $c = 1, 0.8, 0.6, 0.4, 0.2$. See also Figure 3.4.

of the constraint allows to get a much more reliable and faster statistics in the simulations.

For each value of $N$, we determine the empirical frequency $r(N)$ of constrained matrices as the ratio between the number of matrices whose largest rescaled eigenvalue is less than $\zeta$ and the total number of samples ($5\times10^5$). The logarithm of $r(N)$ vs. the size $N$ is then naturally fitted by a parabola $aN^2+bN+\hat{c}$ to test the prediction for $a$ in formulas (3.4.7) and (3.4.28).

The best values for the coefficient $a$ of the leading term are estimated as $-0.006153$ ($c=1$) and $-0.0357$ ($c=0.1$), to be compared respectively with the theoretical prediction $\Phi_-(1;1) \approx -0.006432$ and $\Phi_-(x_+-14;0.1) \approx -0.03666$. Despite the relatively small sizes and the $\mathcal{O}(N)$ corrections, the agreement is already good.

## 3.6 Summary and outlook

In this chapter, we have studied the probability of atypically large negative fluctuations (with respect to the mean) of the largest eigenvalue $\lambda_{\max}$ of a random Wishart matrix. The standard Coulomb gas analogy for the joint probability

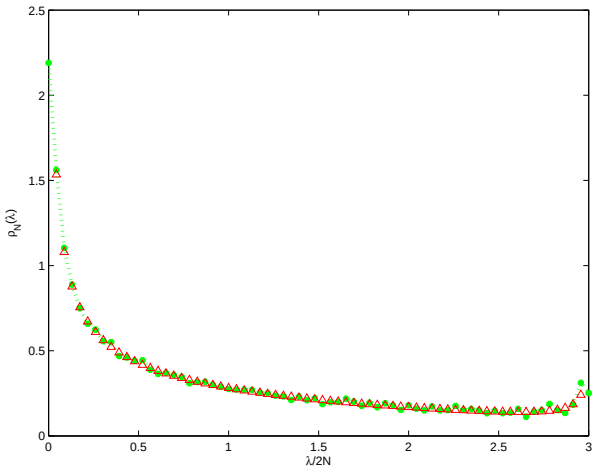


Figure 3.7: Constrained spectral density $\hat{\varrho}_N(\lambda)$ for $N = M = 30$. The barrier is at $\zeta = 3$. In dotted green the histogram of rescaled eigenvalues over an initial sample of $3 \times 10^5$ matrices ($\beta = 2$). In triangled red the theoretical distribution.

distribution of eigenvalues allows to use the tools of statistical physics, such as the functional integral method evaluated for large $N$ by the method of steepest descent. Using these tools, we have analytically computed the probability of large deviations of $\lambda_{\max}$ to the left of its mean. In particular, the main motivation was to compute the probability of a rare event: all eigenvalues are less than the average $\langle\lambda\rangle = N/c$. This implies that the largest eigenvalue itself is less than $\langle\lambda\rangle = N/c$. This question is relevant in estimating the efficiency of the 'principal components analysis' method used in multivariate statistical analysis of data. Our main result is to show that, to leading order in $N$, this probability decays as $\sim \exp[-\frac{\beta}{2}N^2\Phi_-(\frac{2}{\sqrt{c}}+1;c)]$, where $\Phi_-(x;c)$ is a rate function that we have explicitly computed. The quadratic, instead of linear, $N$-dependence of the exponential reflects the eigenvalue correlations.

Furthermore, our method allows us to determine exactly the functional form of the constrained spectral density, i.e., the average charge density of a Coulomb gas constrained to be within a finite box $\lambda \in [0, t]$.

All the analytical results are in excellent agreement with the numerical simulations on samples of hermitian matrices up to $N = 30$, and the estimates of the

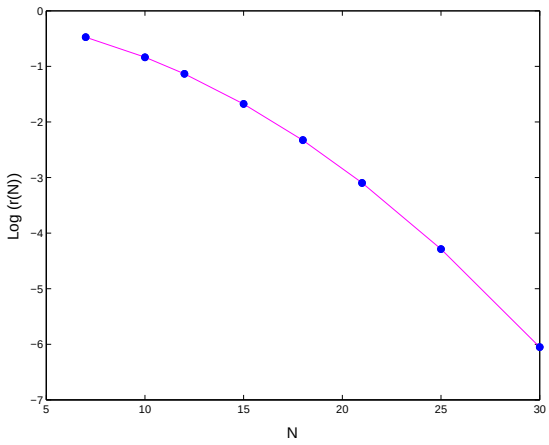


Figure 3.8: Natural logarithm of the probability that all the rescaled eigenvalues are less than $\zeta = 3$ vs. $N$ for the case $c = 1$ ($x_+ = 4$). The data points are fitted with a parabola (solid line).

large deviation prefactor are already good even for $N \sim 15$.

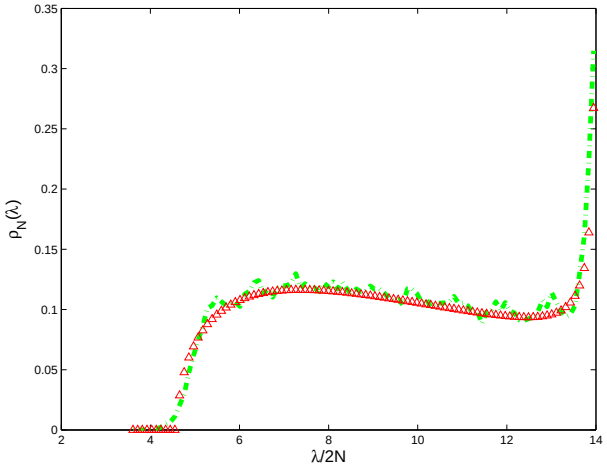


Figure 3.9: Constrained spectral density $\hat{\varrho}_N(\lambda)$ for $N = 10$, $M = 100$ ($c = 0.1$). The barrier is at $\zeta = 14$. In dash-dotted green the histogram of rescaled eigenvalues over an initial sample of $5 \times 10^5$ matrices ($\beta = 2$). In triangled red the theoretical distribution.

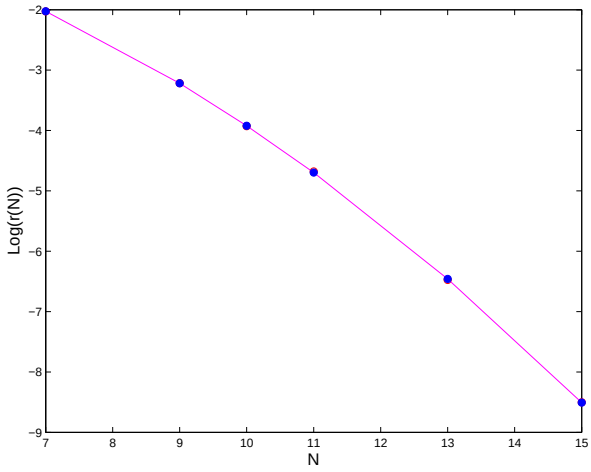


Figure 3.10: Natural logarithm of the probability that all the rescaled eigenvalues are less than $\zeta = 14$ vs. $N$ for the case $c = 0.1$ ($x_+ \approx 17.32$). The data points are fitted with a parabola (solid line).

*There are sadistic scientists who hurry to hunt down errors instead of establishing the truth.*

MARIE CURIE

# Chapter 4

# Deformations of Wishart-Laguerre ensembles

## 4.1 Motivations

In this Chapter, we introduce and solve exactly a one-parameter deformation of the standard Wishart-Laguerre (WL) ensemble for all three $\beta$ classes. What is the motivation to further generalize WL ensembles? In the finance and risk management domain, the empirical covariance of a set of $N$ assets over a temporal window of size $M$ has been under scrutiny for some time [90; 91; 92], and its eigenvalues were shown to be distributed in reasonably good agreement with the Marčenko-Pastur (MP) law, as if they were originated by a completely uncorrelated data series. However, the same analysis repeated by several groups [93; 94; 95] on different data sets have shown that either the part of the spectrum corresponding to extremely low eigenvalues - the most interesting for portfolio selections - or the fat tails are not reproduced by this crude approach. This has led to the appearance of more sophisticated models [95; 96; 97], e.g. the multivariate student distribution where the variance of each matrix entry becomes a random variable. Another deformation of the WL ensemble has been introduced in [98] where sparse matrices $\mathcal{X}$ were considered. This setting has many applications in communication theory and in complex networks (namely in the study of spectral properties of adjacency matrices). All these generalizations lead to a deformation of the MP law, and thus lie outside the WL class. However, the

lack of invariance in such models generally spoils the complete solvability for all correlations functions.

Conversely, a generalized model with power-law tails which is exactly solvable in principle appeared in [97]. However, the analysis in [97] was restricted to the macroscopic spectral density, whereas many more interesting results, and ultimately a complete solution of the model can be obtained. This goal is achieved by exploiting techniques and results introduced in previous works, where the Wigner-Dyson (WD) class was generalized using non-standard entropy maximization and super-statistical approaches [37; 89].

We will follow these lines and provide a complete solution for all three $\beta$ of a generalized WL model with rotational invariance, with an emphasis on the issues of universality and complete integrability for all spectral correlations, both macroscopic and microscopic [43]. After a proper rescaling and normalization, our $N$-independent correlations depend only on a single parameter $\hat{\alpha}$, which controls the power-law decay. In the limit of a large parameter $\hat{\alpha} \gg 1$ we recover all standard WL correlations. For completeness, we also mention another generalization of WL which exploits a different direction. In [99] the unitary WL were generalized to display critical statistics.

This chapter is organized as follows. In the next section 4.2 we define our generalized WL ensembles as a one-parameter deformation, including a general polynomial potential $V$ for all three $\beta = 1, 2$ and 4. The general solution for finite-$N$ is given applying the method of (skew) orthogonal polynomials to an integral transform of the standard WL ensembles.

In the next section 4.3 we take the macroscopic large-$N$ limit for the special case of the confining potential $V(\lambda) = \lambda$. As already mentioned in chapter 2, 'macroscopic' refers to the smooth part of the spectrum, considering correlations on a distance large compared to the mean level-spacing. We re-derive a generalization of the semi-circle and MP spectral density, see refs. [37] and [97] respectively. As a new result we compute the average position of an eigenvalue and the position of a pseudo edge. The former leads to the correct scaling with $N$ and an $N$-independent generalized spectral density displaying a power-law decay.

Section 4.4 is devoted to the microscopic large-$N$ limit, where correlations on the order of the mean level-spacing are computed. Here we can use the known

universal WL results as an input to our model. In the case when the difference of the matrix dimension $M - N$ is kept finite the spectrum has a hard edge at the origin. In two subsections we compute its microscopic density there, generalizing the universal Bessel-law as well as the corresponding smallest eigenvalue distribution for all three $\beta$.

In section 4.5 the nearest neighbor spacing distribution in the bulk of the spectrum is computed using a Wigner's surmise at $N = 2$ for our generalized model. In the appendices B and C technical details are collected.

## 4.2 Definition of the model and finite-$N$ solution for general potential

The joint probability density of our generalized WL ensembles is defined as follows in terms of matrix elements

$$P_\gamma[\mathcal{X}]\, d\mathcal{X} \;\propto\; \left(1 + \frac{n\beta}{\gamma}\mathrm{Tr}V(\mathcal{X}^\dagger\mathcal{X})\right)^{-\gamma} d\mathcal{X} \tag{4.2.1}$$

where $\mathcal{X}$ is a matrix of size $M \times N$ with real, complex or quaternion real elements for the values $\beta = 1, 2$ or $4$, respectively. We define $M = N + \nu$ for later convenience, where $\nu \geq 0$ may be either finite or of order $\mathcal{O}(N)$ in the large-$N$ limit. The integration measure $d\mathcal{X}$ is defined by integrating over all independent matrix elements of $\mathcal{X}$ with a flat measure. Expectation values of an operator $\mathcal{O}$ (denoted by $\langle\mathcal{O}\rangle_\gamma$) are defined with respect to $P_\gamma$ in the usual sense.

The real positive parameter $\gamma$ is to be specified below, and we keep an additional variance-like parameter $n > 0$. The so-called potential $V$ is taken to be a polynomial of finite degree $d$, although some of the universal results we inherit from the WL ensembles are known to hold for a much larger class of functions.

The measure (4.2.1) is well-defined and integrable only if the following condition holds

$$\gamma d \;>\; \frac{\beta}{2}N(N+\nu) \tag{4.2.2}$$

This condition, which is derived in appendix B, can be seen when changing to radial coordinates for the matrix $\mathcal{X}^\dagger\mathcal{X}$, see e.g. [36]. In particular, the large-$N$

behavior of any spectral property cannot be taken for fixed $\gamma$, and a prescription about the way both quantities should approach infinity needs to be given, respecting the inequality eq. (4.2.2).

A similar model was introduced earlier generalizing the (non-chiral) Wigner-Dyson ensembles for a Gaussian potential [37], and a similar interplay between the deformation parameter $\gamma$ and the matrix size $N$ was observed.

In the limit of an infinite deformation parameter

$$\lim_{\gamma\to\infty} P_\gamma[\mathcal{X}] \;=\; \exp[-n\beta \mathrm{Tr} V(\mathcal{X}^\dagger\mathcal{X})] \;\equiv\; P[\mathcal{X}] \tag{4.2.3}$$

we recover the standard WL ensembles denoted by $P[\mathcal{X}]$.

The generalized ensembles can be related to the standard WL through the following integral representation:

$$(1+z)^{-\gamma} = \frac{1}{\Gamma(\gamma)} \int_0^\infty d\xi \; e^{-\xi} \; \xi^{\gamma-1} \; e^{-\xi z} \tag{4.2.4}$$

Inserting this into the definition eq. (4.2.1) we obtain

$$P_\gamma[\mathcal{X}] = \frac{1}{\Gamma(\gamma)} \int_0^\infty d\xi \; e^{-\xi} \; \xi^{\gamma-1} \exp\left[-\xi \, \frac{n\beta}{\gamma} \mathrm{Tr} V(\mathcal{X}^\dagger\mathcal{X})\right] \tag{4.2.5}$$

This relation is crucial to solve our generalized model both for finite- and large-$N$. The same trick was used for the generalization of the Gaussian ensembles introduced previously in [37]. In fact, a similar technique was employed much earlier in [36] when solving the fixed and restricted trace ensembles by writing them as integral transforms of the Gaussian ensembles.

An advantage of our model over some other generalizations of WL [95] is its invariance under orthogonal, unitary or symplectic transformations. In particular, for $\beta = 1$ Burda *et al.* [97] considered a very general family of probability distributions of the form: $P_f[\mathcal{X}] \;\sim\; f(\mathrm{Tr}\; \mathcal{X}^T \mathbf{C}^{-1} \mathcal{X} \mathbf{A}^{-1})$ where $\mathbf{C}$ and $\mathbf{A}$ represent the true correlation and autocorrelation matrices respectively, and $f$ is a non-negative and normalized weight function. Only in the special case $\mathbf{C} = \mathbf{A} = \mathbf{1}$ invariance is recovered. This approach has been modified in [95] to allow for a time-dependent random volatility.

From eq. (4.2.5) (or eq. (4.2.1)) we can immediately go to an eigenvalue basis of the positive definite matrix $\mathcal{X}^\dagger\mathcal{X}$, to obtain the following jpdf

$$\begin{aligned} P_\gamma(\lambda_1,\ldots,\lambda_N) &\equiv \left(1+\frac{n\beta}{\gamma}\sum_{i=1}^N V(\lambda_i)\right)^{-\gamma}\prod_{i=1}^N \lambda_i^{\frac{1}{2}\beta(\nu+1)-1}\prod_{j>k}^N|\lambda_j-\lambda_k|^\beta \\ &= \frac{1}{\Gamma(\gamma)}\int_0^\infty d\xi\; e^{-\xi}\;\xi^{\gamma-1}\;P(\lambda_1,\ldots,\lambda_N;\xi) \end{aligned} \tag{4.2.6}$$

It is expressed through the jpdf of the standard WL[1]

$$P(\lambda_1,\ldots,\lambda_N;\xi) \equiv \prod_{i=1}^N \lambda_i^{\frac{1}{2}\beta(\nu+1)-1}\exp\left[-\xi\,\frac{n\beta}{\gamma}V(\lambda_i)\right]\prod_{j>k}^N|\lambda_j-\lambda_k|^\beta \tag{4.2.7}$$

depending on $\xi$ through its weight $\exp\left[-\xi\,\frac{n\beta}{\gamma}V(\lambda)\right]$. In both jpdf's we have suppressed the constant from the integration over the angular degrees of freedom.

For completeness, we also define the corresponding partition function

$$\begin{aligned} \mathcal{Z}_\gamma &\equiv \int_0^\infty\prod_{i=1}^N d\lambda_i\;\left(1+\frac{n\beta}{\gamma}\sum_{i=1}^N V(\lambda_i)\right)^{-\gamma}\prod_{i=1}^N \lambda_i^{\frac{1}{2}\beta(\nu+1)-1}\prod_{j>k}^N|\lambda_j-\lambda_k|^\beta \\ &= \frac{1}{\Gamma(\gamma)}\int_0^\infty d\xi\; e^{-\xi}\;\xi^{\gamma-1}\mathcal{Z}(\xi) \end{aligned} \tag{4.2.8}$$

which is again an integral over the standard, $\xi$-dependent WL partition function

$$\mathcal{Z}(\xi) \equiv \int_0^\infty\prod_{i=1}^N d\lambda_i\;\lambda_i^{\frac{\beta}{2}(\nu+1)-1}\exp\left[-\xi\,\frac{n\beta}{\gamma}V(\lambda_i)\right]\prod_{j>k}^N|\lambda_j-\lambda_k|^\beta \tag{4.2.9}$$

Because of this linear relation between the generalized and standard ensembles we can immediately express all $k$-point eigenvalue density correlation functions, denoted by $R$ for finite-$N$, in terms of each other. They are defined in the usual way (see [46] and chapter 2):

$$\begin{aligned} R_\gamma(\lambda_1,\ldots,\lambda_k) &\equiv \frac{N!}{(N-k)!}\frac{1}{\mathcal{Z}_\gamma}\int_0^\infty d\lambda_{k+1}\cdots d\lambda_N P_\gamma(\lambda_1,\ldots,\lambda_N) \\ &= \int_0^\infty d\xi\; e^{-\xi}\;\xi^{\gamma-1}\frac{\mathcal{Z}(\xi)}{\Gamma(\gamma)\mathcal{Z}_\gamma}R(\lambda_1,\ldots,\lambda_k;\xi) \end{aligned} \tag{4.2.10}$$

[1]For notational simplicity, we suppress hereafter the subscript WL in the jpdf (2.4.7).

where the $k$-point correlation functions of the standard ensembles depend on $\xi$ through the exponent in the measure

$$R(\lambda_1,\ldots,\lambda_k;\xi) \equiv \frac{(N-k)!}{k!}\frac{1}{\mathcal{Z}(\xi)}\int_0^\infty d\lambda_{k+1}\cdots d\lambda_N P(\lambda_1,\ldots,\lambda_N;\xi) \quad (4.2.11)$$

The latter can be solved using the method of (skew) orthogonal polynomials [46], expressing them through the determinant of the kernel of the orthogonal polynomials for $\beta = 2$, or the Pfaffian of the matrix kernel of skew orthogonal polynomials for $\beta = 1$ and 4. We only recall here the simpler $\beta = 2$ case (see section 2.2) and briefly outline $\beta = 1$ and 4, referring to [46] for more details.

Let us define monic orthogonal polynomials and their norms for $\beta = 2$ as follows

$$\int_0^\infty d\lambda\ \lambda^\nu \exp\left[-\xi\frac{2n}{\gamma}V(\lambda)\right] P_k(\lambda)P_l(\lambda) = h_k\delta_{kl} \quad (4.2.12)$$

Introducing their kernel

$$K_N(\lambda,\mu) \equiv (\lambda\mu)^{\frac{\nu}{2}} e^{-\xi\frac{n}{\gamma}(V(\lambda)+V(\mu))}\sum_{k=0}^{N-1} h_k^{-1}P_k(\lambda)P_k(\mu) \quad (4.2.13)$$

and applying the Christoffel-Darboux identity for $\lambda \neq \mu$

$$\sum_{k=0}^{N-1} h_k^{-1}P_k(\lambda)P_k(\mu) = h_{N-1}^{-1}\frac{P_N(\lambda)P_{N-1}(\mu)-P_N(\mu)P_{N-1}(\lambda)}{\lambda-\mu} \quad (4.2.14)$$

we can express all eigenvalue correlations of the standard ensemble through this kernel [46],

$$R(\lambda_1,\ldots,\lambda_k;\xi) = \det_{1\le i,j\le k}[K_N(\lambda_i,\lambda_j)] \quad (4.2.15)$$

where in the r.h.s. the dependence on $\xi$ is not shown explicitly.

We thus arrive at

$$R_\gamma(\lambda_1,\ldots,\lambda_k) = \int_0^\infty d\xi\ e^{-\xi}\ \xi^{\gamma-1}\frac{\mathcal{Z}(\xi)}{\Gamma(\gamma)\mathcal{Z}_\gamma}\det_{1\le i,j\le k}[K_N(\lambda_i,\lambda_j)] \quad (4.2.16)$$

which is the main result of this section. The simplest example is the spectral density $R_\gamma(\lambda)$ given by the integral over the single kernel $K_N(\lambda,\lambda)$. Notice that it is normalized to[1] $N = \int_0^\infty d\lambda R_\gamma(\lambda)$.

[1] Again, we will use the symbols $R$ or $\rho$ to denote densities normalized to $N$ or 1 respectively.

In order to take $N$ large we only need to know the asymptotic of the polynomials $P_N$, take a finite determinant of size $k$ of the asymptotic kernel and integrate once with respect to $\xi$. In appendix B the orthogonal polynomials, the corresponding densities and partition functions are worked out in detail for finite-$N$ and the potential $V(\lambda) = \lambda$ at $\beta = 2$, given in terms of Laguerre polynomials and their norms.

As pointed out already the same result eq. (4.2.16) holds for $\beta = 1$ and 4 when replacing the determinant by a Pfaffian, $\mathrm{Pf}[\kappa_N(\lambda_i, \lambda_j)]$, where $\kappa_N$ is a $2 \times 2$ matrix kernel. For the weight $V(\lambda) = \lambda$ its skew orthogonal polynomials are explicitly known as well in terms of Laguerre polynomials [100; 101].

For completeness, we also give the partition function occurring inside the integrand in eq. (4.2.16) in terms of the norms $h_i$ of orthogonal polynomials

$$\mathcal{Z}(\xi) \;=\; N! \prod_{i=0}^{N-1} h_i \;=\; N!\, h_0^N \prod_{i=0}^{N-1} r_i^{N-i} \tag{4.2.17}$$

or their ratios $r_i \equiv \frac{h_{i+1}}{h_i}$. An identical result holds for $\beta = 1$ and 4 in terms of the skew orthogonal norms [46].

In the Gaussian case the ratio of partition functions $\mathcal{Z}(\xi)/\Gamma(\gamma)\mathcal{Z}_\gamma$ in eq. (4.2.16) can be obtained most explicitly at finite-$N$ for all 3 values of $\beta$ by changing to radial coordinates, see appendix C for a derivation.

## 4.3 Macroscopic large-$N$ limit for the potential $V(\lambda) = \lambda$

In this section, we restrict ourselves to the potential $V(\lambda) = \lambda$, deriving a generalization of the MP spectral density of WL for all three $\beta$. It exhibits a non-compact support and power-law behavior for large arguments, and we consider two cases. In the first subsection, we deal with matrices that become asymptotically square with $M - N = \nu = \mathcal{O}(1)$. In the standard WL ensembles, as already remarked in section 2.4.2, at large-$N$ the spectral support is a semi-compact support on the positive semi-axis, where the origin represents a hard edge. In the second

subsection, we take the limit

$$\lim_{M,N\to\infty} \frac{N}{M} \equiv c \tag{4.3.1}$$

with $c < 1$, corresponding to the case $M - N = \nu = \mathcal{O}(N)$. In the WL ensembles, the resulting MP macroscopic spectral density takes support on a positive interval. Conversely, in both cases $c = 1$ and $c < 1$ our generalized macroscopic density will have support on the full positive real semi-axis.

### 4.3.1 Generalized semi-circle for $c = 1$

The finite-$N$ density for the WL ensembles $R(\lambda;\xi)$ is well known in terms of Laguerre polynomials, see eq. (C.0.7) for $\beta = 2$ in the appendix C. This results into an explicit integral representation for the spectral density of our generalized ensembles, see eq. (C.0.10). Despite this result, it is rather difficult to extract information about the macroscopic large-$N$ limit from those analytical formulae, both for the standard and generalized WL ensembles.

Hence, we follow here an alternative route, already exploited in [37]: we directly insert the large-$N$ result into eq. (4.2.10)[1]. The $N \gg 1$ asymptotic of the WL density is known and given by the Marčenko-Pastur law, which is in fact the semi-circle law in squared variables at $c = 1$

$$\lim_{N\gg 1} R(\lambda) = \frac{n}{\pi}\sqrt{\frac{2N}{n\lambda} - 1}\,, \quad \text{with} \quad \lambda \in (0, 2N/n] \tag{4.3.2}$$

It is given here for the weight $\exp[-n\beta\lambda]$ for all three $\beta$, and can be derived easily using the Coulomb gas approach and saddle point method (see also [102] and chapter 2).

In order to obtain an $N$-independent macroscopic density we have to rescale the argument of the density by the mean eigenvalue position, $\lambda \to \langle\lambda\rangle x$, and divide by $N$ to normalize the density to unity. The mean position of an eigenvalue or first moment, $\langle\lambda\rangle_\gamma$, can be computed in the generalized model for both finite-$N$

[1]The correctness of this approach will be exhibited at the end of Appendix C.

and -$\nu$ (see appendix B),

$$\begin{aligned} \langle\lambda\rangle_\gamma &\equiv \frac{\int_0^\infty d\lambda\ \lambda\ R_\gamma(\lambda)}{\int_0^\infty d\lambda\ R_\gamma(\lambda)} = \frac{1}{N}\langle \mathrm{Tr}(\mathcal{X}^\dagger\mathcal{X})\rangle_\gamma \\ &= \frac{\gamma(N+\nu)}{2n(\gamma - \frac{\beta}{2}N(N+\nu) - 1)} \end{aligned} \tag{4.3.3}$$

We will comment on the existence of this first moment later, and we will also need this equation again when we consider $c < 1$. It correctly reproduces the known result for WL in the limit $\lim_{\gamma\to\infty}\langle\lambda\rangle_\gamma = \langle\lambda\rangle = (N+\nu)/2n$ (see chapter 2). For the WL case we thus obtain the following known $N$- and $\beta$-independent macroscopic density from eq. (4.3.2)

$$\rho(x) \equiv \lim_{N\to\infty}\frac{1}{N}\langle\lambda\rangle R(x\langle\lambda\rangle) = \frac{1}{2\pi}\sqrt{\frac{4}{x}-1}\ , \quad \text{with} \quad x\in(0,4] \tag{4.3.4}$$

It is normalized to unity and has mean $\langle x\rangle = 1$.

We can now repeat the same steps for our generalized model, where we need eq. (4.3.2) for the weight $\exp[-\xi n\beta\lambda/\gamma]$ (see eq. (4.2.7)). Because of the rescaling with respect to $\langle\lambda\rangle_\gamma$ we now have to specify the $N$-dependence of $\gamma$. We keep the following combination fixed,

$$\hat\alpha \equiv \lim_{N,\gamma\to\infty}\left[\gamma - \frac{\beta}{2}N(N+\nu) - 1\right] \tag{4.3.5}$$

with $\hat\alpha > 0$ finite. This satisfies the constraint (4.2.2). We thus obtain for the generalized macroscopic density

$$\begin{aligned} \rho_{\hat\alpha}(x) &\equiv \lim_{N,\gamma\to\infty}\frac{1}{N}\langle\lambda\rangle_\gamma R_\gamma(x\langle\lambda\rangle_\gamma) \\ &= \lim_{N,\gamma\to\infty}\frac{1}{N}\langle\lambda\rangle_\gamma\int_{\mathcal{J}} d\xi\ e^{-\xi}\xi^{\gamma-1}\frac{\mathcal{Z}(\xi)}{\Gamma(\gamma)\mathcal{Z}_\gamma}\frac{n\xi}{\gamma\pi}\sqrt{\frac{2N\gamma}{n\xi x\langle\lambda\rangle_\gamma}-1} \end{aligned} \tag{4.3.6}$$

where the integration is restricted to the interval $\mathcal{J} = (0, \frac{2N\gamma}{nx\langle\lambda\rangle_\gamma}] = (0, 4\hat\alpha/x]$. In order to compute the integral we still need the following quantity inside the integrand,

$$\frac{\mathcal{Z}(\xi)}{\Gamma(\gamma)\mathcal{Z}_\gamma} = \frac{\xi^{-\frac{\beta}{2}N(N+\nu)}}{\Gamma\left(\gamma - \frac{\beta}{2}N(N+\nu)\right)} \tag{4.3.7}$$

the ratio of partition functions given here for finite-$N$. This result is derived in appendix B, see eq. (B.0.5). Inserting all ingredients into eq. (4.3.6) and taking limits with the definition (4.3.5) we arrive at the following result after changing variables,

$$\begin{aligned}\rho_{\hat{\alpha}}(x) &= \frac{1}{2\hat{\alpha}\pi\Gamma(\hat{\alpha}+1)}\left(\frac{4\hat{\alpha}}{x}\right)^{\hat{\alpha}+2}\int_0^1 dt\ \exp\left[-\frac{4\hat{\alpha}}{x}t\right]\ t^{\hat{\alpha}+1}\sqrt{\frac{1}{t}-1} \\ &= \frac{\Gamma(\hat{\alpha}+\frac{3}{2})}{4\hat{\alpha}\sqrt{\pi}\Gamma(\hat{\alpha}+1)\Gamma(\hat{\alpha}+3)}\left(\frac{4\hat{\alpha}}{x}\right)^{\hat{\alpha}+2}\ {}_1F_1\left(\hat{\alpha}+\frac{3}{2},\hat{\alpha}+3;-\frac{4\hat{\alpha}}{x}\right) \end{aligned} \tag{4.3.8}$$

Here we have introduced the confluent or Kummer hypergeometric function

$${}_1F_1(a,b;z) \ = \ \frac{\Gamma(b)}{\Gamma(b-a)\Gamma(a)}\int_0^1 dt\ e^{zt}\ t^{a-1}(1-t)^{b-a-1} \tag{4.3.9}$$

Eq. (4.3.8) is the main result of this subsection, the macroscopic spectral density of our generalized WL. It has an unbounded support $(0,\infty)$, and the density as well as its first moment are normalized to unity

$$\int_0^\infty dx\rho_{\hat{\alpha}}(x) \ = \ 1 \ = \ \int_0^\infty dx\ x\ \rho_{\hat{\alpha}}(x) \tag{4.3.10}$$

Note that due to this normalization, the parameter $n$ has completely dropped out. We are left with a one-parameter class of densities depicted in fig. 4.1, which approach the WL density for $\hat{\alpha}\to\infty$ as discussed below.

From the expansion for small arguments ${}_1F_1(a,b;z) = 1 + \frac{a}{b}z + \ldots$ we can immediately read off the power law decay of our new density eq. (4.3.8)

$$\lim_{x\to\infty}\rho_{\hat{\alpha}}(x) \ = \ x^{-(\hat{\alpha}+2)}\frac{\Gamma(\hat{\alpha}+\frac{3}{2})}{\sqrt{\pi}\Gamma(\hat{\alpha}+1)\Gamma(\hat{\alpha}+3)}(4\hat{\alpha})^{\hat{\alpha}+1}\ (1+\mathcal{O}(1/x)) \tag{4.3.11}$$

Because of $\hat{\alpha} > 0$ the decay is always faster than quadratic. However, if we drop the requirement for the existence of the first moment we can allow for $\hat{\alpha}$ to take values $-1 < \hat{\alpha} < 0$ while satisfying the constraint eq. (4.2.2). Keeping the same formal rescaling in eq. (4.3.6) we arrive at the same result eq. (4.3.8) now valid for $-1 < \hat{\alpha}$ and $\hat{\alpha} \neq 0$ [1]. Our density can thus describe power laws in between linear and quadratic decay as well, see fig. 4.1. The same feature could be incorporated in the generalized Gaussian model [37].

[1] We use the obvious notation $\hat{\alpha}^{\hat{\alpha}+1} = \exp[(\hat{\alpha}+1)\ln|\hat{\alpha}|]$.

As a check we can take the limit $\hat{\alpha} \to \infty$ on our final result eq. (4.3.8). This amounts to decoupling the $\gamma$- and $N$-dependence, and thus we expect to recover the MP density at $\gamma = \infty$. By taking a saddle point approximation, we find that this is indeed the case, $\lim_{\hat{\alpha}\to\infty} \rho_{\hat{\alpha}}(x) = \rho(x)$. Hence, the density $\rho_{\hat{\alpha}}(x)$ is a well-behaved deformation of the MP density for $c = 1$.

We can also derive the behavior of the density $\rho_{\hat{\alpha}}(x)$ close to the origin. Using the large argument asymptotic for the confluent hypergeometric function at negative argument, $\lim_{z\to\infty} {}_1F_1(a, b; -z) = z^{-a}\Gamma(b)/\Gamma(b-a)(1 + \mathcal{O}(1/z))$, we find that

$$\lim_{x\to 0} \rho_{\hat{\alpha}}(x) \;=\; x^{-\frac{1}{2}} \frac{\Gamma(\hat{\alpha} + \frac{3}{2})}{\pi\Gamma(\hat{\alpha}+1)\sqrt{\hat{\alpha}}} \; (1 + \mathcal{O}(x)) \tag{4.3.12}$$

Therefore all our generalized densities have a square root singularity at the origin, just as the MP density.

To illustrate our findings we first plot eq. (4.3.8) in Fig. 4.1 (left) for different values of $\hat{\alpha}$, and compare it to the semi-circle density eq. (4.3.4). In order to visualize the square root singularity for all $\hat{\alpha}$ we map the density from the positive to the full real axis by defining

$$\vartheta_{\hat{\alpha}}(y) \;\equiv\; |y|\rho_{\hat{\alpha}}(y^2) \tag{4.3.13}$$

that is to a normalized density on $\mathbb{R}$, $\int_{-\infty}^{\infty} dy \vartheta_{\hat{\alpha}}(y) = 1$. In this form it equals the deformed semi-circle law derived from generalizing the Gaussian ensembles in [37], where we have eliminated all irrelevant parameters.

The same map eq. (4.3.13) takes the MP density eq. (4.3.4) to the semi-circle, as mentioned already several times,

$$\vartheta(y) \;=\; \frac{1}{2\pi}\sqrt{4 - y^2} \tag{4.3.14}$$

Both densities are shown in Fig. 4.1 (right). For $\hat{\alpha} = 14$ it already approximates the semi-circle very well. For negative $-1 < \hat{\alpha} < 0$ the height of the maximum in fig. 4.1 (left) goes down again, for $\hat{\alpha} = -0.5$ the curve is even below the semi-circle.

As a final point of this subsection let us discuss the issue of macroscopic universality of our generalized density, eq. (4.3.8). This is a direct consequence

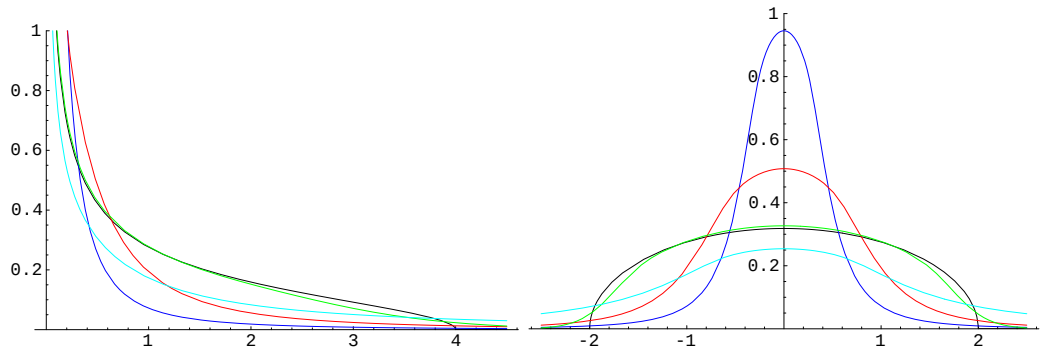


Figure 4.1: The macroscopic generalized density eq. (4.3.8) $\rho_{\hat{\alpha}}(x)$ shown on the positive real line $\mathbb{R}_+$ for $\hat{\alpha} = -0.5,\ 0.1,\ 0.5$ and 14 in light blue, blue, red and green, respectively (left), and its map $\vartheta_{\hat{\alpha}}(y) = |y|\rho_{\hat{\alpha}}(y^2)$ to the full real line $\mathbb{R}$ (right). Note that the MP or semi-circle density given in black for comparison has compact support on $(0, 4]$ and $[-2, 2]$ respectively.

of the (non-)universality of the MP or semi-circular density, due to the linear relationship eq. (4.2.10).

The semi-circle possesses a certain weak universality, being the same for all three Gaussian ensembles at $\beta = 1, 2, 4$, as well as for independently distributed random variables (this was shown already by Wigner). Consequently our generalized density is universal in this weak sense, too.

On the other hand, the polynomial deformation of the confining potential in the definition of our model is clearly *non-universal*, as the semi-circle becomes a polynomial times one or several square root cuts, and we refer to [103] for details at $\beta = 2$. Remarkably, it was found in [103] for $\beta = 2$ that all macroscopic two- or higher $k$-point *connected* density correlation functions are universal under such perturbations $V$, depending only on a finite number of parameters for any degree $d$. Does this universality persist in our model? The answer is no, simply by looking at the definition of the connected two-point density:

$$R_\gamma^{conn}(\lambda, \mu) \ \equiv \ R_\gamma(\lambda, \mu) - R_\gamma(\lambda) R_\gamma(\mu) \tag{4.3.15}$$

We use the same definition for the standard WL density. It no longer relates linearly to the corresponding connected WL two-point density as we would subtract

an integral of the product of two 1-point densities, instead of the product of two integrated 1-point densities:

$$\begin{aligned} R_\gamma^{conn}(\lambda,\mu) &= \int_0^\infty d\xi\ e^{-\xi}\ \xi^{\gamma-1}\frac{\mathcal{Z}(\xi)}{\Gamma(\gamma)\mathcal{Z}_\gamma}R(\lambda,\mu;\xi) \\ &\quad - \int_0^\infty d\xi\ e^{-\xi}\ \xi^{\gamma-1}\frac{\mathcal{Z}(\xi)}{\Gamma(\gamma)\mathcal{Z}_\gamma}R(\lambda;\xi)\int_0^\infty d\xi\ e^{-\xi}\ \xi^{\gamma-1}\frac{\mathcal{Z}(\xi)}{\Gamma(\gamma)\mathcal{Z}_\gamma}R(\mu;\xi) \\ &\neq \int_0^\infty d\xi\ e^{-\xi}\ \xi^{\gamma-1}\frac{\mathcal{Z}(\xi)}{\Gamma(\gamma)\mathcal{Z}_\gamma}\ R^{conn}(\lambda,\mu;\xi) \end{aligned} \tag{4.3.16}$$

The universal macroscopic connected two-point function obtained in the large-$N$ limit $\rho^{conn}(x,y;\xi)$ in [103] will thus mix with the non-universal density $\rho(x;\xi)$, and the same feature persists for higher $k$-point connected correlators. This should not come as a surprise as the same situation was encountered in the fixed or restricted trace ensembles [36], being an integral transformation of the classical Wigner-Dyson ensembles. As observed there, our microscopic correlations will remain universal, see section 4.4.

In the next section we will study the limit $\frac{N}{M} \to c < 1$. The corresponding standard WL ensemble can be mapped to the so-called generalized Penner model [104] with positive definite matrices. The extra determinant from the Jacobian of this change of variables can be written as an extra logarithm in the potential $V \to V + N\ln|\lambda|$. For the same reason as given above the universal findings made in [104] for the unitary ensemble $\beta = 2$ do not translate to the macroscopic limit in the next section either.

### 4.3.2 Generalized Marčenko-Pastur law for $c < 1$

In this subsection we deal with the limit in which the matrix $\mathcal{X}$ remains rectangular, that is both $M$ and $N = cM$ become large such that $\lim_{N,M\to\infty} N/M = c < 1$. This limit is particularly relevant for applications to real data series.

We will follow the same steps as in the previous subsection. We recall that in the standard WL ensembles with weight $\exp[-n\beta\lambda]$, the corresponding density is given by the MP law (see 2.4.2),

$$\lim_{N\gg 1} R(\lambda) = \frac{n}{\pi\lambda}\sqrt{\left(\lambda - \frac{N}{2n}x_-\right)\left(\frac{N}{2n}x_+ - \lambda\right)}\ , \quad \text{with} \quad \lambda \in \left[\frac{N}{2n}x_-, \frac{N}{2n}x_+\right] \tag{4.3.17}$$

We recall here the definition of the bounds for the MP support (see again section 2.4.2)

$$x_\pm \equiv (c^{-\frac{1}{2}} \pm 1)^2 \,, \quad \text{with} \quad 0 < c < 1 \tag{4.3.18}$$

In the limit $c \to 1$ we recover from eq. (4.3.17) the semi-circle eq. (4.3.2) from the last section.

The $N$-independent density is again obtained after rescaling by the mean eigenvalue position

$$\langle\lambda\rangle_\gamma = \frac{\gamma N}{2nc(\gamma - \frac{\beta}{2c}N^2 - 1)} \tag{4.3.19}$$

where we have used $M = N + \nu = N/c$. For large $\gamma$ we obtain the quantity $\langle\lambda\rangle = \frac{N}{2nc}$, which is the average position for the standard WL in our limit $c < 1$. We thus obtain for the rescaled MP density

$$\rho(x) \equiv \lim_{N\to\infty} \frac{1}{N}\langle\lambda\rangle R(x\langle\lambda\rangle) = \frac{1}{2\pi cx}\sqrt{(x - cx_-)(cx_+ - x)} \,, \quad \text{with } x \in [cx_-, cx_+] \tag{4.3.20}$$

It is normalized to unity with mean $\langle x\rangle = 1$.

For the generalized model we have to insert eq. (4.3.17), now with weight $\exp[-\xi\frac{n\beta}{\gamma}\lambda]$, into eq. (4.2.10) and rescale with respect to eq. (4.3.19). As previously we keep fixed

$$\hat\alpha \equiv \lim_{N,\gamma\to\infty}\left[\gamma - \frac{\beta}{2c}N^2 - 1\right] \,, \quad \text{with } \hat\alpha > 0 \tag{4.3.21}$$

as in eq. (4.3.5). The rescaled generalized density is thus given by

$$\begin{aligned}\rho_{\hat\alpha}(x) &\equiv \lim_{N,\gamma\to\infty}\frac{1}{N}\langle\lambda\rangle_\gamma R_\gamma(x\langle\lambda\rangle_\gamma) \\ &= \lim_{N,\gamma\to\infty}\frac{1}{N}\langle\lambda\rangle_\gamma \int_{\mathcal{J}} d\xi\; e^{-\xi}\xi^{\gamma-1}\frac{\mathcal{Z}(\xi)}{\Gamma(\gamma)\mathcal{Z}_\gamma}\frac{n\xi}{\gamma\pi x\langle\lambda\rangle_\gamma}\sqrt{\left(x\langle\lambda\rangle_\gamma - \frac{N\gamma}{2n\xi}x_-\right)\left(\frac{N\gamma}{2n\xi}x_+ - x\langle\lambda\rangle_\gamma\right)}\end{aligned} \tag{4.3.22}$$

where $\mathcal{J} \equiv \left[\frac{c\hat\alpha}{x}x_-, \frac{c\hat\alpha}{x}x_+\right]$. Filling in all definitions and changing variables we finally arrive at the following main result of this subsection:

$$\rho_{\hat\alpha}(x) = \frac{1}{2\pi c\hat\alpha\Gamma(\hat\alpha+1)}\left(\frac{c\hat\alpha}{x}\right)^{\hat\alpha+2}\int_{x_-}^{x_+} dt \exp\left[-\frac{c\hat\alpha}{x}t\right] t^{\hat\alpha}\sqrt{(t - x_-)(x_+ - t)} \tag{4.3.23}$$

Our density in normalized to unity and has first moment $\langle x \rangle = 1$. This result was derived previously (modulo different notations) for $\beta = 1$ in [97], using different methods. The integral in eq. (4.3.23) can be computed in principle in terms of a confluent hypergeometric series in two variables (see [105], formulae 3.385 and 9.261(1)), but the integral form is more convenient for numerical evaluations and an asymptotic analysis. As a first check we recover eq. (4.3.8) in the limit $c \to 1$. Furthermore, one can show that the following limit holds, $\lim_{\hat{\alpha}\to\infty} \rho_{\hat{\alpha}}(x) = \rho(x)$, recovering the MP density eq. (4.3.20). Thus the large-$N$ limit and the large-$\gamma$ limit are again well behaved. We have also checked in appendix C that the convergence with $N$ towards the density eq. (4.3.8) is very fast, see fig. C.1, in fact faster than for WL. Our remark from the previous subsection allowing $-1 < \hat{\alpha} < 0$ applies here too.

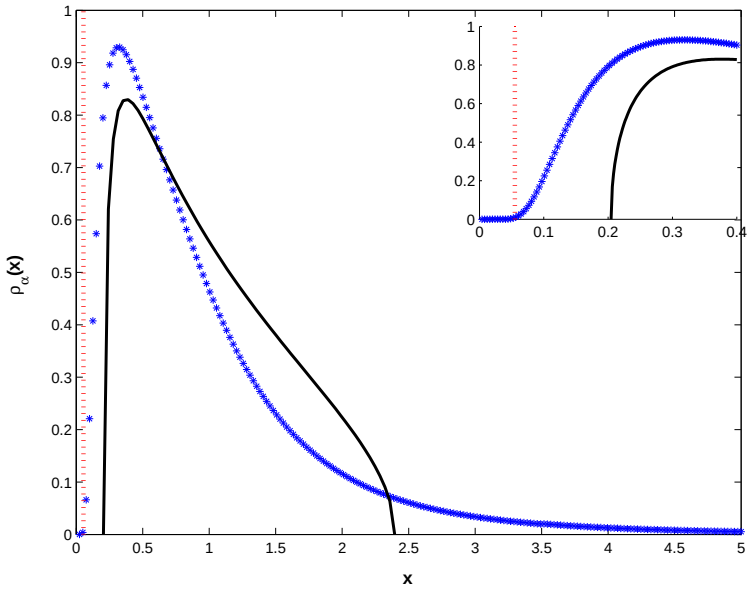


Figure 4.2: The macroscopic generalized density $\rho_{\hat{\alpha}}(x)$ eq. (4.3.23) for $\hat{\alpha} = 3$ and $c = 0.3$ (blue), compared to the MP distribution $\rho(x)$ (4.3.20) (black). In the inset, the behaviour close to the origin is shown. The red dashed line corresponds to the pseudo edge $\mathcal{X}_-$ of our generalized MP density (see main text for details).

It is easy to see how the density decays for large $x \gg 1$

$$\rho_{\hat{\alpha}}(x) \;\sim\; x^{-(\hat{\alpha}+2)} \frac{(c\hat{\alpha})^{\hat{\alpha}+1}}{2\pi\Gamma(\hat{\alpha}+1)}\, \mathcal{C}(1+\mathcal{O}(1/x)) \tag{4.3.24}$$

with the same power law as for $c = 1$. The constant $\mathcal{C}$ is given by

$$\mathcal{C} \;\equiv\; \frac{1}{8}(x_+ - x_-)^2 x_-^{\hat{\alpha}} \pi \; {}_2F_1\left(\frac{3}{2}, -\hat{\alpha}; 3; -\frac{x_+ - x_-}{x_-}\right) \tag{4.3.25}$$

The asymptotic for small values of $x$ is less obvious to obtain, and we find

$$\rho_{\hat{\alpha}}(x) \;\sim\; x^{-\hat{\alpha}-1/2} \exp\left[-\frac{c\hat{\alpha}}{x} x_-\right] \mathcal{D} \tag{4.3.26}$$

where the constant $\mathcal{D} = x_-^{\hat{\alpha}}(x_+ - x_-)^{1/2}(c\hat{\alpha})^{\hat{\alpha}-1/2}/16\Gamma(\hat{\alpha}+1)$.

While the MP density of the standard WL ensemble eq. (4.3.20) has compact support between $[cx_-, cx_+]$, our generalized density is non-vanishing on the entire real positive axis, even for $c < 1$. To the left of the edge in MP, $x < cx_-$, our density decreases but remains non-zero. Below a certain point that we will call pseudo edge, $\mathcal{X}_-$, our density becomes exponentially suppressed. From the asymptotic (4.3.26) it is possible to give an estimate for $\mathcal{X}_-$, below which the density becomes negligible. The reasoning goes as follows: writing the asymptotic (4.3.26) as

$$\rho_{\hat{\alpha}}(x) \;\approx \exp\left[-\left((\hat{\alpha}+1/2)\log x + \frac{c\hat{\alpha}}{x} x_-\right)\right] \tag{4.3.27}$$

the exponential damping conventionally begins at the point $\mathcal{X}_-$ where

$$(\hat{\alpha}+1/2)\log \mathcal{X}_- + \frac{c\hat{\alpha}}{\mathcal{X}_-} x_- \approx 1 \tag{4.3.28}$$

For the case depicted in fig. 4.2 ($c = 0.3$ and $\hat{\alpha} = 3$), the above estimate reads $\mathcal{X}_- \approx 0.055...$, in reasonable agreement with the inset.

## 4.4 Universal microscopic large-$N$ limit for a general potential $V$

In this section we consider a different large-$N$ limit, the microscopic limit, which takes us to the scale of the mean level spacing and thus to the distribution of

individual eigenvalues. Our findings will be universal for a general polynomial potential $V(\lambda)$ for all three $\beta = 1, 2, 4$, inheriting the corresponding universality from the standard ensembles.

We will only consider the case $c = 1$ and the so-called hard edge here, deriving a generalized Bessel-law for the microscopic densities and their first eigenvalue distributions. For $c < 1$ the local distribution at the inner (and outer) soft edge of the standard WL ensembles follows the Tracy-Widom law. Although it would be very interesting to derive the corresponding generalization we have not managed so far, and leave this task for future investigation.

In the first subsection the microscopic densities are derived while the second subsection is devoted to the first eigenvalue distributions. The matching of the two is illustrated in many pictures throughout this section, being an important consistency check.

### 4.4.1 Generalized universal Bessel-law

Let us first recall the definition of the microscopic limit in the standard WL ensembles, resulting into the universal Bessel-law. We will discuss in detail the case $\beta = 2$ and then only quote the results for $\beta = 1, 4$.

For simplicity consider the simplest case $V(\lambda) = \lambda$ first. Starting from the weight $\exp[-n\beta\lambda]$ we first scale out the mean eigenvalue $\lambda \to x\langle\lambda\rangle$, just as in eq. (4.3.4) for the macroscopic limit. On top of that we make a further rescaling by the mean level spacing $4N^2x = y$, keeping $y$ fixed. We therefore define the microscopic limit as

$$\rho_\nu^{(\beta)}(y) \equiv \lim_{N\to\infty} \frac{1}{2N^2}\langle\lambda\rangle R\left(\frac{y}{4N^2}\langle\lambda\rangle\right) \tag{4.4.1}$$

where $R(\lambda)$ is the spectral density for finite-$N$ in one of the three WL ensembles. The result now depends on $\beta$ and $\nu$ as indicated through the indices, in contrast to the semi-circle law. We can then apply the following asymptotic

$$\lim_{k\to\infty} k^{-\nu} L_k^\nu\left(\frac{z^2}{4k}\right) = \left(\frac{z}{2}\right)^{-\nu} J_\nu(z) \tag{4.4.2}$$

to the orthogonal Laguerre polynomials in the finite-$N$ density, see eq. (C.0.7) for $\beta = 2$. We obtain

$$\begin{aligned}\rho_\nu^{(2)}(y) &= \lim_{N\to\infty} \frac{2n}{2N^2}\langle\lambda\rangle \left(\frac{y\langle\lambda\rangle 2n}{4N^2}\right)^\nu e^{-\frac{2ny}{4N^2}\langle\lambda\rangle} \sum_{k=0}^{N-1} \frac{k!}{(k+\nu)!} L_k^\nu\left(\frac{2ny\,k}{4N^2k}\langle\lambda\rangle\right)^2 \\ &= \frac{1}{2}\int_0^1 dt J_\nu(\sqrt{ty})^2 = \frac{1}{2}(J_\nu(\sqrt{y})^2 - J_{\nu-1}(\sqrt{y})J_{\nu+1}(\sqrt{y})) \end{aligned} \tag{4.4.3}$$

after replacing the sum by an integral[1] with variable $t = k/N$. The Bessel density is plotted for different values of $\nu$ in fig. 4.4 together with the first eigenvalue from the next subsection, after changing to the conventional squared variables $y \to y^2$ (see eq. (4.3.13)),

$$\vartheta_\nu^{(2)}(y) = \frac{|y|}{2}(J_\nu(y)^2 - J_{\nu-1}(y)J_{\nu+1}(y)) \tag{4.4.4}$$

This result is universal [106] being valid for any potential $V$ with spectral support including the origin. We only have to rescale in eq. (4.4.1) by the macroscopic density in terms of the squared variables $\pi\vartheta(0)$ for a general potential $V$, instead of the Gaussian macroscopic density eq. (4.3.14) where $\pi\vartheta(0) = 1$. In other words all orthogonal polynomials eq. (4.2.12) tend to Bessel-$J$ functions in the microscopic limit.

We can now repeat the above analysis for our generalized microscopic density. The scaling of $\gamma$ with $N$ ($\hat{\alpha}$ fixed) is kept throughout this entire section. In the previous section we found that the density diverges exactly like the standard density as an inverse square root, see eq. (4.3.12). For that reason the microscopic rescaling is the same, without changing powers of $N$. However, the constant in front of the *macroscopic* density at the origin is not the standard Gaussian result, $1/\pi = \vartheta(0)$, but given by eq. (4.3.12), $\vartheta_{\hat{\alpha}}(0) = b/\pi$ with

$$b \equiv \frac{\Gamma(\hat{\alpha}+\frac{3}{2})}{\Gamma(\hat{\alpha}+1)\sqrt{\hat{\alpha}}} \tag{4.4.5}$$

We therefore define the microscopic limit as

$$\rho_{\hat{\alpha},\nu}^{(\beta)}(y) \equiv \lim_{N,\gamma\to\infty} \frac{1}{2N^2b^2}\langle\lambda\rangle_\gamma R_\gamma\left(\frac{y}{4N^2b^2}\langle\lambda\rangle_\gamma\right) \tag{4.4.6}$$

[1] Instead of eq. (C.0.7) we could have applied the Christoffel-Darboux identity eq. (C.0.9), leading to the same result.

Because of the universality we just stated, we can restrict ourselves to the computation for the orthogonal polynomials with weight $\exp[-2n\xi\lambda/\gamma]$ in eq. (4.2.12). Taking the microscopic limit eq. (4.4.6) and inserting eq. (4.4.3) we obtain

$$\vartheta^{(2)}_{\hat{\alpha},\nu}(y) = \frac{\int_0^\infty d\xi\; e^{-\xi}\; \xi^{\hat{\alpha}}\, \frac{\xi|y|}{2\hat{\alpha}b^2} \left( J_\nu\left(\frac{y}{b}\sqrt{\xi/\hat{\alpha}}\right)^2 - J_{\nu-1}\left(\frac{y}{b}\sqrt{\xi/\hat{\alpha}}\right) J_{\nu+1}\left(\frac{y}{b}\sqrt{\xi/\hat{\alpha}}\right)\right)}{\Gamma(\hat{\alpha}+1)} \tag{4.4.7}$$

This is the first main result of this subsection given here in terms of squared values. The integral could be expressed in terms of generalized hypergeometric functions, but for plots this representation is preferable. Note that in our calculation we have inserted the ratio of partition functions eq. (4.3.7) for the Gaussian models. This quantity is again universal as in the large-$N$ limit not only the polynomials themselves, but also their norms become universal. Starting from eq. (4.2.17) the standard WL partition functions is given as follows

$$\begin{aligned} \lim_{N\to\infty} \left(\log[\mathcal{Z}(\xi)] - \log[N!\, h_0^N]\right) \;&=\; \lim_{N\to\infty} N \sum_{i=0}^{N-1} \left(1 - \frac{i}{N}\right) \log[r_i] \;= \\ &= \int_0^1 dt(1-t)\log[r(t)] \end{aligned} \tag{4.4.8}$$

The $\xi$-dependent ratios of the norms determined by the so-called string or recursion equation at finite-$N$ have a universal limit $r(t)$ [106]. Re-exponentiating and inserting this universal result eq. (4.4.8) into eq. (4.2.8), the generalized partition function $\mathcal{Z}_\gamma$ also becomes universal in the large-$N$ limit, and thus the ratio eq. (4.3.7) as well. The constant factor that we have subtracted on the left hand side of eq. (4.4.8) cancels out when taking the ratio.

The new microscopic density eq. (4.4.7) generalizing the Bessel-law eq. (4.4.4) is shown in figs. 4.3 and 4.4 for various values of $\hat{\alpha}$ and $\nu$. The plots include the corresponding first eigenvalues to be derived later. As a check we can take the limit $\hat{\alpha} \to \infty$ to analytically reobtain eq. (4.4.4) from eq. (4.4.7). This is illustrated in fig. 4.3 where we observe that the convergence is rather slow. We have checked that for $\hat{\alpha} \sim \mathcal{O}(150)$ the first three maxima become indistinguishable.

The procedure for $\beta = 1$ and 4 is the same as above and so we can be more concise. The corresponding microscopic densities of the WL ensembles are again

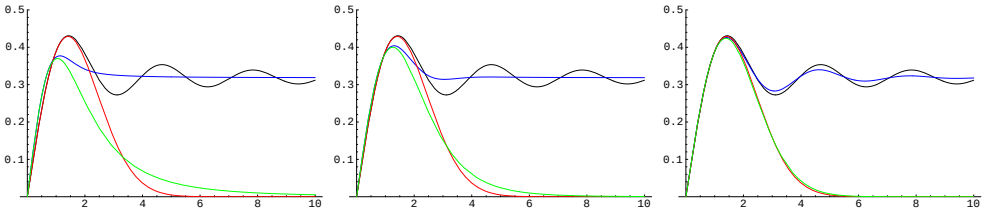

Figure 4.3: Varying $\hat{\alpha}$ at $\beta = 2$: the generalized microscopic density $\vartheta^{(2)}_{\hat{\alpha},\nu}(y)$ eq. (4.4.7) (blue) and its first eigenvalue (green) at $\hat{\alpha} = 0.1$ (left), $\hat{\alpha} = 2$ (middle), and $\hat{\alpha} = 20$ (right), vs the corresponding WL Bessel density $\vartheta^{(2)}_{\nu}(y)$ eq. (4.4.4) (black) and its first eigenvalue (red).

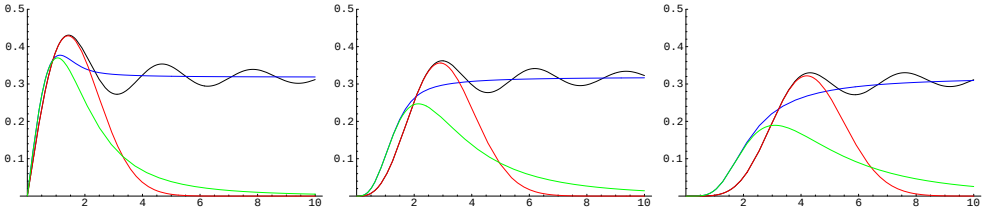

Figure 4.4: Varying $\nu$ at $\beta = 2$: the generalized microscopic density $\vartheta^{(2)}_{\hat{\alpha},\nu}(y)$ eq. (4.4.7) (blue) and its first eigenvalue (green) at $\hat{\alpha} = 0.1$ vs the corresponding WL Bessel density $\vartheta^{(2)}_{\nu}(y)$ eq. (4.4.4) (black) and its first eigenvalue (red): $\nu = 0$ (left), $\nu = 1$ (middle) and $\nu = 2$ (right). It is clearly visible that even the first eigenvalue of the generalized model has fat tails.

universal [107]. Computed initially in [100; 101] the obtained expressions can be simplified. They can be expressed through the $\beta = 2$ density eq. (4.4.4) plus extra terms as shown for $\beta = 1$ [108] and $\beta = 4$ [109],

$$\vartheta^{(1)}_{\nu}(y) = \vartheta^{(2)}_{\nu}(y) + \frac{1}{2} J_{\nu}(|y|) \left( 1 - \int_0^{|y|} dt J_{\nu}(t) \right) \tag{4.4.9}$$

$$\vartheta^{(4)}_{\nu}(y) = \vartheta^{(2)}_{2\nu}(2y) - \frac{1}{2} J_{2\nu}(2|y|) \int_0^{2|y|} dt J_{2\nu}(t) \tag{4.4.10}$$

The generalized densities immediately follow. Because of the linear relationship

they are also expressed through the generalized $\beta = 2$ density eq. (4.4.7):

$$\vartheta^{(1)}_{\hat{\alpha},\nu}(y) = \vartheta^{(2)}_{\hat{\alpha},\nu}(y) + \frac{\int_0^\infty d\xi\ e^{-\xi}\ \xi^{\hat{\alpha}} \sqrt{\frac{\xi}{\hat{\alpha}b^2}} \frac{1}{2} J_\nu\Big(\frac{|y|}{b}\sqrt{\xi/\hat{\alpha}}\Big)\Big(1 - \int_0^{|y|\sqrt{\xi/\hat{\alpha}b^2}} dt J_\nu(t)\Big)}{\Gamma(\hat{\alpha}+1)}$$

$$\vartheta^{(4)}_{\hat{\alpha},\nu}(y) = \vartheta^{(2)}_{\hat{\alpha},2\nu}(2y) - \frac{\int_0^\infty d\xi\ e^{-\xi}\ \xi^{\hat{\alpha}} \sqrt{\frac{\xi}{\hat{\alpha}b^2}} \frac{1}{2} J_{2\nu}\Big(\frac{2|y|}{b}\sqrt{\xi/\hat{\alpha}}\Big) \int_0^{2|y|\sqrt{\xi/\hat{\alpha}b^2}} dt J_{2\nu}(t)}{\Gamma(\hat{\alpha}+1)}$$

For a given $\nu$ the inner integral over the single Bessel-$J$ function can be performed analytically. It is given in terms of Bessel-$J$ functions for odd values of $\nu$, e.g. $\int_0^v dt J_1(t) = J_0(v)$, and additional Struve functions for even $\nu$.

The generalized microscopic densities $\vartheta^{(\beta)}_{\hat{\alpha},\nu}(y)$ are compared to the standard ones below in fig. 4.5 for $\beta = 1$, and in fig. 4.6 for $\beta = 4$.

Higher order correlation functions can be computed along the same lines by inserting the asymptotic Bessel kernels into eq. (4.2.16), and we only quote the simplest final result for $\beta = 2$:

$$\vartheta^{(2)}_{\hat{\alpha},\nu}(y_1,\ldots,y_k) = \frac{\prod_{i=1}^k \frac{1}{2}|y_i|}{\Gamma(\hat{\alpha}+1)} \int_0^\infty d\xi\ e^{-\xi}\ \xi^{\hat{\alpha}} \prod_{j=1}^k \sqrt{\frac{\xi}{\hat{\alpha}}} \frac{|y_j|}{b}$$
$$\cdot \det_{1\le i,j\le k} \left[ \frac{J_\nu\Big(\frac{y_i}{b}\sqrt{\xi/\hat{\alpha}}\Big) J_{\nu+1}\Big(\frac{y_j}{b}\sqrt{\xi/\hat{\alpha}}\Big) - (i \leftrightarrow j)}{y_i - y_j} \right] \tag{4.4.11}$$

The corresponding results for $\beta = 1, 4$ are given in terms of a Pfaffian of a matrix kernel [101], and for a discussion of a relation between the three universal kernels we refer to [107].

A feature we observe for all three $\beta$ is that for $\hat{\alpha} \le \mathcal{O}(1)$ the oscillations of the Bessel density are completely smoothed out, apart from the first peak. A similar feature was observed in a generalization of the unitary WL ensemble for critical statistics [99]. However, no power law tails seem to be present in such a model where only the generalized microscopic density and number variance were computed.

It is known that for standard WL the maxima of the Bessel density correspond to the location of individual eigenvalues [110], as we will see in the next subsection. On the other hand the microscopic density of the WL ensembles in the bulk is completely flat, equalling $\frac{1}{\pi}$ in our normalization. We may thus suspect that in

the generalized model the bulk is approached much faster than in the standard WL, where localized maxima persist to $y \gg 10$. We therefore focus mainly on the first eigenvalue distribution in the generalized model which is the subject of the next subsection.

### 4.4.2 Generalized universal first eigenvalue distribution at the hard edge

The probability that the interval $(0, s]$ is empty of eigenvalues is defined as follows (see also chapter 2),

$$E_\gamma(s) \equiv \frac{1}{\mathcal{Z}_\gamma} \int_s^\infty d\lambda_1 \cdots d\lambda_N P_\gamma(\lambda_1, \ldots, \lambda_N) \tag{4.4.12}$$

$$= \int_0^\infty d\xi \; e^{-\xi} \; \xi^{\gamma-1} \frac{\mathcal{Z}(\xi)}{\Gamma(\gamma)\mathcal{Z}_\gamma} E(s;\xi) \tag{4.4.13}$$

where the gap probability of the WL ensembles is defined as

$$E(s;\xi) \equiv \frac{1}{\mathcal{Z}(\xi)} \int_s^\infty d\lambda_1 \cdots d\lambda_N P(\lambda_1, \ldots, \lambda_N; \xi) \tag{4.4.14}$$

Both quantities are normalized to unity at $s = 0$ and vanish at $s = \infty$. The distribution of the first eigenvalue $p(s)$ simply follows by differentiation.

$$p_\gamma(s) \equiv -\frac{\partial}{\partial s} E_\gamma(s) \tag{4.4.15}$$

and likewise for WL. In WL the gap probability $E(s)$ and the first eigenvalue distribution $p(s)$ are explicitly known and universal in the microscopic large-$N$ limit for all $\nu$ at $\beta = 2$, for odd values of $\nu$ and 0 at $\beta = 1$, and for $\nu = 0$ at $\beta = 4$. This has been shown by various authors independently [110; 111; 112; 113]. In some cases only finite-$N$ results are know in terms of a hypergeometric function of a matrix argument (see [114; 115] and appendix D), from which limits are difficult to extract.

Although $p(s)$ follows from $E(s)$, the most compact universal formulas are known directly for $p(s)$ for all three $\beta$ [110]. There, also the second and higher eigenvalue distributions are given, which we will not consider here.

We start once more with an explicit calculation for $\beta = 2$ and the Gaussian ensemble. At $\nu = 0$ the pre-exponential factor is absent and we have for WL with weight $\exp[-2n\lambda]$

$$E(s) \;=\; \frac{1}{\mathcal{Z}}\int_s^\infty d\lambda_1 \cdots d\lambda_N \exp\left[-2n\sum_{i=1}^N \lambda_i\right]\prod_{j>k}^N |\lambda_j - \lambda_k|^2 \;=\; \exp[-2nNs] \tag{4.4.16}$$

shifting all integration variables by $s$ and using the invariance of the Vandermonde determinant. This result is exact for any $N$ and identical to the properly rescaled large-$N$ result when keeping $Ns$ fixed.

The generalized ensemble follows easily, by inserting this result into eq. (4.4.13)

$$E_\gamma(s) \;=\; \int_0^\infty d\xi\; e^{-\xi}\;\xi^{\gamma-1}\frac{\mathcal{Z}(\xi)}{\Gamma(\gamma)\mathcal{Z}_\gamma}\exp\left[-\frac{2n\xi Ns}{\gamma}\right] \;=\; \left(1+\frac{2nNs}{\gamma}\right)^{-(\gamma-N^2)} \tag{4.4.17}$$

which is also exact for finite and infinite $N$. This very fact implies that we have full control of the large-$N$ limit.

Now, the microscopic limit can be taken following eq. (4.4.1) for WL:

$$\mathcal{E}_\nu^{(\beta)}(y) \;\equiv\; \lim_{N\to\infty} E\left(\frac{y}{4N^2}\langle\lambda\rangle\right) \tag{4.4.18}$$

where we explicitly indicate the dependence on $\beta$ and $\nu$, as in the previous subsection. As a result we obtain for $\beta = 2$ and $\nu = 0$

$$\mathcal{E}_{\nu=0}^{(2)}(y) \;=\; \exp\left[-\frac{1}{4}y\right] \tag{4.4.19}$$

and for the corresponding generalized gap probability

$$\mathcal{E}_{\hat\alpha,\,\nu=0}^{(2)}(y) \equiv \lim_{N,\gamma\to\infty} E_\gamma\left(\frac{y}{4N^2b^2}\langle\lambda\rangle_\gamma\right) \;=\; \left(1+\frac{y}{4\hat\alpha b^2}\right)^{-(\hat\alpha+1)} \tag{4.4.20}$$

The first eigenvalue distribution can be compared to the microscopic densities $\vartheta_{\hat\alpha}(y)$ in squared variables:

$$\wp_{\nu=0}^{(2)}(y) \;\equiv\; -\frac{\partial}{\partial y}\mathcal{E}_0^{(2)}(y^2) \;=\; \frac{1}{2}|y|\exp\left[-\frac{1}{4}y^2\right] \tag{4.4.21}$$

for WL, and for the generalized ensemble

$$\wp_{\hat\alpha,\,\nu=0}^{(2)}(y) \;\equiv\; -\frac{\partial}{\partial y}\mathcal{E}_{\hat\alpha,0}^{(2)}(y^2) \;=\; |y|\,\frac{(\hat\alpha+1)}{2\hat\alpha b^2}\left(1+\frac{y^2}{4\hat\alpha b^2}\right)^{-(\hat\alpha+2)} \tag{4.4.22}$$

These distributions are all normalized to unity,

$$\int_0^\infty dy\ \wp^{(\beta)}_{\hat\alpha,\nu}(y) \ = \ 1 \tag{4.4.23}$$

The restriction to a confining potential $V(\lambda) = \lambda$ in the discussion above can be lifted, as the first eigenvalue distributions for all $\nu$ are universal, including the ratio of partition functions that we have inserted again. Eqs. (4.4.21) and (4.4.22) are compared to the corresponding densities eqs. (4.4.4) and (4.4.7) in fig. 4.3 for various values of $\hat\alpha$.

Next we give the first eigenvalue distribution for general $\nu$. Here we directly use the most compact universal expression [110] for $\wp^{(2)}_\nu(y)$ in WL, without making the detour over $\mathcal{E}^{(2)}(y)$ [113],

$$\wp^{(2)}_\nu(y) \ = \ \frac{1}{2}|y| \exp\left[-\frac{1}{4}y^2\right] \det_{1\le i,j\le\nu}\left[I_{i-j+2}(|y|)\right] \tag{4.4.24}$$

In addition to the exponential in eq. (4.4.21) it contains a determinant of finite size $\nu\times\nu$ over the modified Bessel-$I$ function, which is absent at $\nu = 0$. Knowing that the properly rescaled microscopic gap probability is a function of the form $\mathcal{E}^{(2)}_\nu(y;\xi) = \mathcal{E}^{(2)}_\nu(\sqrt{\xi y/\hat\alpha b^2})$, see eq. (4.4.7), we obtain for the generalized first eigenvalues distribution in terms of squared eigenvalues

$$\begin{aligned}\wp^{(2)}_{\hat\alpha,\nu}(y) &= \frac{1}{\Gamma(\hat\alpha+1)}\int_0^\infty d\xi\ e^{-\xi}\ \xi^{\hat\alpha}(-)\frac{\partial}{\partial y}\mathcal{E}^{(2)}(y\sqrt{\xi/\hat\alpha b^2}) \\ &= \frac{1}{\Gamma(\hat\alpha+1)}\int_0^\infty d\xi\ e^{-\xi}\ \xi^{\hat\alpha}\frac{\xi|y|}{2\hat\alpha b^2}\exp\left[-\frac{\xi y^2}{4\hat\alpha b^2}\right]\det_{1\le i,j\le\nu}\left[I_{i-j+2}\Big(\frac{|y|}{b}\sqrt{\xi/\hat\alpha}\Big)\right]\end{aligned} \tag{4.4.25}$$

For $\nu = 1$, the integral contains only one Bessel-$I$ and can be evaluated in terms of a hypergeometric function

$$\begin{aligned}\wp^{(2)}_{\hat\alpha,1}(y) &= \frac{|y|}{2\hat\alpha b^2\Gamma(\hat\alpha+1)}\int_0^\infty d\xi\ e^{-\xi}\ \xi^{\hat\alpha+1}\exp\left[-\frac{\xi y^2}{4\hat\alpha b^2}\right]I_2\Big(\frac{y}{b}\sqrt{\xi/\hat\alpha}\Big) \\ &= \frac{\Gamma(\hat\alpha+3)}{|y|\Gamma(\hat\alpha+1)}\left(1+\frac{y^2}{4\hat\alpha}\right)^{-(\hat\alpha+3)}\ {}_1F_1\left(\hat\alpha+3,3;\left(1+\frac{4\hat\alpha}{y^2}\right)^{-1}\right)\end{aligned} \tag{4.4.26}$$

It is shown in fig. 4.4 (middle), together with $\nu = 2$ (right). For increasing $\nu$ however, the integral representation eq. (4.4.25) is more convenient.

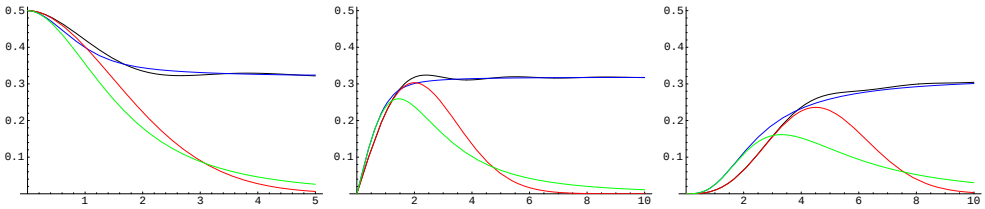

Figure 4.5: Varying $\nu$ for $\beta = 1$: the generalized microscopic density $\vartheta^{(1)}_{\hat{\alpha},\nu}(y)$ (blue) with its first eigenvalue (green) at $\hat{\alpha} = 0.1$ vs the corresponding WL Bessel density $\vartheta^{(1)}_{\nu}(y)$ eq. (4.4.9) (black) and its first eigenvalue (red) at $\nu = 0$ (left), $\nu = 1$ (middle), and $\nu = 3$ (right).

We now turn to $\beta = 1$. Here the first eigenvalue distribution of the WL ensembles is only known explicitly for odd values of $\nu$ in the large-$N$ limit [110], given by a Pfaffian with indices running over half integers:

$$\wp^{(1)}_{\nu}(y) \;=\; const.\; |y|^{(3-\nu)/2} \exp\left[-\frac{1}{8}y^2\right] \mathrm{Pf}_{-\frac{\nu}{2}+1\le i,j\le \frac{\nu}{2}-1}\left[(i-j)I_{i+j+3}(|y|)\right] \tag{4.4.27}$$

The constant in front is determined by the normalization to unity and can be computed case by case. An exception is $\nu = 0$ where the distribution was calculated in [111]

$$\wp^{(1)}_{0}(y) \;=\; \frac{1}{4}(2+|y|)\exp\left[-\frac{|y|}{2}-\frac{y^2}{8}\right] \tag{4.4.28}$$

For $\nu = 1$ and 3 we have from eq. (4.4.27)

$$\wp^{(1)}_{1}(y) \;=\; \frac{1}{4}|y|\exp\left[-\frac{1}{8}y^2\right] \tag{4.4.29}$$

$$\wp^{(1)}_{3}(y) \;=\; \frac{1}{2}\exp\left[-\frac{1}{8}y^2\right] I_3(|y|) \tag{4.4.30}$$

The corresponding generalized formula for general odd $\nu$ thus reads

$$\begin{aligned}\wp^{(1)}_{\hat{\alpha},\nu}(y) \;=\; const.\; \frac{1}{\Gamma(\hat{\alpha}+1)}\int_0^\infty d\xi\; e^{-\xi}\,\xi^{\hat{\alpha}}\sqrt{\frac{\xi}{\hat{\alpha}b^2}}\left(\frac{|y|}{b}\sqrt{\frac{\xi}{\hat{\alpha}}}\right)^{(3-\nu)/2}\exp\left[-\frac{1}{8\hat{\alpha}b^2}\xi y^2\right]\\ \cdot\,\mathrm{Pf}_{-\frac{\nu}{2}+1\le i,j\le\frac{\nu}{2}-1}\left[(i-j)I_{i+j+3}\Big(\frac{|y|}{b}\sqrt{\xi/\hat{\alpha}}\Big)\right]\end{aligned} \tag{4.4.31}$$

up to the normalization constant. For the simplest examples $\nu = 0, 1$ and 3 displayed in fig. 4.5 we have

$$\begin{aligned}
\wp^{(1)}_{\hat{\alpha},0}(y) &= \frac{1}{4\sqrt{\hat{\alpha}}\,\Gamma(\hat{\alpha}+1)b}\int_0^\infty d\xi\; e^{-\xi}\xi^{\hat{\alpha}+\frac{1}{2}}\Big(2+\frac{|y|}{b}\sqrt{\frac{\xi}{\hat{\alpha}}}\Big)\exp\left[-\frac{|y|}{2b}\sqrt{\frac{\xi}{\hat{\alpha}}}-\frac{\xi y^2}{8\hat{\alpha}b^2}\right]\\
\wp^{(1)}_{\hat{\alpha},1}(y) &= \frac{(\hat{\alpha}+1)}{4\hat{\alpha}b^2}\,|y|\left(1+\frac{y^2}{8\hat{\alpha}b^2}\right)^{-(\hat{\alpha}+2)}\\
\wp^{(1)}_{\hat{\alpha},3}(y) &= \frac{1}{\Gamma(\hat{\alpha}+1)}\int_0^\infty d\xi\; e^{-\xi}\;\xi^{\hat{\alpha}}\sqrt{\frac{\xi}{\hat{\alpha}b^2}}\frac{1}{2}\exp\left[-\frac{\xi y^2}{8\hat{\alpha}b^2}\right]I_3\Big(\frac{|y|}{b}\sqrt{\xi/\hat{\alpha}}\Big)
\end{aligned}$$

While the density is modified only rather mildly compared to WL, the first eigenvalue changes considerably. We have checked that the curves converges to WL for large $\hat{\alpha}$, where the convergence to the density is much faster than for $\beta = 2$. The case $\nu = 0$ in fig. 4.5 (left) is the only example where the microscopic densities do not vanish at $x = 0$. The fact that they both have the same limit $\frac{1}{2}$ can also be seen analytically, exploiting that $J_\nu(0) = \delta_{\nu,0}$ (see eqs. (4.4.9) and following). As mentioned above for $\nu = 2k$ with $k \in \mathbb{N}_+$ the first eigenvalue is not available to date.

Finally we turn to $\beta = 4$. In principle the result is known in the WL ensemble,

$$\wp^{(4)}_0(y) \;=\; const.\;\; |y|^{\nu+\frac{3}{2}}\exp\left[-\frac{1}{2}y^2\right]Z_{3/2}(\{|y|\}_{2\nu+1}) \tag{4.4.32}$$

Here $Z_{3/2}(\{y\}_{2\nu+1})$ is the large-$N$ matrix model partition function at topological charge 3/2 with $2\nu+1$ degenerate masses at value $y$, and we refer to [110] for a more detailed discussion of these objects. This partition function is generally known explicitly only for an even number of masses, except at $\nu = 0$. There we have

$$\wp^{(4)}_0(y) \;=\; \frac{1}{2}\sqrt{2\pi}\,|y|^{\frac{3}{2}}\exp\left[-\frac{1}{2}y^2\right]I_{3/2}(y) \;=\; |y|\,\Big(\cosh(y)-\frac{1}{y}\sinh(y)\Big)\exp\left[-\frac{1}{2}y^2\right] \tag{4.4.33}$$

Thus the generalized distribution depicted in fig. 4.6 is given by

$$\begin{aligned}
\wp^{(4)}_0(y) = \frac{1}{\hat{\alpha}\Gamma(\hat{\alpha}+1)b^2}\int_0^\infty d\xi\; e^{-\xi}\;\xi^{\hat{\alpha}+1}\cdot\\
\cdot\left(|y|\cosh\Big(\frac{y}{b}\sqrt{\xi/\hat{\alpha}}\Big)-b\sqrt{\frac{\hat{\alpha}}{\xi}}\sinh\Big(\frac{|y|}{b}\sqrt{\xi/\hat{\alpha}}\Big)\right)\exp\left[-\frac{\xi y^2}{2\hat{\alpha}b^2}\right]
\end{aligned} \tag{4.4.34}$$

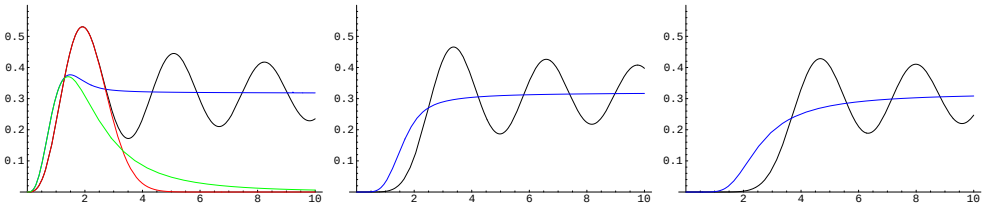

Figure 4.6: Varying $\nu$ for $\beta = 4$: the generalized microscopic density $\vartheta^{(4)}_{\hat{\alpha},\nu}(y)$ (blue) at $\hat{\alpha} = 0.1$ vs the corresponding WL Bessel density $\vartheta^{(4)}_{\nu}(y)$ eq. (4.4.10) (black) at $\nu = 0$ (left), $\nu = 1$ (middle), and $\nu = 2$ (right). For $\nu = 0$ we also display the respective first eigenvalue for the generalized (green) and WL ensemble (red).

We note that the oscillations get smoothed out as already observed at $\beta = 2$. The convergence in $\hat{\alpha}$ to the WL quantity is again slow, as for $\beta = 2$.

## 4.5 The generalized Wigner's surmise in the bulk

In this section we study the spacing distribution between eigenvalues in the bulk in our generalized model. In contrast to the previous sections we do not take $N$ to be large, but use the $N = 2$ results, following the original idea of Wigner.

In the Wigner-Dyson ensembles with a Gaussian potential, the spacing distribution has the simple form (see (2.4.5))

$$\mathcal{P}^{(\beta)}_{\mathrm{G}}(s) \;=\; A s^{\beta} e^{-Bs^2} \tag{4.5.1}$$

known as Wigner's surmise. The known constants $A, B$ follow from normalization. For the WL case the corresponding expression can be computed from the jpdf (2.4.7), where we have introduced the notation $\bar{\nu} = \frac{\beta}{2}(\nu + 1) - 1$:

$$\mathcal{P}^{(\beta)}(s) = C s^{\beta+\bar{\nu}+1/2} K_{-1/2-\bar{\nu}}(n\beta s) \tag{4.5.2}$$

where $K_{\mu}(x)$ is a modified Bessel function and the constant $C$ is given by:

$$C = \left( 2^{-1/2+\beta+\bar{\nu}} (n\beta)^{-3/2-\beta-\bar{\nu}} \Gamma\left(\frac{1+\beta}{2}\right) \Gamma\left(1 + \bar{\nu} + \frac{\beta}{2}\right) \right)^{-1} \tag{4.5.3}$$

Only for $\bar{\nu} = 0$, one recovers the Wigner's surmise, using $K_{-1/2}(x) = \sqrt{\pi/2x}\, e^{-x}$ (apart from squared variables in the exponent there). For general $\bar{\nu}$ one easily gets

an exponential decay for large spacing $\sim s^{\beta+\bar{\nu}}e^{-n\beta s}$, from the asymptotic expression of the Bessel function. However, we expect that only the $\bar{\nu}=0$ expression will lead to a good approximation of the infinite-$N$ case.

Conversely, for the generalized model the spacing distribution has a different expression:

$$\mathcal{P}_{\gamma}^{(\beta)}(s) = C_{\gamma} s^{\beta+\bar{\nu}} \left(\frac{\gamma}{2n\beta}+\frac{s}{2}\right)^{\bar{\nu}+1-\gamma} {}_2F_1\left(-\bar{\nu},\bar{\nu}+1;-\bar{\nu}+\gamma;\frac{1}{2}-\frac{\gamma}{2n\beta s}\right) \tag{4.5.4}$$

where ${}_2F_1(a,b;c;z)$ is a hypergeometric function. The constant $C_\gamma$ can be computed as

$$C_{\gamma} = \frac{2^{1-\gamma}B(\bar{\nu}+1,-2\bar{\nu}-1+\gamma)\Gamma(\gamma)\Gamma(1+\beta/2)}{\Gamma(\bar{\nu}+1)\Gamma(1+\beta)\Gamma(\bar{\nu}+1+\beta/2)\Gamma(\gamma-2-\beta-2\bar{\nu})}\left(\frac{n\beta}{\gamma}\right)^{2+2\bar{\nu}+\beta-\gamma} \tag{4.5.5}$$

where $B(\alpha,\beta)$ is a Beta function. The large-$s$ decay is now a pure power law $\sim s^{-(\varpi+1)}$ where we have defined

$$\varpi \;\equiv\; \gamma-\beta-2\bar{\nu}-2 \;>\; 0 \tag{4.5.6}$$

required to be positive for convergence[1].

For $\bar{\nu}=0$, the spacing distribution takes a much simpler form:

$$\mathcal{P}_{\gamma}^{(\beta)}(s) \;=\; \frac{n(n\beta/\gamma)^{\beta}\Gamma(\gamma-1)}{\gamma\Gamma(\beta)\Gamma(\gamma-\beta-2)}\, s^{\beta}\left(1+\frac{sn\beta}{\gamma}\right)^{1-\gamma} \tag{4.5.7}$$

It agrees with the corresponding quantity in the generalized WD ensembles found in [37]. In this particular case, we can compute the mean level spacing explicitly:

$$\langle\langle s\rangle\rangle_{\gamma} = \int_0^{\infty} s\; \mathcal{P}_{\gamma}^{(\beta)}(s)ds = \left(\frac{\gamma}{n\beta}\right)\frac{1+\beta}{\gamma-\beta-3} \tag{4.5.8}$$

which converges to the WL Wigner surmise value for $\gamma\to\infty$:

$$\langle\langle s\rangle\rangle = \int_0^{\infty} s\; \mathcal{P}^{(\beta)}(s)ds = \frac{1+\beta}{n\beta} \tag{4.5.9}$$

After defining the rescaled quantities having mean spacing 1,

$$\hat{\mathcal{P}}_{\gamma}^{(\beta)}(x) = \langle\langle s\rangle\rangle_{\gamma}\mathcal{P}_{\gamma}^{(\beta)}\Big(\langle\langle s\rangle\rangle_{\gamma}x\Big) \tag{4.5.10}$$

$$\hat{\mathcal{P}}^{(\beta)}(x) = \langle\langle s\rangle\rangle\mathcal{P}^{(\beta)}\Big(\langle\langle s\rangle\rangle x\Big) \tag{4.5.11}$$

[1]This condition coincides with eq. (4.2.2) derived for the partition function at $N=2$.

we can compare the curves for all three $\beta$ at $\bar{\nu} = 0$ (and $n = 1$), in fig. 4.7. The power-law tail modification compared to the standard WL spacing distribution is evident in the plots. Because in the large-$N$ limit $\gamma$ scales with $N$, we keep the combination $\varpi$ in eq. (4.5.6) fixed to be able to compare to spacing distributions at large-$N$.

Both in this and the previous section the power-law tail of the macroscopic density is seen to persist on the microscopic level of the mean level-spacing. It would be very interesting to confirm this on real data sets.

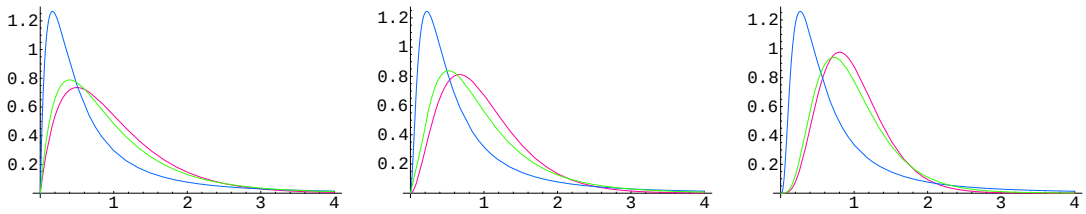


Figure 4.7: Comparison between $\hat{\mathcal{P}}_{\gamma}^{(\beta)}(x)$ (blue, green) and $\hat{\mathcal{P}}^{(\beta)}(x)$ (red), for $\beta = 1, 2, 4$ (from left to right). The $\gamma$ value for the blue curves is chosen is chosen in such a way that the combination $\varpi$ is kept constant to the value 2. The green curves have value $\gamma = 12, 12, 25$ from left to right, and correctly approach the limiting WL curve.

## 4.6 Summary and outlook

In this chapter, we have considered a generalization of the standard WL or chiral ensembles of random matrices, replacing the exponential of a polynomial potential by a fat-tailed distribution with parameter $\gamma$. In the limit $\gamma \to \infty$ we can recover the exponential and thus the standard ensembles. This modification led to the appearance of power law distributions governed by a single parameter. Such a behavior is found in many systems in nature, e.g. in the wide area of complex networks. WL ensembles are often used as a 'null' model, whose spectral properties can be compared with covariance matrices of real data sets. To illustrate the potential of our results we show a comparison to financial data in fig. 4.8.

The eigenvalues of the covariance matrix from time series of stock data clearly show power law behavior. These are well described by our generalized Marčenko-Pastur density, refining previous comparisons to the standard Marčenko-Pastur law.

The solution of our generalized model relied heavily on the possibility of writing it as an integral transform of the standard WL ensembles. This generalization is thus in the spirit of superstatistics, where other models have been constructed already. The virtue of our model is its invariance for all three symmetry classes, allowing to go to an eigenvalues basis and to study universality. We could show that while the macroscopic density was only weakly universal, all microscopic densities were universal under any invariant deformations by polynomial potentials. This macroscopic/microscopic dichotomy should not come as a surprise, being observed previously for restricted trace ensembles.

We exploited the linear relation to standard WL by solving our model exactly at finite-$N$ for any polynomial potential, using the formalism of orthogonal polynomials therein. In the subsequent large-$N$ double scaling limit, where $\gamma$ is scaled with $N$, we derived all density correlations in the macroscopic limit, and the microscopic limit at the hard edge for all three $\beta$. We have mainly focused on the spectral density itself and the first eigenvalue distribution. The general formalism for higher density or individual eigenvalue correlation functions was provided and is straightforward to use if such quantities will be needed.

While the hard edge was solved exhaustively, persisting in our model for asymptotically quadratic matrices, we only provided the Wigner's surmise in the bulk. Here, more detailed correlation functions could be investigated, including a possible generalization of the Tracy-Widom distribution at the soft edge. This is left for future investigations.

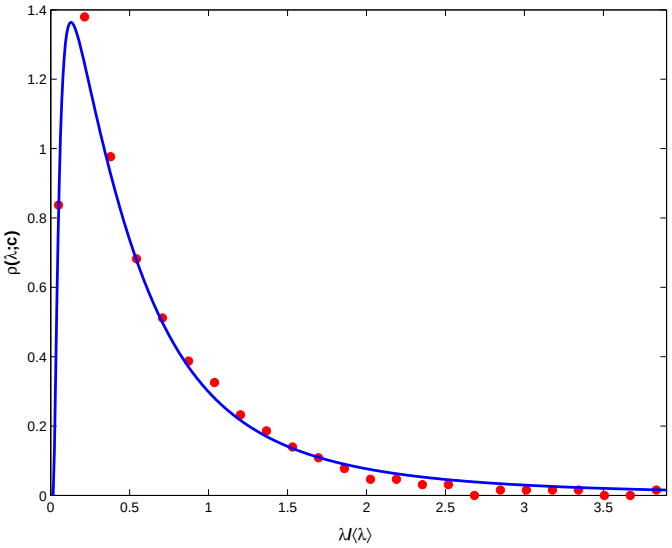


Figure 4.8: Comparison between the rescaled eigenvalue distribution from financial data [116] and the macroscopic density for the generalized model (4.3.8), in red dots and solid blue respectively. The best fit gives a value of $\hat{\alpha} \approx 0.95$, which corresponds to a power-law decay as $\rho_{\hat{\alpha}}(x) \approx \hat{\alpha}^{-2.95}$.

*Research is to see what everybody else has seen, and to think what nobody else has thought.*

ALBERT SZENT-GYÖRGI

# Chapter 5

# Quantum conductance: the Jacobi ensemble

## 5.1 The scattering theory framework

Conductance in mesoscopic systems is currently a very active area of research, both from the theoretical and the experimental point of view. A common experimental setting is the so-called *quantum dot*, 'a cavity of sub-micron dimensions, etched in a semiconductor' [11]. This cavity is coupled to two electronic reservoirs, and then brought out of equilibrium by passing a current through the system. A statistical theory of electronic transport within the cavity has been formulated independently by Landauer, Imry and Büttiker and a comprehensive account is provided in [11].

If we imagine that $N_1$ and $N_2$ electronic channels are lodged in each of the two attached leads, the main object to consider is the scattering matrix $S$:

$$S = \begin{pmatrix} r & t' \\ t & r' \end{pmatrix} \tag{5.1.1}$$

This is a unitary matrix with a block structure, which encodes the linear transformation law between the incoming and the outgoing electronic wave function coefficients in a given basis. The submatrices $r, r'$ represent the reflection (left-left and right-right) respectively, while $t, t'$ are transmission matrices (from left to right and from right to left, respectively).

Unitarity $S^{-1} = S^\dagger$ is implied by current conservation: as a consequence, the Hermitian matrices $tt^\dagger$, $t't'^\dagger$, $1 - rr^\dagger$ and $1 - r'r'^\dagger$ all share the same set of eigenvalues $T_1, \ldots, T_N$ (where $N = \min(N_1, N_2)$), which are real number between 0 and 1.

Many quantities of interest for the experiments can be extracted from the knowledge of the transmission eigenvalues $\{T_i\}$: in the following we will mainly focus on moments of the form $\mathcal{T}_m = \mathrm{Tr}(tt^\dagger)^m$. In particular, the first two moments are related to the average dimensionless conductance ($G/G_0 = \mathcal{T}_1$) thanks to the Landauer-Büttiker formula [117], and to the average shot noise ($P/P_0 = \mathcal{T}_1 - \mathcal{T}_2$) [118]. These quantities will be introduced in more detail in next section.

As long as one is interested in *universal* properties of quantum transport in chaotic cavities, i.e. those which do not depend much on the sample size or the amount of disorder, it comes as no surprise that RMT sets in quite naturally.

The starting point is the assumption that the relevant statistical properties of transmission eigenvalues depend only on few general symmetry requirements, and are essentially insensitive to the fine details of the scattering matrix $S$. This leads immediately to the postulate that $S$ is just a random unitary matrix distributed *uniformly* in the unitary group: no other constraint needs to be imposed if time-reversal symmetry is broken ($\beta = 2$), whereas $S$ must be also symmetric ($\beta = 1$) or self-dual ($\beta = 4$) if time-reversal symmetry is present, and spin-rotation symmetry is present or absent respectively.

The postulate of uniform distribution of $S$ within the unitary group is consistent with a maximum entropy approach *à la* Balian [119], where one seeks for a distribution $P(S)$ within the unitary group that maximizes the information entropy:

$$\mathcal{S} = -\int d\mu(S) P(S) \ln P(S) \tag{5.1.2}$$

given some constraints[1] ($\mu(S)$ being the Haar measure of the group). The only requirements of symmetry ($\beta = 1$) or self-duality ($\beta = 4$) lead to the condition $P(S) = \text{const}$ which characterizes Dyson's circular ensembles [2; 120].

[1] A similar approach (using Tsallis' entropy) can be used to derive the probability density in (4.2.1).

Additional constraints, leading to more intricate distributions on the unitary group, have been considered in the literature: in particular, the so-called *Poisson kernel*

$$P(S) \propto |\det(I - \bar{S}^\dagger S)|^{-\beta(N_1+N_2-1+2/\beta)} \tag{5.1.3}$$

generalizes the circular ensemble to the case of non-zero average scattering matrix $\bar{S}$ and has proven useful for dealing with chaotic cavities coupled to the leads with tunnel barriers [11].

In this chapter, we confine ourselves to the simplest case (equiprobability in matrix space), and derive exact expressions for i) the density of transmission eigenvalues at arbitrary number of open channels; ii) moments of transmission eigenvalues at arbitrary number of open channels, encoding the full counting statistics of the cavity; iii) large deviations for the probability distribution of conductance and shot noise in the limit of large number of channels [44].

## 5.2 Density of transmission eigenvalues for fixed and finite number of open channels

Suppose that one is interested in computing the average shot noise $\langle P \rangle$, where:

$$P = P_0 \sum_{p=1}^{N} T_p(1 - T_p), \qquad N = \min(N_1, N_2) \tag{5.2.1}$$

$P_0$ being a constant related to the physical properties of the conductor [121; 122; 123]. Within the random scattering matrix approach, this quantity is a random variable between 0 and $N/4$.

Until 2005, results for $\langle P \rangle$ were known only in the limiting cases $N_{1,2} \gg 1$ [11; 124; 125], $N_1 = N_2 = 1$ [126] or few open channels [127]. Very recently, a compact form has been found for $\langle P \rangle / P_0$ using two different methods, based on a semiclassical expansion [128] and on recurrence relations for the Selberg integral [129] (see also [130] for an alternative derivation). The latter nicely exploits the remarkably simple expression for the jpdf of transmission eigenvalues:

$$P_\beta(T_1, \ldots, T_N) = \mathcal{N}_\beta^{-1} \prod_{j<k} |T_j - T_k|^\beta \prod_{i=1}^{N} T_i^{\frac{\beta}{2}(|N_2-N_1|+1)-1}, \qquad 0 \le T_j \le 1 \tag{5.2.2}$$

where the normalization constant is given by [46; 129]:

$$\mathcal{N}_\beta = \prod_{j=0}^{N-1} \frac{\Gamma\left(1+\frac{\beta}{2}+j\frac{\beta}{2}\right)\Gamma\left(\frac{\beta}{2}(|N_2-N_1|+1)+j\frac{\beta}{2}\right)\Gamma\left(1+j\frac{\beta}{2}\right)}{\Gamma\left(1+\frac{\beta}{2}\right)\Gamma\left(\frac{\beta}{2}(|N_2-N_1|+1)+1+(N+j-1)\frac{\beta}{2}\right)} \tag{5.2.3}$$

A few comments about (5.2.2) are in order. The jpdf in (5.2.2) is stated in [11] without proof and attributed to Brouwer. A formal proof has been given (using three different methods) by Forrester [131] in 2006, where the author also highlighted the connection with the jpdf of the Jacobi ensemble of random matrices [46; 132]. In fact, one observes that the change of variables $y_j = 1 - 2T_j$ brings (5.2.2) to the form (see (2.4.11)):

$$P_\beta(y_1,\ldots,y_N) = \tilde{\mathcal{N}}_\beta^{-1} \prod_{j<k} |y_j - y_k|^\beta \prod_{i=1}^{N} (1-y_i)^{\frac{\beta}{2}(|N_2-N_1|+1)-1}, \qquad -1 \le y_j \le 1 \tag{5.2.4}$$

allowing to use the machinery and results already known from Random Matrix Theory.

In particular, the average density of transmission eigenvalues:

$$R_\beta(T;N_1,N_2) = \langle \sum_{i=1}^{N} \delta(T-T_i)\rangle = N \int_{[0,1]^{N-1}} dT_2 \ldots dT_N P_\beta(T,T_2,\ldots,T_N) \tag{5.2.5}$$

is of interest for computing linear statistics, i.e. observables of the form $\langle \mathrm{tr}\ a(tt^\dagger)\rangle$:

$$\langle \mathrm{tr}\ a(tt^\dagger)\rangle = \int_0^1 dT R_\beta(T;N_1,N_2) a(T) \tag{5.2.6}$$

where $a(x)$ is a given smooth function. The average of moments $\mathcal{T}_m$ for a real number $m$ can be computed in principle from the knowledge of the average density as:

$$\langle \mathcal{T}_m \rangle = \int_0^1 dT\ T^m R_\beta(T;N_1,N_2) \tag{5.2.7}$$

where the range for $m$ is constrained by the convergence of the integral. As already mentioned, the first two moments are directly related to the normalized conductance (a random variable between 0 and $N$) thanks to the Landauer-Büttiker formula, and to the shot noise. More generally, the moments are related to quantities more accessible to measurements, the charge cumulants $\langle\langle Q_n\rangle\rangle$,

which quantify the fluctuations in the amount of charge transmitted over an interval of time [133]:

$$\sum_{n=1}^{\infty} \frac{x^n}{n!} \langle\langle Q_n \rangle\rangle = -\sum_{m=1}^{\infty} \frac{(-1)^m}{m} \langle \mathcal{T}_m \rangle (e^x - 1)^m \tag{5.2.8}$$

Surprisingly, the connection with the Jacobi ensemble mentioned above has not been fully appreciated so far, with the consequence that the average spectral density $R_\beta(T; N_1, N_2)$ for *finite* and *arbitrary* number of open channels $(N_1, N_2)$ is still deemed unknown (see e.g. [129; 134]). On the other hand, the density is known in the above mentioned limiting cases [11; 127; 135; 136; 137].

In the mesoscopic literature the Jacobi ensemble is mentioned in the paper by Araújo and Macêdo [127], where the authors derived the average density of transmission eigenvalues *for a small number of open channels and* $\beta = 2$ using an auxiliary non-linear sigma model. Their result reads:

$$R_2(T; N_1, N_2 < 11) = T^\mu \sum_{n=0}^{N-1} (2n + \mu + 1) \{P_n^{(\mu,0)}(1 - 2T)\}^2 \tag{5.2.9}$$

where

$$\mu = \frac{\beta}{2}(|N_2 - N_1| + 1) - 1 = |N_2 - N_1| \tag{5.2.10}$$

$$N = \min(N_1, N_2) \tag{5.2.11}$$

and $P_n^{(\alpha,\beta)}(y)$ is a Jacobi polynomial.

The authors state in [127]:

> ...we believe (although we have no formal proof) that Eq. (5.2.9) is valid for arbitrary $N_1$ and $N_2$. This result is consistent with the random-matrix approach of Ref. [135; 136], which predicts for the same system a joint distribution of transmission eigenvalues given by the Jacobi ensemble, from which Eq. (5.2.9) can be derived. We have thus found independent evidence for the application of the Jacobi ensemble in this problem.

However, the invoked references [135; 136] do not mention the Jacobi ensemble, and work out the only case $N_1 = N_2$. More precisely:

1. Ref. [135] reports the jpdf (5.2.2) *restricted to the case* $N_1 = N_2$ *and* $\beta = 1, 2$. For the case $\beta = 2$, the term $T_i^{\frac{\beta}{2}(|N_2-N_1|+1)-1}$ in the jpdf (5.2.2) then disappears, making the use of Legendre polynomials appropriate. For this subcase, the authors derive the average density and the 2-point function, and finally take the large $N_1 = N_2$ limit to get the smoothed macroscopic density $R_2(T; N_1 = N_2 \gg 1) \approx N/\pi\sqrt{T(1-T)}$;

2. Ref. [136] deals with all symmetry classes $\beta = 1, 2, 4$ and considers the two cases $N_1 = N_2 \gg 1$ or $N_1 = N_2 = 1$. In the first subcase, the authors derive some quantities of interest with the use of a Coulomb gas approach after the change of variable $T_i = 1/(1+y_i)$, $y_i \in [0, \infty)$.

We wish to clarify that the average density of transmission eigenvalues for *any* $N_1$ and $N_2$ is exactly given by the density of the Jacobi ensemble, where the argument of the Jacobi polynomials is $1-2T$ (i.e. nothing but (5.2.9), for $\beta = 2$), and this result descends from the application of the standard Orthogonal Polynomial Technique (see [46; 138] and Chapter 2) to the (modified) jpdf (5.2.4). In fact, the Jacobi polynomials $P_n^{(\mu,0)}$ appearing in (5.2.9) are precisely *the* orthogonal polynomials over $[-1, 1]$ with respect to the weight $(1-y)^\mu$ in (5.2.4). The cases $\beta = 1$ and $\beta = 4$ are more complicated, but can be tackled in the same framework (see [139] and references therein). Also, $n$-th order correlation functions can be derived for all three symmetry classes [46; 139]. For example, for $\beta = 2$ one defines the kernel (see [46] - Sections 5.7 and 19.1, and chapter 2):

$$K_N(x,y) = x^{\mu/2} y^{\mu/2} \sum_{n=0}^{N-1} (2n+\mu+1) P_n^{(\mu,0)}(1-2x) P_n^{(\mu,0)}(1-2y) \tag{5.2.12}$$

and the $n$-th order correlation function is written in terms of the $(n \times n)$ determinant:

$$\begin{aligned} R_2(T_1, \ldots, T_n) &= \frac{N!}{(N-n)!} \int_{[0,1]^{N-n}} dT_{n+1} \ldots dT_N P_\beta(T_1, \ldots, T_N) \\ &= \det[K_N(T_j, T_k)]_{1 \le j,k \le n} \end{aligned} \tag{5.2.13}$$

In particular, the average spectral density (1-point function) is exactly given by:

$$R_2(T; N_1, N_2) = T^\mu \sum_{n=0}^{N-1} (2n+\mu+1) \{P_n^{(\mu,0)}(1-2T)\}^2 \tag{5.2.14}$$

extending the result (5.2.9) to an arbitrary number of open channels. In Appendix E, we will show that for $\mu \to 0$ eq. (5.2.14) recovers the result by Baranger and Mello [135].

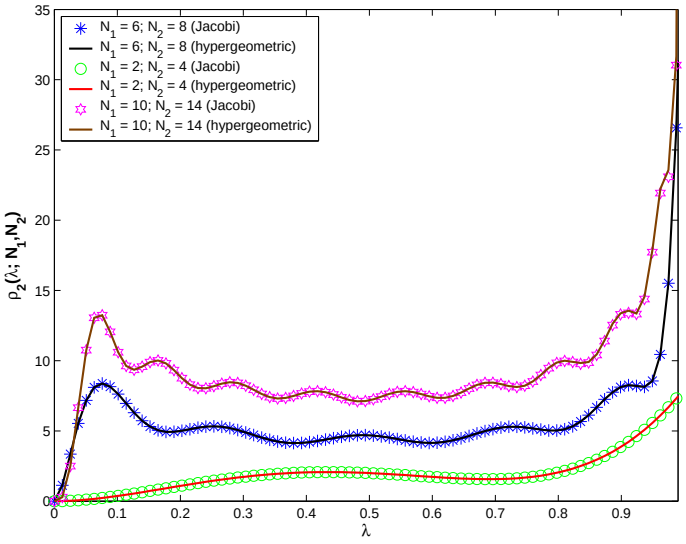


Figure 5.1: Density of transmission eigenvalues for $\beta = 2$ and different values for the pair $(N_1, N_2)$. The plot symbols are used for RMT formula (5.2.14), whereas solid lines represent the alternative formula (5.2.21)

We can also derive an alternative expression for the average density of transmission eigenvalues and higher order correlation functions for *finite* $N_1$ and $N_2$ and $\beta = 2, 4$, starting from the jpdf (5.2.2). Exploiting a variant of the Selberg integral evaluated by Kaneko [140], all correlation functions can be expressed in terms of a hypergeometric function of a matrix argument, instead of a determinant of a kernel as in (5.2.13) (for $\beta = 2$).

Consider again the joint probability density of transmission eigenvalues (5.2.2):

$$P_\beta(T_1, \ldots, T_N) = \mathcal{N}_\beta^{-1} \prod_{j<k} |T_j - T_k|^\beta \prod_{i=1}^{N} T_i^{\frac{\beta}{2}(|N_2 - N_1|+1)-1}, \qquad 0 \le T_j \le 1 \quad (5.2.15)$$

where $N = \min(N_1, N_2)$, $\beta = 1, 2, 4$ and the normalization constant is given by (5.2.3).

The density of eigenvalues is given by the following multiple integral:

$$R_\beta(T_1; N_1, N_2) = N \int_0^1 \dots \int_0^1 dT_2 \dots dT_N \; P_\beta(T_1, \dots, T_N) \tag{5.2.16}$$

such that the normalization $\int_0^1 R_\beta(T; N_1, N_2) dT = N$ holds (where again $N = \min(N_1, N_2)$).

It turns out that the integral above can be evaluated without the use of the Orthogonal Polynomial technique, which would lead to the formula (5.2.14), if one resorts to the following extension of Selberg integral given by Kaneko [140]:

$$\int_{[0,1]^n} \prod_{j=1}^n dx_j \prod_{j=1}^n x_j^{\ell_1}(1-x_j)^{\ell_2} \prod_{\substack{1\le i\le n \\ 1\le k\le m}} (x_i - t_k) \prod_{j<k} |x_j - x_k|^\beta = C_1 \; {}_2F_1^{(\beta/2)}\left(-n, \frac{2}{\beta}(\ell_1+\ell_2+m+1)+n-1; \frac{2}{\beta}(\ell_1+m); \{t_1, \dots, t_m\}\right), \tag{5.2.17}$$

where $C_1$ is a known constant and ${}_2F_1^{(\alpha)}$ is a hypergeometric function of a matrix argument. Details about these objects are provided in the appendix D.

From (5.2.16), one has:

$$R_\beta(T_1; N_1, N_2) = \frac{N T_1^{\frac{\beta}{2}(|N_2-N_1|+1)-1}}{\mathcal{N}_\beta} \int_{[0,1]^{N-1}} dT_2 \dots dT_N \prod_{j<k} |T_j - T_k|^\beta \cdot \prod_{i=2}^N T_i^{\frac{\beta}{2}(|N_2-N_1|+1)-1} \tag{5.2.18}$$

Now, the Vandermonde coupling can be decomposed as:

$$\prod_{j<k} |T_j - T_k|^\beta = \prod_{j<k, j=2} |T_j - T_k|^\beta \prod_{j=2}^N |T_1 - T_j|^\beta \tag{5.2.19}$$

and, for $\beta = 2, 4$ the absolute value in all products is immaterial. Hence:

$$R_\beta(T_1; N_1, N_2) = \frac{N T_1^{\frac{\beta}{2}(|N_2-N_1|+1)-1}}{\mathcal{N}_\beta} \int_{[0,1]^{N-1}} dT_2 \dots dT_N \prod_{j<k, j=2} |T_j - T_k|^\beta \cdot \prod_{i=2}^N T_i^{\frac{\beta}{2}(|N_2-N_1|+1)-1} \prod_{j=2}^N (T_j - T_1)^\beta \tag{5.2.20}$$

Comparing (5.2.20) and (5.2.17), after the following identification:

$$\begin{cases} n &= N-1 \\ \ell_1 &= \frac{\beta}{2}(|N_2-N_1|+1)-1 \\ \ell_2 &= 0 \\ t_k &= T_1 \qquad k=1,\dots,m \\ m &= \beta \end{cases}$$

one eventually obtains:

$$R_\beta(T_1;N_1,N_2) = \frac{N\ C_1\ T_1^{\frac{\beta}{2}(|N_2-N_1|+1)-1}}{\mathcal{N}_\beta} \cdot\ {}_2F_1^{(\beta/2)}\left(1-N,|N_2-N_1|+N+1;|N_2-N_1|+3-2/\beta;T_1\mathbf{1}_\beta\right) \quad (5.2.21)$$

where we have introduced a customary matrix notation in the last argument of the hypergeometric function. Note that the result (5.2.21) is still formally valid for any even integer $\beta$.

We also observe that higher order correlation functions can be easily written down, exploiting the very same eq. (5.2.17). For example, the two-point function $R_\beta^{(2)}(T_1,T_2;N_1,N_2)$ can be written (ignoring prefactors) as:

$$\begin{aligned} R_\beta^{(2)}(T_1,T_2;N_1,N_2) \propto\ & (T_1T_2)^{\frac{\beta}{2}(|N_2-N_1|+1)-1}|T_2-T_1|^\beta \\ & \cdot \int_{[0,1]^{N-2}} dT_3\dots dT_N \prod_{i=3} T_i^{\frac{\beta}{2}(|N_2-N_1|+1)-1} \prod_{j<k,j=3} |T_j-T_k|^\beta \\ & \cdot \prod_{j=3}^{N}|T_j-T_1|^\beta \prod_{j=3}^{N}|T_j-T_2|^\beta \end{aligned} \quad (5.2.22)$$

and the $(N-2)$-fold integral is again of the same form as (5.2.17) for the following values of parameters:

$$\begin{cases} n &= N-2 \\ \ell_1 &= \frac{\beta}{2}(|N_2-N_1|+1)-1 \\ \ell_2 &= 0 \\ t_k &= T_1 \qquad k=1,\dots,\beta \\ t_k &= T_2 \qquad k=\beta+1,\dots,2\beta \\ m &= 2\beta \end{cases}$$

Hence, this time the matrix argument of the hypergeometric function is $\mathbf{X}^{(2)} := \mathrm{diag}\left(\underbrace{T_1,\dots,T_1}_{\beta\text{ times}},\underbrace{T_2,\dots,T_2}_{\beta\text{ times}}\right)$. Note that the 2-point correlation function

$R_\beta^{(2)}(T_1, T_2; N_1, N_2)$ is manifestly symmetric in the two arguments as it should, due to the symmetry of Jack polynomials (see appendix D). It is worth mentioning that higher order correlation functions can be written down easily along the same lines.

Thanks to a very efficient MATLAB® implementation of this kind of hypergeometric functions by Koev and Edelman [141], the density itself, linear statistics (one-dimensional integrals over the density) and $n$-th order correlation functions can be numerically tackled very easily. In particular, these results entirely avoid the use of (quaternion) determinants and (skew-)orthogonal polynomials which would arise from the canonical RMT treatment and can get computationally demanding for high $N_{1,2}$ and $n$. Conversely, the computational complexity of the algorithm in [141] is only *linear* in the size of the matrix argument ($\beta n$).

In the following, we shall provide some plots of the spectral density for different numbers of incoming and outgoing leads, and $\beta = 2$ (Fig. 5.1). The agreement between the two alternative formulas (5.2.14) and (5.2.21) is excellent.

As a final check, we also numerically compute the prototype of linear statistics, i.e. the (normalized) average shot noise power $\langle P\rangle/P_0$ (see (5.2.1)), defined as:

$$\langle P\rangle/P_0 = \int_0^1 dT R_\beta(T; N_1, N_2) T(1-T) \tag{5.2.23}$$

where $R_\beta(T; N_1, N_2)$ is taken from (5.2.21). The result has to agree with the analytical expression [128; 129]:

$$\frac{\langle P\rangle}{P_0} = \frac{N_1(N_1 - 1 + 2/\beta)N_2(N_2 - 1 + 2/\beta)}{(\tilde{N} - 2 + 2/\beta)(\tilde{N} - 1 + 2/\beta)(\tilde{N} - 1 + 4/\beta)} \tag{5.2.24}$$

where $\tilde{N} = N_1 + N_2$. We compare in Table 5.1 the theoretical result (5.2.24) with the numerical integration of (5.2.23), obtained in MATLAB® with a standard integration routine. The agreement we found is excellent, thus confirming the correctness of (5.2.21).

| $N_1$ | $N_2$ | $\beta$ | Theory | Numerical |
|---|---|---|---|---|
| 4 | 7 | 2 | 0.5939393 | 0.5939393 |
| 8 | 11 | 2 | 1.1321637 | 1.1321639 |
| 3 | 9 | 2 | 0.4248251 | 0.4248251 |
| 4 | 7 | 4 | 0.5805422 | 0.5805424 |
| 3 | 5 | 4 | 0.4326923 | 0.4326923 |

Table 5.1: Comparison between the theoretical expression for the average shot-noise power (5.2.24) and the numerical integration of (5.2.23), for different values of $N_1$, $N_2$ and $\beta$.

## 5.3 Full counting statistics: exact results for moments of the transmission eigenvalues

For simplicity, we consider again the $\beta = 2$ case as in [127]. The moments $\langle \mathcal{T}_m \rangle$ can be computed as a simple linear statistic on the transmission eigenvalues:

$$\langle \mathcal{T}_m \rangle = \int_0^1 dT\ T^m R_2(T; N_1, N_2) \tag{5.3.1}$$

Known results about $\langle \mathcal{T}_m \rangle$ include:

1. *Approximate* evaluation *for all positive integer* $m$ (but valid in the regime $N_1, N_2 \gg 1$) [142; 143]; also, the generating function for all moments in this limit was first computed in [137].

2. *Exact* evaluation (valid for all $N_1, N_2, \beta$) but only up to $m = 4$ (see [134] and references therein).

Assuming $N_1 < N_2$ without loss of generality, we can use (5.2.14) and (5.3.1) with $N_1 = N$ and $N_2 = \mu + N$:

$$\langle \mathcal{T}_m \rangle = \sum_{n=0}^{N-1} (2n + \mu + 1) \int_0^1 dT\ T^{\mu+m} P_n^{(\mu,0)}(1-2T) P_n^{(\mu,0)}(1-2T) \tag{5.3.2}$$

After the change of variables $T = (1-t)/2$ and the definition of Jacobi polynomials as:

$$P_n^{(\mu,0)}(t) = \frac{1}{n!} \sum_{k=0}^{n} \frac{(-n)_k (\mu + n + 1)_k (\mu + k + 1)_{n-k}}{k!} \left( \frac{1-t}{2} \right)^k \tag{5.3.3}$$

(where $(a)_k = \Gamma(a+k)/\Gamma(a)$ is a Pochhammer symbol), we obtain:

$$\langle \mathcal{T}_m \rangle = \frac{1}{2^{\mu+m+1}} \sum_{n=0}^{N-1} \frac{2n+\mu+1}{n!} \sum_{k=0}^{n} \frac{(-n)_k (\mu+n+1)_k (\mu+k+1)_{n-k}}{2^k \; k!} \cdot \\ \cdot \int_{-1}^{1} dt \; (1-t)^{\mu+m+k} P_n^{(\mu,0)}(t) \tag{5.3.4}$$

The integral above can be computed for $m > -\mu - 1$ ([105], formula 7.391.2) in terms of a hypergeometric function ${}_3F_2(-n, \mu+n+1, \mu+m+k+1; \mu+1, \mu+m+k+2; 1)$. Since the first argument is a negative integer, the series gets truncated to give eventually:

$$\langle \mathcal{T}_m \rangle = \sum_{n=0}^{N-1} (2n+\mu+1) \sum_{k,\ell=0}^{n} \frac{g(k) g(\ell)}{\mu+m+k+\ell+1} \tag{5.3.5}$$

where:

$$g(\kappa) = (-1)^\kappa \binom{n}{\kappa} \binom{n+\mu+\kappa}{\mu+\kappa} \tag{5.3.6}$$

Despite lacking the aesthetic appeal of subcases already considered in the literature [134; 142], formula (5.3.5) is nevertheless valid for any $(N_1, N_2)$ and $m > -\mu - 1$, and is fully non-perturbative. After implementing (5.3.5) in MATHEMATICA®, one can check by direct inspection that:

1. the formula (5.3.5) agrees with the approximate result in [142] (valid for $N_1, N_2 \gg 1$):

$$\langle \mathcal{T}_m \rangle = (\mu + 2N) \sum_{p=1}^{m} \binom{m-1}{p-1} (-1)^{p-1} c_{p-1} \left( \frac{N(\mu+N)}{(\mu+2N)^2} \right)^p \tag{5.3.7}$$

   where $c_p = \frac{1}{p+1}\binom{2p}{p}$ (see Table 5.2).

2. The shot noise power $\langle P \rangle / P_0$, defined as $\langle \mathcal{T}_1 \rangle - \langle \mathcal{T}_2 \rangle$, can be extracted from (5.3.5). Thanks to multiple cancellations, the result can be cast in the very simple form:

$$\frac{\langle P \rangle}{P_0} = \frac{N^2 (\mu+N)^2}{(\mu+2N-1)(\mu+2N)(\mu+2N+1)} \tag{5.3.8}$$

   which agrees with the known exact result [128; 129] (see also eq. (5.2.24) below).

3. The average conductance $\langle G\rangle/G_0 = \langle \mathcal{T}_1\rangle$ from (5.3.5) can be brought to the simple form:
$$\frac{\langle G\rangle}{G_0} = \frac{N(\mu+N)}{\mu+2N} \tag{5.3.9}$$
which agrees with the known result [135].

| $\mu$ | $N$ | m | Exact (5.3.5) | Approximate (5.3.7) |
|---|---|---|---|---|
| 4 | 57 | 3 | 18.4240 | 18.4248 |
| 4 | 87 | 7 | 18.637 | 18.638 |
| 12 | 47 | 19 | 6.7672 | 6.77002 |
| 15 | 57 | 29 | 6.67909 | 6.68199 |
| 25 | 75 | 59 | 6.34394 | 6.34704 |

Table 5.2: Comparison between the moments $\langle \mathcal{T}_m\rangle$ computed by Novaes [142] and our exact derivation (5.3.5). Note that the normalization $\int_0^1 dT\ R_\beta(T;N_1,N_2) = N_1$ implies that the moments are not constrained between 0 and 1.

Another alternative formula for the moments has been found very recently by M. Novaes [144]. In contrast with (5.3.5), where the number of terms in the sum grows with $N_{1,2}$ (whereas the value of $m$ does not matter much), Novaes' formula (valid only for integer $m$) is given by:
$$\langle \mathcal{T}_m\rangle = \sum_{p=0}^{m-1} G_{m,p} \tag{5.3.10}$$
where:
$$G_{m,p} = \frac{(-1)^p}{m!}\binom{m-1}{p}\frac{(N_1-p)_m(N_2-p)_m}{(N_1+N_2-p)_m} \tag{5.3.11}$$
where the notation $(x)_n$ is standard for the Pochhammer symbol.

The agreement between (5.3.10) and (5.3.5) (for integer $m$) can be checked numerically to arbitrary precision. Nevertheless, a *direct* proof of their equivalence is still elusive. It is indeed possible to recast (5.3.5) in a form similar to (5.3.10), by exploiting the Christoffel-Darboux formula for Jacobi polynomials in (5.3.2) and using the binomial theorem. This leads to:
$$\langle \mathcal{T}_m\rangle = \sum_{p=0}^{m-1} \Psi_{m,p} \tag{5.3.12}$$

where:

$$\Psi_{m,p} = \frac{N_1(\mu+N_1)}{(\mu+2N_1)2^{\mu+m}}(-1)^p \binom{m-1}{p} \phi_p(\mu, N_1) \tag{5.3.13}$$

$$\phi_p(\mu, N_1) = \int_{-1}^{1} dt\ t^p(1-t)^{\mu+1}\left[P_N^{(\mu,0)\prime}(t)P_{N-1}^{(\mu,0)}(t) - P_{N-1}^{(\mu,0)\prime}(t)P_N^{(\mu,0)}(t)\right] \tag{5.3.14}$$

It would be thus tempting to conclude that $G_{m,p} = \Psi_{m,p}$ and try to prove this equality: unfortunately, this is not the case (and can be easily shown numerically). So, although the full $p$-sums eventually coincide, the individual summands do not. The question of how to prove the equivalence of (5.3.10) and (5.3.5) is still open. On top of that, from none of the three formulas presented above it appears straightforward to deduce the asymptotic behavior (5.3.7): this is yet another puzzle that we leave for further investigation.

## 5.4 Large deviations and linear statistics

So far, we have considered the quantum conductance problem for a fixed and finite number of open channels. In the case of symmetric cavities ($N_1 = N_2 \to \mu = 0$) with many open channels $N_{1,2} \gg 1$, there are many results available for the average and the variance of the above quantities (conductance, shot noise...) [11; 137; 142]. In particular, a general formula for the variance of any linear statistics $A = \sum_{i=1}^{N} a(\lambda_i)$ (where $\lambda_i = (1+T_i)^{-1}$) is known from Beenakker [145]. However, at least for the case $A = \mathcal{T}_n$ (integer moments), this formula is of little practical use. Is it possible to obtain it following another route? It turns out that this problem is intimately related to the following: what is the *full* probability distribution of the quantities of interest (conductance, shot noise, moments) and any linear statistics in general?

In contrast with the simple mean and variance, for which a wealth of results is available, much less is known for their distributions: for the conductance, an explicit expression was obtained for $N_1 = N_2 = 1, 2$ [135; 136; 146]. For the shot noise, the distribution was known only for $N_1 = N_2 = 1$ [126]. Only very recently, Sommers *et al.* [147] announced two rather intricate formulas for the distribution of the conductance and the shot noise, valid at arbitrary number of open channels. An integrable theory of quantum transport has been also brought forward

in very recent times, where interesting connections with Painlevé trascendents and integrable hierarchies have been presented [148]. Hardly anything is known about the distribution of moments or other linear statistics, even though an exact treatment involving Painlevé functions may be within reach with the techniques presented in [148; 149].

Given some recent experimental progresses [150], which made eventually possible to explore the full distribution for the conductance (and not just its mean and variance), it is of great interest to deepen our knowledge about distributions of other quantities, whose experimental test may be soon within reach.

It is the purpose of the present section to establish exact large deviation formulas for the distribution of any linear statistics on the transmission eigenvalues of a symmetric cavity with $N_1 = N_2 = N \gg 1$ open channels. More precisely, for any linear statistics $A$ whose probability distribution is denoted as $\mathcal{P}_A(A, N)$, we have[1]:

$$\lim_{N\to\infty} \left[ -\frac{2 \log \mathcal{P}_A(Nx, N)}{\beta N^2} \right] = \Psi_A(x) \tag{5.4.1}$$

where the rate function $\Psi_A(x)$ is computed exactly for the conductance ($A = G$) and shot noise ($A = P$). For the case of integer moments, a complete solution is not yet available, although we can use our partial results to provide an explicit formula for the variance of $\mathcal{T}_n$ (see below). The method can be extended to the case of asymmetric cavities $N_1 = \kappa N_2$, and is based on a combination of the very same Dean-Majumdar method [40] (already used in Chapter 3), this time in Laplace space.

In fact, given a linear statistics of interest $A = \sum_{i=1}^{N} a(T_i)$, the main idea is to work with the Laplace transform of the probability density $P_A(A, N)$, defined as:

$$\mathcal{P}_A(A, N) = \mathcal{N}_\beta^{-1} \int_0^1 \cdot \int_0^1 \prod_{i=1}^{N} dT_i \exp\left( \frac{\beta}{2} \sum_{j\neq k} \log|T_j - T_k| + \left(\frac{\beta}{2} - 1\right) \sum_{i=1}^{N} \log T_i \right) \cdot \cdot \delta\left( \sum_{i=1}^{N} a(T_i) - A \right) \tag{5.4.2}$$

[1]Hereafter we will use the abbreviated notation $\mathcal{P}_A(A, N) \asymp \exp\left(-\frac{\beta}{2} N^2 \Psi_A(A/N)\right)$ to mean exactly (5.4.1), in complete agreement with Chapter 3.

We can write the Laplace transform of (5.4.2) as:

$$\int_0^\infty \mathcal{P}_A(A,N)e^{-\frac{\beta}{2}NpA}dA = \mathcal{N}_\beta^{-1}\int_0^1\cdots\int_0^1 dT_1\cdots dT_N \exp\left(\frac{\beta}{2}\sum_{j\neq k}\log|T_j-T_k|+\right.$$
$$\left.+\left(\frac{\beta}{2}-1\right)\sum_{i=1}^N\log T_i - \frac{\beta}{2}pN\sum_{i=1}^N a(T_i)\right) \tag{5.4.3}$$

Now, introducing the counting function (density) $\varrho(T) = N^{-1}\sum_i \delta(T-T_i)$, we can treat the transmission eigenvalues as a continuous fluid of charged particles living on the real interval $[0,1]$. To the leading order in $N$, this amounts to replacing the multiple integral on the rhs of (5.4.3) with a functional integral over the density $\varrho$, in complete analogy with the treatment in section 3.3:

$$\int_0^\infty \mathcal{P}_A(A,N)e^{-\frac{\beta}{2}NpA}dA = \mathcal{N}_\beta^{-1}\int \mathcal{D}[\varrho]e^{-\frac{\beta}{2}N^2S_p[\varrho]} \tag{5.4.4}$$

It is then clear that the density of fluid particles will be such that the free energy of the gas $S_p[\varrho]$ is minimized. Thus, $\varrho_p(T)$ will generically obey a Poisson equation of the form:

$$pa'(T) = \mathcal{P}\int_0^1 \frac{\varrho_p(T')}{T-T'}dT' \tag{5.4.5}$$

where $\mathcal{P}$ denotes the Cauchy principal part.

A very interesting feature of (5.4.5) is that, depending on the value of the Laplace parameter $p$, several different profiles of the density $\varrho_p(T)$ appear, and the fluid of charged particles undergoes a series of real phase transitions in the Laplace space. As a consequence, the large deviation functions introduced earlier, which can be determined from the density $\varrho_p(T)$, display some critical points, characterized by a discontinuous third derivative. Similar phase transitions have been reported recently in the context of the quantum entanglement problem [151].

As an example, we consider the case of the conductance ($a(T) = T$) (see subsection 5.4.2 for details). In fig. 5.2, we plot schematically the density of transmission eigenvalues $\varrho_p(T)$ (solution of (5.4.5) with $A = G$), for three different intervals on the real $p$ line:

- when $p \geq 4$, the external potential $pT/2$ is strong enough (compared to the logarithmic repulsion) to keep the fluid particles confined between the hard

wall at $T = 0$ and a point $T^{(+)} = 4/p$. The gas particles accumulate towards $T \to 0^+$, where the density develops an inverse square root divergence, while $\varrho_p(T_c) = 0$. This situation is depicted in the left panel of fig. 5.2;

- when $p$ hits the critical value $p^{(+)} = 4$ from above, the density profile changes abruptly. The external potential $pT/2$ is no longer overcoming the logarithmic repulsion, which takes over, so the fluid particles spread over the whole support $(0, 1)$, feeling the hard edges at $T = 0, 1$: thus, the density generically exhibits an inverse square root divergence at both endpoints ($T \to 0^+$ and $T \to 1^-$). This phase keeps holding for all the values of $p$ down to the second critical point $p^{(-)} = -4$ (see the second panel in fig. 5.2), when the negative slope of the potential is so steep that the particles can no longer sustain a delocalized phase over $(0, 1)$, but prefer to be located near the right hard edge at $T = 1$.

- In the third phase ($p < -4$), the fluid particles are pushed away from the origin and accumulate towards the right hard wall at $T \to 1$ (see the rightmost panel in fig. 5.2). The density thus vanishes below the point $T^{(-)} = 1 - 4/|p|$.

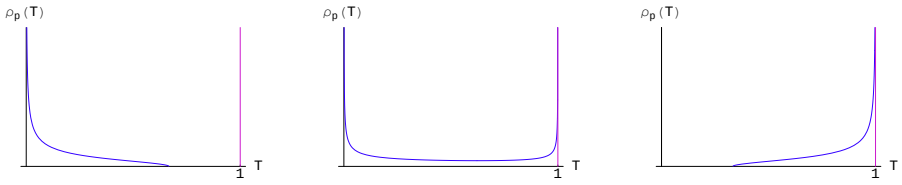


Figure 5.2: Phases of the density of transmission eigenvalues for the conductance case.

In the following, we present first a summary of results, and in two separate subsection the detailed calculations in both the conductance and shot noise cases.

### 5.4.1 Statement of results

The exact expressions for the rate functions in the case of conductance ($G$) and shot noise ($P$) are given as follows:

$$\Psi_G(x) = \begin{cases} \frac{1}{2} - \log(4x) & \text{for} \quad 0 \le x \le \frac{1}{4} \\ 8\left(x - \frac{1}{2}\right)^2 & \text{for} \quad \frac{1}{4} \le x \le \frac{3}{4} \\ \frac{1}{2} - \log[4(1-x)] & \text{for} \quad \frac{3}{4} \le x \le 1 \end{cases} \tag{5.4.6}$$

$$\Psi_P(x) = \begin{cases} \frac{1}{4} - 2\log 2 - \frac{1}{2}\log x & \text{for} \quad 0 \le x \le \frac{1}{16} \\ 64\left(\frac{1}{8} - x\right)^2 & \text{for} \quad \frac{1}{16} \le x \le \frac{3}{16} \\ \frac{1}{4} - 2\log 2 - \frac{1}{2}\log\left(\frac{1}{4} - x\right) & \text{for} \quad \frac{3}{16} \le x \le \frac{1}{4} \end{cases} \tag{5.4.7}$$

All the rate functions above are continuous everywhere. Only the third derivative is discontinuous at the critical points ($x = 1/4, 3/4$ for the conductance etc.). From the expressions (5.4.6) and (5.4.7), together with (5.4.1), one observes that the distributions (to the leading order in $N$) have a Gaussian behavior close to the maximum, flanked on both sides by power-law tails.

Combining the explicit formulas above with the general large deviation expression (5.4.1), we can write e.g. for the conductance the following large deviation law close to the maximum:

$$\mathcal{P}_G(G,N) \asymp \exp\left(-\frac{\beta}{2}N^2\Psi_G\left(\frac{G}{N}\right)\right) = \exp\left[-\frac{\beta}{2}N^2 \cdot 8\left(\frac{G}{N} - \frac{1}{2}\right)^2\right] = \exp\left[-\frac{1}{2(1/8\beta)}\left(G - \frac{N}{2}\right)^2\right] \tag{5.4.8}$$

from which one reads off very easily the well-known values for mean and variance $\langle G\rangle = N/2$ and $\mathrm{var}(G) = 1/8\beta$. The large-$N$ behavior (5.4.1) is generic for any linear statistics on the transmission eigenvalue, and the functional formalism developed here may also help to derive new interesting formulae for mean and variances. Consider for example the case of integer moments $\mathcal{T}_n = \sum_{i=1}^N T_i^n$. The rate function close to the maximum is given by [152]: $\Psi_{\mathcal{T}_n}(x) = (4A_n)^{-1}(x - B_n)^2 \qquad \text{for } x_n^{(-)} < x < x_n^{(+)}$, where $x_n^{(\pm)}$ are $n$-dependent edge points and the constants $A_n$ and $B_n$ are given by $A_n = (2n-1)\Gamma(n+1/2)\Gamma(n-1/2)/16\pi n\Gamma^2(n)$ and $B_n = 4^{-n}\binom{2n}{n}$.

This implies from (5.4.1): $\mathcal{P}_{\mathcal{T}_n}(\mathcal{T}_n, N) \asymp \exp\left[-\frac{1}{2(4A_n/\beta)}\left(\mathcal{T}_n - B_n N\right)^2\right]$. From this Gaussian shape, the mean (in agreement with [142]) and variance of $\mathcal{T}_n$ can be read off very easily:

$$\langle \mathcal{T}_n \rangle = B_n N = \frac{N}{4^n}\binom{2n}{n} \tag{5.4.9}$$

$$\mathrm{var}(\mathcal{T}_n) = \frac{4A_n}{\beta} = \frac{1}{4\beta\pi}\frac{(2n-1)\Gamma(n+1/2)\Gamma(n-1/2)}{n\Gamma^2(n)} \tag{5.4.10}$$

whose asymptotic value is easily computed as:

$$v^\star = \lim_{n\to\infty} v(n) = \frac{1}{2\beta\pi} \tag{5.4.11}$$

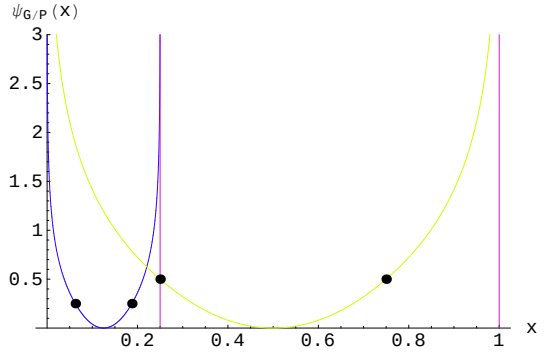


Figure 5.3: Rate functions $\Psi_G(x)$ (green) and $\Psi_P(x)$ (blue) (see eq. (5.4.6)). The black dots highlight the two critical points on each curve.

### 5.4.2 Distribution of the conductance

We start with the simplest case of linear statistics, namely the conductance $G = \sum_{i=1}^N T_i$ (where we have absorbed the constant $G_0$). Starting from the jpdf of transmission eigenvalues for the case of symmetric cavities ($N_1 = N_2 = N$) (5.2.2):

$$P(T_1, \ldots, T_N) = \mathcal{N}_\beta^{-1} \prod_{j<k} |T_j - T_k|^\beta \prod_{i=1}^N T_i^{\beta/2-1} \tag{5.4.12}$$

the object we are interested in is the distribution $\mathcal{P}_G(G,N)$:

$$\mathcal{P}_G(G,N) = \mathcal{N}_\beta^{-1} \int_0^1 \cdot \int_0^1 \prod_{i=1}^N dT_i \exp\left(\frac{\beta}{2}\sum_{j\neq k}\log|T_j - T_k| + \left(\frac{\beta}{2}-1\right)\sum_{i=1}^N \log T_i\right) \cdot \cdot \delta\left(\sum_{i=1}^N T_i - G\right) \tag{5.4.13}$$

Taking the Laplace transform of (5.4.13):

$$\int_0^\infty \mathcal{P}_G(G,N) e^{-\frac{\beta}{2}NpG} dG = \mathcal{N}_\beta^{-1} \int_0^1 \cdots \int_0^1 dT_1 \cdots dT_N \exp\left(\frac{\beta}{2}\sum_{j\neq k}\log|T_j - T_k| + \right. \\ \left. + \left(\frac{\beta}{2}-1\right)\sum_{i=1}^N \log T_i - \frac{\beta}{2}pN\sum_{i=1}^N T_i\right) \tag{5.4.14}$$

Introducing the counting function $\varrho(T) = N^{-1}\sum_i \delta(T - T_i)$, we can go from the multiple integral on the r.h.s. of (5.4.14) to a functional integral over $\varrho(T)$ [40] as:

$$\int_0^\infty \mathcal{P}_G(G,N) e^{-\frac{\beta}{2}NpG} dG = \mathcal{N}_\beta^{-1} \int \mathcal{D}[\varrho] e^{-\frac{\beta}{2}N^2 S_p[\varrho]} \tag{5.4.15}$$

where in the exponential we have kept only the leading $\mathcal{O}(N^2)$ terms. Note that the term $\prod_i T_i^{\beta/2-1}$ in (5.4.12) does not contribute to the leading action $S_p[\varrho]$ for the symmetric case $N_1 = N_2 \gg 1$, while it would for $N_1 = \kappa N_2 \gg 1$ for $\kappa \neq 1$. This case will be tackled in a forthcoming publication.

The action $S_p[\varrho(T)]$ in (5.4.15) is given by:

$$S_p[\varrho] = p\int_0^1 \varrho(T) T dT - \int_0^1\int_0^1 dT dT' \varrho(T)\varrho(T')\log|T-T'| + B\left[\int_0^1 \varrho(T)dT - 1\right] \tag{5.4.16}$$

where the Lagrange multiplier $B$ enforces the normalization of $\varrho(T)$ to 1.

The leading contribution to the r.h.s. of (5.4.15) comes from the density function which makes the action (5.4.16) stationary $\frac{\delta S_p[\varrho]}{\delta \varrho} = 0$. This implies that the density must satisfy:

$$pT + B = 2\int_0^1 \varrho(T')\log|T - T'|dT' \tag{5.4.17}$$

Eq. (5.4.17) will be essential for determining the constant $B$ in different cases. Now, differentiating (5.4.17) once more with respect to $T$:

$$\frac{p}{2} = \mathcal{P}\int_0^1 \frac{\varrho(T')}{T-T'}dT' \tag{5.4.18}$$

where $\mathcal{P}$ denotes the Cauchy principal part.

The task is then to find a solution $\varrho_p^\star(T)$ for the integral equation of Tricomi type (5.4.18). Physically, we can foresee three possible phases for the density $\varrho_p^\star(T)$ according to the strength and sign of the external potential (see also the discussion above):

1. For large and positive $p$, the fluid particles (transmission eigenvalues) will feel a strong confining potential which will keep them close to the left hard edge $T \to 0+$. Thus, $\varrho_p^\star(T)$ will have a semi-compact support $(0, L_1]$, with $0 < L_1 < 1$,

2. For intermediate values of $p$, the particles will spread over the full range $(0, 1)$.

3. For large and negative $p$, the fluid particles will be pushed towards the right edge and the support of $\varrho_p^\star(T)$ will be $[L_2, 1)$, with $0 < L_2 < 1$.

These three cases will correspond to different solutions for the Tricomi equation (5.4.18) above, and the positivity constraint for the obtained densities will fix the range of variability for $p$ in each case. Once a solution $\varrho_p^\star(T)$ for each case (different ranges for $p$) is obtained, this will be substituted into the action (5.4.16) and from (5.4.15) we can read off the asymptotic decay of the Laplace transform of the conductance:

$$\int_0^\infty \mathcal{P}_G(G,N)e^{-\frac{\beta}{2}NpG}dG \asymp \exp\left(-\frac{\beta}{2}N^2\{S_p[\varrho_p^\star] - S_0[\varrho_0^\star]\}\right) = \exp\left(-\frac{\beta}{2}N^2 J_G(p)\right) \tag{5.4.19}$$

where in (5.4.19) we have used the fact that, for $p = 0$:

$$\int_0^\infty \mathcal{P}_G(G,N)dG = 1 \asymp \mathcal{N}_\beta^{-1}\exp\left(-\frac{\beta}{2}N^2 S_0[\varrho_0^\star]\right) \tag{5.4.20}$$

which determines the normalization $\mathcal{N}_\beta^{-1}$ as $\mathcal{N}_\beta^{-1} \asymp \exp\left(\frac{\beta}{2}N^2 S_0[\varrho_0^\star]\right)$.

We are now ready to consider the three cases separately.

#### 5.4.2.1 Large $p$: support on $(0, L_1]$

The general solution of the Tricomi equation (5.4.18) reads:

$$\varrho_p^\star(T) = -\frac{1}{\pi^2\sqrt{T(L_1-T)}}\left[\frac{p}{2}\,\mathcal{P}\int_0^{L_1}\frac{\sqrt{T'(L_1-T')}}{T-T'}dT' + B_1\right] \tag{5.4.21}$$

where $B_1$ is an arbitrary constant.

Evaluating the principal value integral in (5.4.21), we obtain:

$$\varrho_p^\star(T) = \frac{p}{2\pi\sqrt{T}}\sqrt{L_1-T} \tag{5.4.22}$$

The normalization of $\varrho_p^\star(T)$ determines $L_1$ as $4/p$ and the condition $L_1 < 1$ implies $p > 4$. As expected, this solution hold for large values of $p$ (i.e. for a strong confining potential).

Coming back to (5.4.17):

$$pT + B = 2\int_0^1 \varrho(T')\log|T-T'|dT' \tag{5.4.23}$$

we can determine the Lagrange multiplier $B$ in the action by putting $T = 0$ there[1]:

$$B = 2\int_0^1 \varrho_p^\star(T')\log T' dT' \tag{5.4.24}$$

Eq. (5.4.23) can be also used to simplify the action (5.4.16) at the saddle point. First, we multiply (5.4.23) by $\varrho(T)$ and we integrate both sides between 0 and 1 in $T$. Then, using (5.4.24), we can write:

$$\int_0^1\int_0^1 dTdT'\varrho(T)\varrho(T')\log|T-T'| = \frac{p}{2}\int_0^1 T\varrho(T)dT + \int_0^1 \varrho(T)\log(T)dT \tag{5.4.25}$$

The action (5.4.16) at the saddle point thus reads:

$$S_p[\varrho_p^\star] = \frac{p}{2}\int_0^1 \varrho_p^\star(T)TdT - \int_0^1 \varrho_p^\star(T)\log(T)dT \tag{5.4.26}$$

Substituting the solution $\varrho_p^\star(T)$ (5.4.22) into (5.4.26) gives:

$$S_{(p>4)}[\varrho_{(p>4)}^\star] = 3/2 + \log p \tag{5.4.27}$$

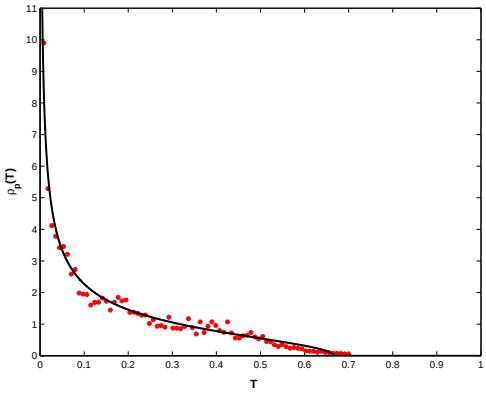


Figure 5.4: Density of transmission eigenvalues (conductance case) for $N = 4$ and $p = 6$ (theory vs. numerics).

In fig. 5.4 we perform a Montecarlo simulation to test the prediction (5.4.22) for the average density of eigenvalues in Laplace space under the effect of a strong confining potential ($p$ large). The numerical density for $N$ eigenvalues (here and for all the subsequent cases) is obtained as:

$$\varrho_p^\star(x_1) \approx \frac{\left\langle e^{-pN\sum_{i=1}^N x_i} \prod_{j<k} |x_j - x_k|^2 \right\rangle_{N-1}}{\left\langle e^{-pN\sum_{i=1}^N x_i} \prod_{j<k} |x_j - x_k|^2 \right\rangle_{N}} \tag{5.4.28}$$

where the average $\left\langle \cdot \right\rangle$ is taken over $N-1$ random numbers $x_2, \ldots, x_N$ (numerator) with a flat measure over $[0,1]$, with $x_1$ spanning the interval $(0,1)$. In the denominator, the normalization constant is obtained with the same procedure, this time averaging over $N$ random variables uniformly drawn from $(0,1)$. In all cases, the agreement with the theoretical results is fairly good already for $N = 4, 5$.

#### 5.4.2.2 Intermediate $p$: support on $(0,1)$

In this case, the solution of (5.4.18) from (5.4.21) reads:

$$\varrho_p^\star(T) = \frac{p}{2\pi\sqrt{T(1-T)}}\,[K - T] \tag{5.4.29}$$

[1] More care is needed for the evaluation of B in the case 5.4.2.3 below.

The normalization of $\varrho_p^\star(T)$ determines the arbitrary constant $K$ as $(4+p)/2p$. Now, there are 2 positivity constraints ($\varrho_p^\star(T) > 0$ everywhere) to take into account depending on whether $p$ is greater or smaller than 0:

1. if $p > 0$, the positivity constraint $K - 1 > 0$ at the edge point $T = 1$ implies $p < 4$.

2. if $p < 0$, the positivity constraint $K < 0$ at the edge point $T = 0$ implies $p > -4$.

Substituting this solution into the simplified action (5.4.26) (which holds in this case as well) gives:

$$S_{(-4<p<4)}[\varrho^\star_{(-4<p<4)}] = -\frac{p^2}{32} + \frac{p}{2} + 2\log 2 \tag{5.4.30}$$

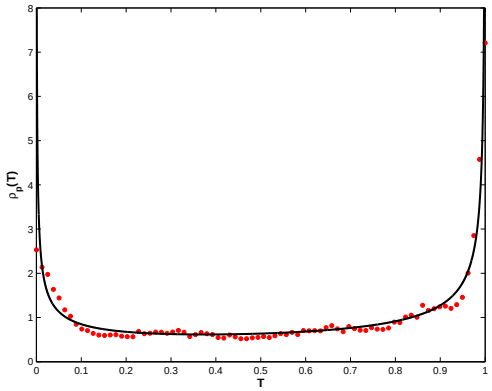


Figure 5.5: Density of transmission eigenvalues (conductance case) for $N = 5$ and $p = -1$ (theory vs. numerics).

#### 5.4.2.3 Large negative $p$: support on $[L_2, 1)$

In this case, the general solution of (5.4.18) reads:

$$\varrho_p(T) = -\frac{1}{\pi^2\sqrt{(T-L_2)(1-T)}}\left[\frac{p}{2}\mathcal{P}\int_{L_2}^{1} dT' \frac{\sqrt{(T'-L_2)(1-T')}}{T-T'} + C\right] \tag{5.4.31}$$

where $C$ is an arbitrary constant. Evaluating the principal value integral in (5.4.31) and imposing the normalization $\int_{L_2}^{1} \varrho_p(T)dT = 1$, we get:

$$\varrho_p^\star(T) = \frac{|p|}{2\pi\sqrt{1-T}}\sqrt{T-(1-4/|p|)} \tag{5.4.32}$$

The condition $L_2 = 1 - 4/|p| > 0$ implies $p < -4$. Substituting this result into the action (5.4.16) gives:

$$S_{(p<-4)}[\varrho^\star_{(p<-4)}] = 3/2 + p + \log(-p) \tag{5.4.33}$$

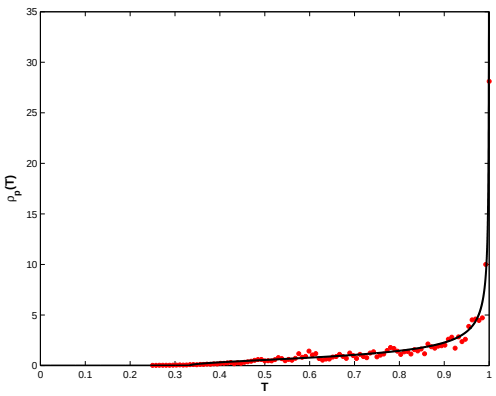


Figure 5.6: Density of transmission eigenvalues (conductance case) for $N = 5$ and $p = -6$ (theory vs. numerics).

#### 5.4.2.4 Summary for the conductance case

To summarize, the density of eigenvalues (solution of the saddle point equation (5.4.18)) has the following form:

$$\varrho_p^\star(T) = \begin{cases} \frac{p}{2\pi\sqrt{T(1-T)}}\left[\frac{4+p}{2p} - T\right] & 0 \le T \le 1 \qquad -4 \le p \le 4 \\ \frac{p}{2\pi\sqrt{T}}\sqrt{\frac{4}{p} - T} & 0 \le T \le 4/p \qquad p \ge 4 \\ \frac{|p|}{2\pi\sqrt{1-T}}\sqrt{T-(1-4/|p|)} & 1-4/|p| \le T \le 1 \qquad p \le -4 \end{cases} \tag{5.4.34}$$

One may easily check that $\varrho_p^\star(T)$ is continuous at $p = \pm 4$, but develops two phase transitions characterized by different supports.

The action (5.4.16) at the saddle point is given by:

$$S_p[\varrho_p^\star] = \begin{cases} -\frac{p^2}{32} + \frac{p}{2} + 2\log 2 & -4 \le p \le 4 \\ 3/2 + \log p & p \ge 4 \\ 3/2 + p + \log(-p) & p \le -4 \end{cases} \tag{5.4.35}$$

which is again continuous at $p = \pm 4$.

From (5.4.19), the expression of $J_G(p)$ is:

$$J_G(p) = S_p[\varrho_p^\star] - S_0[\varrho_0^\star] = \begin{cases} -\frac{p^2}{32} + \frac{p}{2} & -4 \le p \le 4 \\ 3/2 + \log(p/4) & p \ge 4 \\ 3/2 + p + \log(-p/4) & p \le -4 \end{cases} \tag{5.4.36}$$

The form of (5.4.19) suggests that, for large $N$:

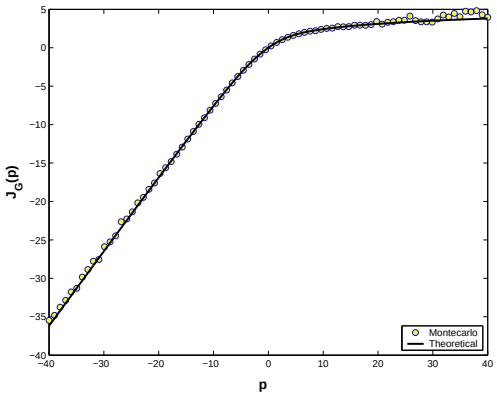


Figure 5.7: $J_G(p)$: theory vs. Montecarlo.

$$\mathcal{P}_G(G, N) \asymp \exp\left(-\frac{\beta}{2} N^2 \Psi_G\left(\frac{G}{N}\right)\right) \tag{5.4.37}$$

Inserting this ansatz into (5.4.19), we get:

$$\int_0^\infty \exp\left\{-\frac{\beta}{2} N^2 \left[p\frac{G}{N} + \Psi_G\left(\frac{G}{N}\right)\right]\right\} dG \to \exp\left\{-\frac{\beta}{2} N^2 \min_x \left[px + \Psi_G(x)\right]\right\} \tag{5.4.38}$$

Comparing (5.4.38) and (5.4.19), we have:

$$J_G(p) = \min_x \left[ px + \Psi_G(x) \right] \tag{5.4.39}$$

Thus:

$$\Psi_G(x) = \max_p \left[ -xp + J_G(p) \right] \tag{5.4.40}$$

and from (5.4.36) the rate function $\Psi_G(x)$ is readily computed:

$$\Psi_G(x) = \begin{cases} 8\left(x - \frac{1}{2}\right)^2 & \frac{1}{4} \le x \le \frac{3}{4} \\ \frac{1}{2} - \log(4x) & 0 \le x \le \frac{1}{4} \\ \frac{1}{2} - \log[4(1-x)] & \frac{3}{4} \le x \le 1 \end{cases} \tag{5.4.41}$$

From this formula, one can derive the leading behavior of the tails of $\mathcal{P}_G(G, N)$ as:

$$\mathcal{P}_G(G, N) \overset{G \to 0}{\asymp} \exp\left\{ -\frac{\beta}{2} N^2 \left[ -\log\left(4G/N\right) \right] \right\} = G^{\beta N^2/2} \tag{5.4.42}$$

$$\mathcal{P}_G(G, N) \overset{G \to N}{\asymp} \exp\left\{ -\frac{\beta}{2} N^2 \left[ -\log\left(4(1 - G/N)\right) \right] \right\} = (N-G)^{\beta N^2/2} \tag{5.4.43}$$

$$\tag{5.4.44}$$

in agreement with [147].

The most interesting feature of (5.4.41) is the appearance of discontinuities in higher-order derivatives at the critical points: more precisely, the third derivative of $\Psi_G(x)$ is discontinuous at $x = 1/4$ and $x = 3/4$. This was already highlighted by Sommers *et al.* [147], who found many more non-analyticities for finite $N_1, N_2$. Only two of them survive to the leading order for $N \to \infty$ and, in our picture, those correspond to a physical phase transition in Laplace space.

In summary, the following exact limit holds:

$$\lim_{N \to \infty} \left[ -\frac{2 \log \mathcal{P}_G(Nx, N)}{\beta N^2} \right] = \Psi_G(x) \tag{5.4.45}$$

where the rate function $\Psi_G(x)$ is given in (5.4.41).

The rate function in Laplace space (5.4.36) as been compared with numerical simulations[1] over the range $p = (-40, 40)$ and already for $N = 5$ the agreement

[1] From a numerical point of view, this approach is far more convenient than dealing with the rate function $\Psi_G(x)$ itself.

is excellent. For a given $p$ between $-40$ and 40, the numerical $J_G(p)$ is computed as:

$$J_G(p) \approx -\frac{1}{N^2} \log \frac{\left\langle e^{-pN\sum_{i=1}^N x_i} \prod_{j<k} |x_j - x_k|^2 \right\rangle}{\left\langle \prod_{j<k} |x_j - x_k|^2 \right\rangle} \tag{5.4.46}$$

where the average is taken over $N$ random variables $\{x_i\}$ drawn from a uniform distribution over $(0, 1)$.

We are now ready to tackle the shot noise case.

### 5.4.3 Distribution of the shot noise

The dimensionless shot noise is defined as $P = \sum_{i=1}^N T_i(1 - T_i)$, where we have absorbed the constant $P_0$ (see discussion above). It is convenient to rewrite it in the form $P = N/4 - \sum_{i=1}^N (1/2 - T_i)^2 = N/4 - Q$. The probability distribution of $P$ and $Q$ are related by:

$$\mathcal{P}_P(P, N) = \mathcal{P}_Q\left(\frac{N}{4} - P, N\right) \tag{5.4.47}$$

It is also necessary to make the change of variable in the jpdf (5.2.2) $\mu_i = 1/2 - T_i$, so that $-1/2 \leq \mu_i \leq 1/2$. The jpdf (5.2.2) expressed in terms of the new variables $\mu_i$ reads:

$$P(\mu_1, \ldots, \mu_N) = \mathcal{N}_\beta^{-1} \prod_{j<k} |\mu_j - \mu_k|^\beta \prod_{i=1}^N \left(\frac{1}{2} - \mu_i\right)^{\frac{\beta}{2}-1} \tag{5.4.48}$$

and we are interested in the large $N$ decay of the logarithm of $\mathcal{P}_Q(Q, N)$, where $Q = \sum_i \mu_i^2$. We have:

$$\mathcal{P}_Q(Q, N) = \mathcal{N}_\beta^{-1} \int_{-1/2}^{1/2} \cdots \int_{-1/2}^{1/2} d\mu_1 \cdots d\mu_N \exp\left(\frac{\beta}{2} \sum_{j \neq k} \log|\mu_j - \mu_k| + \left(\frac{\beta}{2} - 1\right) \sum_{i=1}^N \log\left(\frac{1}{2} - \mu_i\right)\right) \delta\left(\sum_{i=1}^N \mu_i^2 - Q\right) \tag{5.4.49}$$

Again, taking the Laplace transform and transforming multiple integrals to functional integrals we obtain:

$$\int_0^\infty \mathcal{P}_Q(Q, N) e^{-\frac{\beta}{2} NpQ} dQ = \mathcal{N}_\beta^{-1} \int \mathcal{D}[\varrho] e^{-\frac{\beta}{2} N^2 S_p[\varrho]} \tag{5.4.50}$$

where for notational simplicity we keep the same symbols $\varrho$ and $S_p$ as before. Of course, the new action $S_p$ reads:

$$S_p[\varrho] = p\int_{-1/2}^{1/2}\varrho(\mu)\mu^2 d\mu - \int_{-1/2}^{1/2}\int_{-1/2}^{1/2} d\mu d\mu' \varrho(\mu)\varrho(\mu')\log|\mu-\mu'| + C\left[\int_{-1/2}^{1/2}\varrho(\mu)d\mu - 1\right] \tag{5.4.51}$$

The stationary point of the action $S$ is given by the solution of the following Tricomi equation:

$$p\mu = \mathcal{P}\int_{-1/2}^{1/2}\frac{\varrho(\mu')}{\mu-\mu'}d\mu' \tag{5.4.52}$$

In terms of the solution $\varrho_p^\star(\mu)$ of (5.4.52), the action (5.4.51) can be simplified

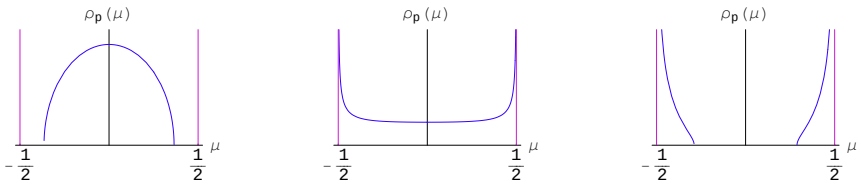


Figure 5.8: Density of the shot noise (schematic).

as:

$$S_p[\varrho_p^\star] = \frac{p}{2}\int_{-1/2}^{1/2}\varrho_p^\star(\mu)\mu^2 dx - \frac{C}{2} \tag{5.4.53}$$

where the Lagrange multiplier $C$ will be determined in complete analogy with the conductance case. Now, we can write the asymptotic decay of $Q$ as:

$$\int_0^\infty \mathcal{P}_Q(Q,N)e^{-\frac{\beta}{2}NpQ}dQ \asymp \exp\left(-\frac{\beta}{2}N^2\{S_p[\varrho_p^\star] - S_0[\varrho_0^\star]\}\right) = \exp\left(-\frac{\beta}{2}N^2 J_Q(p)\right) \tag{5.4.54}$$

Again, in order to solve (5.4.52) we need first to foresee the allowed supports for $\varrho_p^\star(\mu)$. This time, the symmetry constraint $\varrho_p^\star(\mu) = \varrho^\star(-\mu)$ reduces the possible behaviors of $\varrho_p^\star(\mu)$ to the following three cases: I) $\varrho_p^\star(\mu)$ has compact support $[-L, L]$ with $L < 1/2$, or II) $\varrho_p^\star(\mu)$ has non-compact support $(-1/2, 1/2)$, or III) the support of $\varrho_p^\star(\mu)$ is the union of two disjoint semi-compact intervals $(-1/2, -L] \cup [L, 1/2)$ with $L > 0$. Again, these cases correspond to different ranges of variability for the Laplace parameter $p$, as detailed below.

We analyze now the three cases separately.

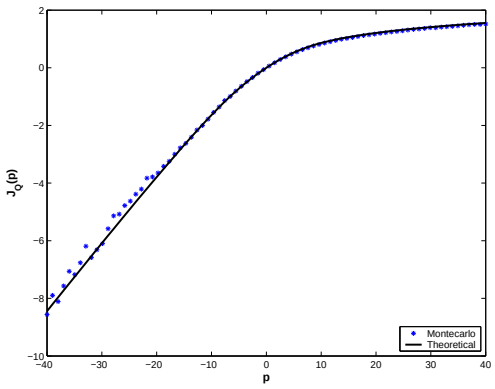


Figure 5.9: $J_Q(p)$: theory vs. Montecarlo.

#### 5.4.3.1 Large $p$: support on $[-L, L]$ with $L < 1/2$

A compact support between $[-L, L]$ is expected when the external potential $\propto p\mu^2/2$ is stronger than the logarithmic repulsion. The fluid particles cannot escape towards $\mu = \pm 1/2$ and gather close to the origin. The general solution of (5.4.52) in this case is given by:

$$\varrho_p^\star(\mu) = \frac{p}{\pi\sqrt{L^2 - \mu^2}}[a - \mu^2] \tag{5.4.55}$$

The constant $a$ is clearly determined as $a = L^2$ by the condition that $\varrho_p^\star(\pm L) = 0$. Thus, the solution within the bounds $[-L, L]$ with $L < 1/2$ is the semicircle:

$$\varrho_p^\star(\mu) = \frac{p}{\pi}\sqrt{L^2 - \mu^2} \tag{5.4.56}$$

where the edge point $L$ is determined by the normalization $\int_{-L}^{L} \varrho_p^\star(\mu)d\mu = 1$. This gives $L = \sqrt{2/p}$. In turn, the constraint $L < 1/2$ implies $p > 8$. So, eventually:

$$\varrho_{p>8}^\star(\mu) = \frac{p}{\pi}\sqrt{\frac{2}{p} - \mu^2} \tag{5.4.57}$$

Evaluating the action (5.4.53):

$$S_{p>8}[\varrho_{p>8}^\star] = \frac{3}{4} + \frac{1}{2}\log 2 + \frac{1}{2}\log p \tag{5.4.58}$$

From (5.4.54), the value of $J_Q(p) = S_p[\varrho_p^\star] - S_0[\varrho_0^\star]$ for $p \geq 8$ is given by:

$$J_Q(p) = \frac{3}{4} + \frac{1}{2}\log\left(\frac{p}{8}\right) \tag{5.4.59}$$

Again, the rate function $\Psi_Q(x)$ is given by the inverse Legendre transform of (5.4.59), i.e.:

$$\Psi_Q(x) = \max_p \left[-xp + J_Q(p)\right] = \frac{1}{4} - 2\log 2 - \frac{1}{2}\log x \tag{5.4.60}$$

valid for $0 \leq x \leq 1/16$. From the relation (5.4.47), we have the following relation among the rate functions for $Q$ and $P$:

$$\Psi_P(x) = \Psi_Q\left(\frac{1}{4} - x\right) \tag{5.4.61}$$

implying for $\Psi_P(x)$ the following expression:

$$\Psi_P(x) = \frac{1}{4} - 2\log 2 - \frac{1}{2}\log\left(\frac{1}{4} - x\right) \qquad \text{for} \quad \frac{3}{16} \leq x \leq \frac{1}{4} \tag{5.4.62}$$

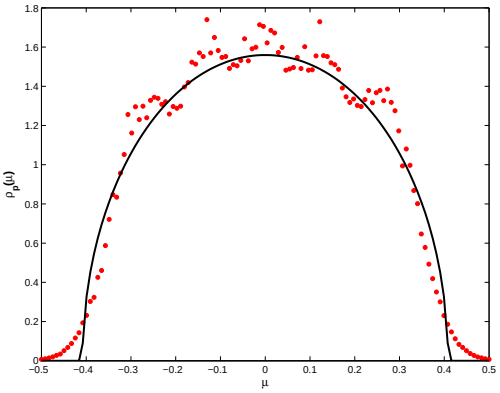


Figure 5.10: Density of shifted transmission eigenvalues $\mu$ for $N = 5$ and $p = 12$ (theory vs. numerics) for the shot noise case. The strong fluctuations around the theoretical results are due to small $N$ effects.

#### 5.4.3.2 Intermediate $p$: support on $(-1/2, 1/2)$

This case is expected when $p$ is lowered below some critical value ($p = 8$, from the discussion in previous section), so that the external potential $\propto p\mu^2/2$ no longer overcomes the logarithmic repulsion, which takes over. The fluid particles spread

over the entire support $(-1/2, 1/2)$, feeling the hard edges at $\mu = \pm 1/2$. Thus, a divergence in the density is expected at the edge points.

The general solution of (5.4.52) in this case is given by:

$$\varrho_p^\star(\mu) = \frac{p}{\pi\sqrt{1/4-\mu^2}}[b-\mu^2] \tag{5.4.63}$$

The constant $b$ is clearly determined by the normalization $\int_{-1/2}^{1/2}\varrho_p^\star(\mu)d\mu = 1$. This gives $b = 1/p + 1/8$. In turn, the positivity constraint for the density implies $-8 < p < 8$, in agreement with the qualitative discussion above. So, eventually:

$$\varrho^\star_{-8<p<8}(\mu) = \frac{p}{\pi\sqrt{1/4-\mu^2}}\left[\frac{1}{p}+\frac{1}{8}-\mu^2\right] \tag{5.4.64}$$

Evaluating the action (5.4.53):

$$S_{-8<p<8}[\varrho^\star_{-8<p<8}] = \frac{p}{8} - \frac{p^2}{256} + 2\log 2 \tag{5.4.65}$$

From (5.4.54), the value of $J_Q(p) = S_p[\varrho_p^\star] - S_0[\varrho_0^\star]$ for $-8 \le p \le 8$ is given by:

$$J_Q(p) = -\frac{p^2}{256} + \frac{p}{8} \tag{5.4.66}$$

Again, the rate function $\Psi_Q(x)$ is given by the inverse Legendre transform of (5.4.66), i.e.:

$$\Psi_Q(x) = \max_p\left[-xp + J_Q(p)\right] = 64\left(x-\frac{1}{8}\right)^2 \tag{5.4.67}$$

valid for $1/16 \le x \le 3/16$. From the relation (5.4.61), we have for $\Psi_P(x)$ the following expression:

$$\Psi_P(x) = 64\left(\frac{1}{8}-x\right)^2 \qquad \text{for} \quad \frac{1}{16} \le x \le \frac{3}{16} \tag{5.4.68}$$

#### 5.4.3.3 Large negative $p$: support on $(-1/2, -L] \cup [L, 1/2)$

In this case (large negative $p$), the fluid charges tend to cluster towards $T = \pm 1/2$ and the density is nonzero over two disconnected (and symmetric) domains $(-1/2, -L] \cup [L, 1/2)$. In this case, the general solution of Tricomi equation

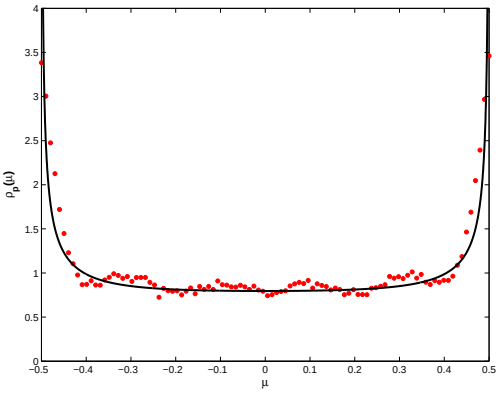


Figure 5.11: Density of shifted transmission eigenvalues $\mu$ for $N = 6$ and $p = 2$ (theory vs. numerics) for the shot noise case.

(5.4.52), which assumes a single-support solution, no longer applies. In order to obtain the sought solution of the integral equation (5.4.52), we first rewrite it as:

$$p\mu = \int_{-1/2}^{-L} \frac{\varrho_p(\mu')d\mu'}{\mu - \mu'} + \mathcal{P}\int_{L}^{1/2} \frac{\varrho_p(\mu')d\mu'}{\mu - \mu'} \qquad \text{for } \mu > 0 \tag{5.4.69}$$

$$p\mu = \mathcal{P}\int_{-1/2}^{-L} \frac{\varrho_p(\mu')d\mu'}{\mu - \mu'} + \int_{L}^{1/2} \frac{\varrho_p(\mu')d\mu'}{\mu - \mu'} \qquad \text{for } \mu < 0 \tag{5.4.70}$$

Let us focus on the case $\mu > 0$: the left half will follow by symmetry. Rewriting (5.4.69):

$$p\mu = \underbrace{\int_{-1/2}^{-L} \frac{\varrho_p(\mu')d\mu'}{\mu - \mu'}}_{\mathcal{I}_1} + \mathcal{P}\int_{L}^{1/2} \frac{\varrho_p(\mu')d\mu'}{\mu - \mu'} \tag{5.4.71}$$

In $\mathcal{I}_1$, we make a change of variables $\mu' = -y'$:

$$\mathcal{I}_1 = \int_{L}^{1/2} \frac{\varrho_p(-y')dy'}{\mu + y'} \tag{5.4.72}$$

Using $\varrho_p(-\mu) = \varrho_p(\mu)$, we get:

$$\mathcal{I}_1 = \int_{L}^{1/2} \frac{\varrho_p(y')dy'}{\mu + y'} \tag{5.4.73}$$

Substituting (5.4.73) into (5.4.71), we get:

$$p\mu = \mathcal{P}\int_{L}^{1/2} \varrho_p(\mu') \left[\frac{1}{\mu + \mu'} + \frac{1}{\mu - \mu'}\right] \tag{5.4.74}$$

implying:

$$\frac{p}{2} = \mathcal{P}\int_L^{1/2} \frac{\varrho_p(\mu')d\mu'}{\mu^2 - \mu'^2} \tag{5.4.75}$$

Making another change of variables in (5.4.75), $\mu'^2 = y'$ and denoting $\mu^2 = y$:

$$p = \mathcal{P}\int_{L^2}^{1/4} \frac{\varrho_p(\sqrt{y'})}{\sqrt{y'}} \frac{dy'}{y - y'} \tag{5.4.76}$$

Calling $g(y') = \varrho_p(y')/\sqrt{y'}$, we get an equation of Tricomi type in the unknown $g(x)$:

$$p = \mathcal{P}\int_{L^2}^{1/4} \frac{g(y')dy'}{y - y'} \tag{5.4.77}$$

whose general solution reads:

$$g(y) = -\frac{1}{\pi^2\sqrt{(y - L^2)(1/4 - y)}}\left[p\mathcal{P}\int_{L^2}^{1/4} \frac{\sqrt{(y' - L^2)(1/4 - y')}dy'}{y - y'} + C\right] \tag{5.4.78}$$

where $C$ is an arbitrary constant, leading to:

$$g(y) = \frac{p}{\pi\sqrt{(1/4 - y)(y - L^2)}}[A - y] \tag{5.4.79}$$

where $A$ is an arbitrary constant.

From the definition of $g(y)$ above, we have:

$$\varrho_p(\mu) = \mu g(\mu^2) = \frac{p\mu}{\pi\sqrt{(1/4 - \mu^2)(\mu^2 - L^2)}}\left[A - \mu^2\right] \tag{5.4.80}$$

and imposing the condition $\varrho_p(L) = 0$, we determine $A = L^2$.

Thus:

$$\varrho_p(\mu) = \frac{-p\mu\sqrt{\mu^2 - L^2}}{\pi\sqrt{1/4 - \mu^2}} \tag{5.4.81}$$

Since $p$ is negative, we have $-p = |p|$. The constant $L$ is determined by the condition $\int_L^{1/2} \varrho_p(\mu)d\mu = 1/2$, giving $L = \sqrt{1/4 - 2/|p|}$. In turn, the existence of the square root is ensured if $p < -8$.

Hence, eventually, the density reads:

$$\varrho^\star_{p<-8}(\mu) = \frac{|p\mu|\sqrt{\mu^2 - 1/4 + 2/|p|}}{\pi\sqrt{1/4 - \mu^2}} \tag{5.4.82}$$

and the corresponding $J_Q(p)$ is given by:

$$J_Q(p) = \frac{3}{4} + \frac{1}{2}\log\left(\frac{|p|}{8}\right) - \frac{|p|}{4} \tag{5.4.83}$$

The rate function is again given by the inverse Legendre transform of (5.4.83):

$$\Psi_Q(x) = \frac{1}{4} - 2\log 2 - \frac{1}{2}\log\left(\frac{1}{4} - x\right) \tag{5.4.84}$$

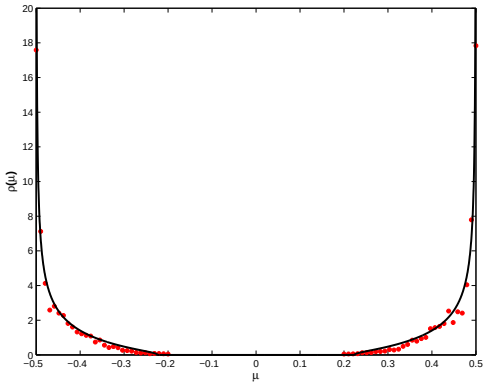


Figure 5.12: Density of shifted transmission eigenvalues $\mu$ for $N = 4$ and $p = -10$ (theory vs. numerics) for the shot noise case.

#### 5.4.3.4 Summary for the shot noise case

To summarize, the density of the shifted eigenvalues $\{\mu_i\}$ (solution of the saddle point equation (5.4.52)) has the following form:

$$\varrho_p^\star(\mu) = \begin{cases} \frac{p}{\pi}\sqrt{\frac{2}{p} - \mu^2} & -\sqrt{\frac{2}{p}} \le \mu \le \sqrt{\frac{2}{p}} \qquad p \ge 8 \\ \frac{p}{\pi\sqrt{1/4-\mu^2}}\left[\frac{8+p}{8p} - \mu^2\right] & -1/2 \le \mu \le 1/2 \qquad -8 \le p \le 8 \\ \frac{|p\mu|\sqrt{\mu^2-1/4+2/|p|}}{\pi\sqrt{1/4-\mu^2}} & -1/2 \le \mu \le -\sqrt{1/4-2/|p|} \vee \sqrt{1/4-2/|p|} \le \mu \le 1/2 \end{cases} \tag{5.4.85}$$

One may easily check that $\rho_p(\mu)$ is continuous at $p = \pm 8$, but develops two phase transitions characterized by different supports.

The saddle-point action (5.4.53) is given by:

$$S_p[\varrho_p^\star] = \begin{cases} \frac{3}{4} + \frac{1}{2}\log 2 + \frac{1}{2}\log p & p > 8 \\ \frac{p}{8} - \frac{p^2}{256} + 2\log 2 & -8 \le p \le 8 \\ \frac{3}{4} + \frac{1}{2}\log\left(\frac{|p|}{8}\right) - \frac{|p|}{4} + 2\log 2 & p \le -8 \end{cases} \tag{5.4.86}$$

which is again continuous at $p = \pm 8$.

From (5.4.19), the expression of $J_Q(p)$ is:

$$J_Q(p) = S_p[\varrho_p^\star] - S_0[\varrho_0^\star] = \begin{cases} \frac{3}{4} + \frac{1}{2}\log\left(\frac{p}{8}\right) & p \ge 8 \\ \frac{-p^2}{256} + \frac{p}{8} & -8 \le p \le 8 \\ \frac{3}{4} + \frac{1}{2}\log\left(\frac{|p|}{8}\right) - \frac{|p|}{4} & p \le -8 \end{cases} \tag{5.4.87}$$

from which one can derive (in complete analogy with the conductance case) the rate function for the auxiliary quantity $Q$:

$$\Psi_Q(x) = \begin{cases} \frac{1}{4} - 2\log 2 - \frac{1}{2}\log x & 0 \le x \le 1/16 \\ 64\left(x - \frac{1}{8}\right)^2 & 1/16 \le x \le 3/16 \\ \frac{1}{4} - 2\log 2 - \frac{1}{2}\log\left(\frac{1}{4} - x\right) & 3/16 \le x \le 1/4 \end{cases} \tag{5.4.88}$$

and from the relation $\Psi_P(x) = \Psi_Q(1/4 - x)$ one readily obtains the rate function for the shot noise. Since the shot noise has range between 0 and $N/4$, the support of $\Psi_P(x)$ is clearly $[0, 1/4]$. Once again, the central region of the distribution is a Gaussian, and the decay on both sides is given by a power-law distribution.

## 5.5 Summary and outlook

In this chapter, we have investigated several aspects of the quantum conductance problem in chaotic cavities, and its relation with the Jacobi ensemble of random matrices. Exploiting this very simple mapping, and another less known result by Kaneko, we provided two different (but equivalent) expressions for the density of transmission eigenvalues (and higher order correlation functions), valid at arbitrary number of open channels in the two attached leads. Using these results, we obtained a new analytical formula for the moments of transmission eigenvalues, again valid at arbitrary number of open channels. Together with very recent analytical results by Novaes [142; 144], our findings lead to interesting combinatorial

puzzles, that we highlighted and left for future investigations. In the last section, we tackled the more general problem of the full distribution of statistical quantities (conductance and shot noise, mainly) in the limit of large number of open channels. Using the very same functional methods exploited in connection with the large deviation properties of Wishart matrices (this time in Laplace space), we provided exact large deviation expressions for the probability distributions of conductance and shot noise. Using the same approach, a new result for the variance of integer moments has been obtained. All the results have been checked by numerical simulations with good agreement.

*Computers are useless. They can only give you answers.*

PABLO PICASSO

# Chapter 6

# Conclusions and open problems

In this thesis, we have considered classical random matrix models where the rotational invariance is retained but the independence of matrix entries is dropped. More specifically, we considered the Wishart-Laguerre (WL) ensemble in its 'canonical' form, a one-parameter deformation of WL with a power-law distribution of entries, and a classical Jacobi ensemble.

The WL ensemble, probably one of the first appearances of random matrix in multivariate statistical analysis, is composed by covariance (positive definite) matrices of random data: its applications range from data analysis (e.g. in finance) to low-energy sectors of gauge theories, and several results are available in both the physics and mathematics literature. The Jacobi ensemble arises naturally as a particular combination of WL matrices, and has significant importance in multivariate statistics and more recent applications in the quantum conductance problem.

In this work, we presented new analytical results concerning these two 'classical' ensembles: we made extensive use of a variant of the well-known Dyson's Coulomb gas analogy, devised by Dean and Majumdar in a recent publication. This technique is invaluable in extreme value statistics, as it provides very quickly the leading large-$N$ decay (or rate function) in many cases of interest.

For the ensembles considered in this work, the eigenvalue jpdf has been known since a long time, and constitutes the starting point of all our analytical results. We believe we have proved that, despite the very 'classical' nature of the RMT ensembles considered, after dozens of years still many fruitful and fertile lines

of research (ranging from purely mathematical questions to more applicative issues) can stem from the very well-known and dated eigenvalue representations, combined with insightful techniques (e.g. the Dean-Majumdar one [40]) and experimental developments (e.g. quantum dots) that became available in more recent times.

If it is true what I. Calvino said about classics: 'A classic is a book that has never finished saying what it has to say.', we can safely say that the ensembles considered in this work certainly deserve to be regarded as classics in RMT.

In this thesis, we first considered the issue of large deviations of the maximum eigenvalue (to the left of its mean) for the Wishart-Laguerre ensemble, obtaining exact results for the rate function. This is one of the few cases (up to date) where the rate functions for *correlated* random variables are known explicitly, completing the rigorous analysis by Johansson [41]. Next, we studied a one-parameter deformation of the Wishart-Laguerre ensemble with power-law tails. The motivation comes from covariance matrices of empirical data (especially from finance), and we noticed that an integral representation already used in some superstatistical approaches to RMT could be used to obtain a complete solution of the model for finite matrix size $N$, and in both the macroscopic and microscopic large $N$ limit, improving earlier results [97]. Finally, we turned to the quantum conductance problem in chaotic cavities: after recalling an obvious but fairly neglected connection with the Jacobi ensemble, we provided exact results for densities and moments of transmission eigenvalues, valid at a fixed and finite number of open channels in the two attached leads. These results may be useful for comparison with more realistic experimental settings, where typically the number of open channels is very far from infinite. Eventually, we exploited the very same Dean-Majumdar formalism [40] (this time in Laplace space) to obtain large deviation formulas for the full probability distribution of quantities of interest for the experiments: conductance, shot noise, integer moments.

Before concluding, it is appropriate to give a list of open problems and directions for future research that may stem from the present thesis:

- Although very powerful, the Dean-Majumdar method is obviously limited to *leading order* results (complexity of random energy landscapes, rate func-

tions etc.). It is natural and very appealing to ask whether sub-leading results (such as $\mathcal{O}(N)$ corrections) may be obtained, and with what methods. A very promising, though quite intricate framework has been proposed recently by Kanzieper [149], and it certainly deserves further investigations.

- Besides the Gaussian and WL ensembles, the large deviation issue for the largest eigenvalue may arise in many other invariant matrix models, such as Jacobi or the free Lévy models [153]. Even though we are not aware of specific applications, it is an interesting question in its own right to provide exact result for the large deviation function (or constant) for these models. It is expected that the Dean-Majumdar technique may be applied straightforwardly and help providing the answer. Also, with little effort, analogous results about the large deviation properties of the *smallest* eigenvalue could be probably obtained in all the cases mentioned above.

- Further generalizations of the WL ensemble can be considered within the same superstatistical approach. The jpdf of entries can be written as an integral transform analogous to (4.2.4), where the 'superstatistical' weight $f(\xi) = e^{-\xi}\xi^{\gamma-1}$ is replaced by a more general distribution (see the list of possible weights in [154]). It is likely that analytical results for spectral density, higher-correlation functions and gap distributions may be obtained also for different weights $f(\xi)$, in analogy with Abul-Magd's findings for the Gaussian models [38]. Eventually, a comparison with empirical data (e.g. from finance) may be attempted for different choices of the weight function $f(\xi)$ in order to determine the 'best fitting' function for spectral properties of empirical covariance matrices.

- In the context of deformed invariant models with power-law tails, it would be of great interest to derive the corresponding generalization of Tracy-Widom distribution for the largest (smallest) eigenvalues at the soft edges. It would be interesting to check whether Painlevé functions may arise in this context as well.

- For the quantum conductance problem, apart from the interesting puzzles highlighted in section 5.3, it is not yet clear whether the results for moments

of transmission eigenvalues could be straightforwardly extended to the case $\beta = 1$ or 4. For the full probability distributions of experimental quantities, some technical difficulties related to the applicability of Tricomi's theorem have prevented us from obtaining complete results for integer moments so far, and it would be very interesting to complete the picture sketched in section 5.4.

Since RMT is such a beautiful, deep and long-lasting construction stemming from the intuition of few pioneers, it seems appropriate to end this final chapter recalling the inspiring and still very actual words of one of them, Eugene Wigner, in his celebrated *The Unreasonable Effectiveness of Mathematics in the Natural Sciences*:

> The miracle of the appropriateness of the language of mathematics for the formulation of the laws of physics is a wonderful gift which we neither understand nor deserve. We should be grateful for it and hope that it will remain valid in future research and that it will extend, for better or for worse, to our pleasure, even though perhaps also to our bafflement, to wide branches of learning.

# Appendix A

# Rate function for $c < 1$

We evaluate in closed form the action $S(\zeta) := S[\hat{f}^\star(x); \zeta]$ (see (3.3.11)) for the case $c < 1$, where $\hat{f}^\star(x)$ is given by (3.4.23).

The rate function $\Phi_-(x; c)$ for $c < 1$, given by:

$$\Phi_-(x; c) = S\left(x_+ - x\right) - S\left(x_+\right) \tag{A.0.1}$$

can be evaluated immediately.

The action (3.3.11) in this case reads:

$$\begin{aligned} S[\hat{f}(x); \zeta] = &\int_{L_1}^{\zeta} x\hat{f}(x)dx - \alpha \int_{L_1}^{\zeta} \hat{f}(x) \log(x)dx + \\ &- \int_{L_1}^{\zeta}\int_{L_1}^{\zeta} \hat{f}(x)\hat{f}(x') \log|x - x'|dxdx' + \\ &+ C_1 \left[\int_{L_1}^{\zeta} \hat{f}(x)dx - 1\right] \end{aligned} \tag{A.0.2}$$

where we have replaced 0 with $L_1$ (3.4.22) as the lower bound of the integrals.

From (3.3.14) (where again 0 is replaced with $L_1$), we can determine the value of the constant $C_1$ by putting $x = L_1$ there:

$$C_1 = \alpha \log L_1 - L_1 + 2\int_{L_1}^{\zeta} dx' \hat{f}(x') \log(x' - L_1) \tag{A.0.3}$$

Then, multiplying (3.3.14) by $\hat{f}(x)$ and integrating over $x$ from $L_1$ to $\zeta$, we get:

$$\int_{L_1}^{\zeta}\int_{L_1}^{\zeta}\hat{f}(x)\hat{f}(x')\log|x-x'|dxdx' = \frac{1}{2}\int_{L_1}^{\zeta}dx\ x\hat{f}(x) - \frac{\alpha}{2}\int_{L_1}^{\zeta}dx\ \hat{f}(x)\log x + \frac{C_1}{2} \tag{A.0.4}$$

Substituting this expression for the double integral into (A.0.2), we get:

$$S[\hat{f}(x);\zeta] = \frac{1}{2}\int_{L_1}^{\zeta}x\hat{f}(x)dx - \frac{\alpha}{2}\int_{L_1}^{\zeta}\hat{f}(x)\log(x)dx + \frac{C_1}{2}$$

where $C_1$ is now taken from (A.0.3). Eventually:

$$\begin{aligned} S(\zeta) = &\frac{1}{2}\int_{L_1}^{\zeta}\hat{f}(x)xdx - \frac{\alpha}{2}\int_{L_1}^{\zeta}\hat{f}(x)\log(x)dx + \\ &- \int_{L_1}^{\zeta}\hat{f}(x)\log(x-L_1)dx + \frac{L_1}{2} - \frac{\alpha}{2}\log(L_1) \end{aligned} \tag{A.0.5}$$

After the substitution $x = (\zeta - L_1)t + L_1$ in the integrals in (A.0.5) and some simple algebra, $S(\zeta)$ can be expressed as:

$$S(\zeta) = -\frac{\alpha}{2}\Theta_1 - \Theta_2 + \frac{\zeta - L_1}{2}\Xi + \frac{L_1}{2} - \frac{\alpha}{2}\log(L_1) \tag{A.0.6}$$

where $\Theta_k$ and $\Xi$ are the following functions of $c$ and $\zeta$:

$$\begin{aligned} \Theta_k = &\frac{\zeta - L_1}{2\pi}\left\{\log(\zeta - L_1)\left[\frac{A}{\zeta - L_1}\mathfrak{I}_0\left(\frac{L_1}{\zeta - L_1}\right) - \frac{\pi}{2}\right] + \right. \\ &\left. + \frac{A}{\zeta - L_1}\mathfrak{I}_k\left(\frac{L_1}{\zeta - L_1}\right)\right\} \\ \Xi = &\frac{A}{4} - \frac{3}{16}\zeta - \frac{L_1}{16} + \frac{\alpha}{2\pi}\mathfrak{I}_3\left(\frac{L_1}{\zeta - L_1}\right) + \frac{1}{2} - \log(2) \end{aligned} \tag{A.0.7}$$

The functions $\mathfrak{I}_k(x)$ are given by the following integrals:

$$\mathfrak{I}_0(x) = \frac{d}{dx}\mathfrak{I}_3(x) \tag{A.0.8}$$

$$\mathfrak{I}_1(x) = \int_0^1 dt\frac{\log(t+x)}{t+x}\sqrt{\frac{t}{1-t}} \tag{A.0.9}$$

$$\mathfrak{I}_2(x) = \int_0^1 dt\frac{\log t}{t+x}\sqrt{\frac{t}{1-t}} \tag{A.0.10}$$

$$\mathfrak{I}_3(x) = \int_0^1 dt\log(t+x)\sqrt{\frac{t}{1-t}} \tag{A.0.11}$$

which, following very closely ref. [88] paper I, appendix B, can be computed explicitly in closed form.

The integral $\mathcal{I}_3(x)$ (and thus also $\mathcal{I}_0(x)$) can be computed by Mathematica®:

$$\mathcal{I}_3(x) = \frac{\pi}{2}\left[1 + 2x - 2\sqrt{x(1+x)} + 2\log\left[1 + \sqrt{1+\frac{1}{x}}\right] + \right.$$
$$\left. + \log\left(\frac{x}{4}\right)\right] \tag{A.0.12}$$

while $\mathcal{I}_1(x)$ and $\mathcal{I}_2(x)$ are given in terms of derivatives of hypergeometric functions. More explicit expressions can be given as follows, starting with $\mathcal{I}_1(x)$. Exploiting the identity $h^\lambda \log h = \partial_\lambda h^\lambda$, we can rewrite the integral as:

$$\mathcal{I}_1(x) = \left[\partial_\lambda \int_0^1 dt (t+x)^\lambda \sqrt{\frac{t}{1-t}}\right]\Big|_{\lambda=-1} \tag{A.0.13}$$

and the integral in (A.0.13) can be evaluated in terms of Kummer's hypergeometric function:

$$\mathcal{I}_1(x) = \frac{\pi}{2}\left\{\partial_\lambda\left[x^\lambda\ {}_2F_1\left(-\lambda, \frac{3}{2}; 2; -\frac{1}{x}\right)\right]\right\}\Big|_{\lambda=-1} \tag{A.0.14}$$

Now, applying the transformation formulas [155] [15.3.7 pag. 559] and evaluating the derivatives of Gamma functions that arise, we finally get:

$$\mathcal{I}_1(x) = \frac{\pi}{2}\left[-2\log 4 + 2\ \hat{i}_1(x) - 2\sqrt{\frac{x}{1+x}}\log\left(\frac{4x}{e^2}\right) + \right.$$
$$\left. - 2\sqrt{x}\ \hat{i}_2(x)\right] \tag{A.0.15}$$

where:

$$\hat{i}_1(x) = \left[\partial_\mu\ {}_2F_1(1-\mu, -\mu; -\mu+1/2; -x)\right]\Big|_{\mu=0} \tag{A.0.16}$$

$$\hat{i}_2(x) = \left[\partial_\mu\ (1+x)^{\mu-1/2}\ {}_2F_1(\mu, \mu+1; \mu+3/2; -x)\right]\Big|_{\mu=0} \tag{A.0.17}$$

To evaluate $\hat{i}_1(x)$ and $\hat{i}_2(x)$, we use the series expansion for hypergeometric functions [155] [15.1.1 pag. 556] and upon differentiation we get:

$$\hat{i}_1(x) = -\sum_{n=1}^{\infty} B\left(\frac{1}{2}, n\right)(-x)^n \tag{A.0.18}$$

where $B(v,w) = \frac{\Gamma(v)\Gamma(w)}{\Gamma(v+w)}$ is Euler's Beta function. Introducing the integral representation of the Beta function:

$$B(x,y) = \int_0^1 dt\ t^{x-1}(1-t)^{y-1} \tag{A.0.19}$$

into (A.0.18) and upon exchanging summation and integral, we arrive with the help of $\sum_{n=0}^{\infty}(-xt)^n = (1+xt)^{-1}$ to:

$$\hat{i}_1(x) = x\int_0^1 \frac{dt}{\sqrt{1-t}(1+xt)} = 2\sqrt{\frac{x}{1+x}}\text{arcsinh}(\sqrt{x}) \tag{A.0.20}$$

Following the same procedure, we get for $\hat{i}_2(x)$:

$$\hat{i}_2(x) = \frac{1}{\sqrt{1+x}}\left[\log(1+x) - i_1(x)\right] \tag{A.0.21}$$

where $i_1(x)$ is defined in ref. [88] as:

$$i_1(x) = -2 + 2\sqrt{\frac{1+x}{x}}\text{arctanh}\left(\sqrt{\frac{x}{1+x}}\right) \tag{A.0.22}$$

From (A.0.15) we get the final result for $\mathfrak{I}_1(x)$:

$$\begin{aligned}\mathfrak{I}_1(x) = \pi\Bigg\{&-\log 4 + \sqrt{\frac{x}{1+x}}\left[2\text{arcsinh}(\sqrt{x}) + \right.\\ &\left. + 2\sqrt{1+\frac{1}{x}}\text{arctanh}\left(\sqrt{\frac{x}{1+x}}\right) - \log[4x(1+x)]\ \right]\Bigg\}\end{aligned} \tag{A.0.23}$$

Following the very same procedure as in the previous case, we find for $\mathfrak{I}_2(x)$:

$$\mathfrak{I}_2(x) = \pi\left[-\log 4 + \sqrt{\frac{x}{x+1}}\left(2\text{arcsinh}(\sqrt{x}) - \log(x)\right)\right] \tag{A.0.24}$$

Now we compute the limit $c \to 1^-$ in (A.0.6) to recover (3.4.6). Given that, for $c \to 1^-$, $L_1 \to 0$, $\alpha \to 0$ and $A \to (\zeta+4)/2$, we have to evaluate the integrals $\mathfrak{I}_k(x)$ for $x \to 0$. This gives:

$$\mathfrak{I}_0(0) \sim \pi \tag{A.0.25}$$

$$\mathfrak{I}_1(0) \sim -\pi\log 4 \tag{A.0.26}$$

$$\mathfrak{I}_2(0) \sim -\pi\log 4 \tag{A.0.27}$$

$$\mathfrak{I}_3(0) \sim -\frac{\pi}{2}(\log 4 - 1) \tag{A.0.28}$$

Then, $S[\hat{f}^\star(x);\zeta]\Big|_{c\to 1^-} \sim \left[-\Theta_2 + \frac{\zeta}{2}\Xi\right]\Big|_{c\to 1^-} = 2\log 2 - \log\zeta + \frac{\zeta}{2} - \frac{\zeta^2}{32}$ as it should (see (3.4.6)).

# Appendix B

# Partition function and first moment of the Gaussian models

The purpose of this appendix is threefold. First, we derive the condition under which our generalized model defined in eq. (4.2.1) is convergent. Second, we compute both the generalized and standard Gaussian partition functions in order to determine their $\xi$-dependent ratio needed in the computation of all eigenvalue correlation functions. Third, we compute the first moment as a function of $N$, $\nu$, $\beta$ and $\gamma$ which is needed for the rescaling of the eigenvalues in the large-$N$ limit.

All three steps will be performed by changing variables from independent matrix elements or its eigenvalues to radial coordinates, following [36].

The generalized partition function reads in terms of eigenvalues

$$\begin{aligned}\mathcal{Z}_\gamma &= \int_0^\infty \prod_{i=1}^N d\lambda_i \prod_{i=1}^N \lambda_i^{\frac{1}{2}\beta(\nu+1)-1} \prod_{j>k}^N |\lambda_j-\lambda_k|^\beta \frac{1}{\left(1+\frac{n\beta}{\gamma}\sum_{i=1}^N V(\lambda_i)\right)^\gamma} \\ &= \int_{\Omega(N)} da_N \int_0^\infty dr r^{N-1} r^{N(\frac{1}{2}\beta(\nu+1)-1)} \prod_{i=1}^N \left(\frac{\lambda_i}{r}\right)^{\frac{1}{2}\beta(\nu+1)-1} r^{\frac{N(N-1)}{2}\beta} \cdot \\ &\cdot \frac{\prod_{j>k}^N \left|\frac{\lambda_j}{r}-\frac{\lambda_k}{r}\right|^\beta}{\left(1+\frac{n\beta}{\gamma}\sum_{i=1}^N V(r\frac{\lambda_i}{r})\right)^\gamma}\end{aligned} \tag{B.0.1}$$

Here we have changed to radial coordinates of the $N$-component vector of the eigenvalues $(\lambda_1, \ldots, \lambda_N)$, and $da_N$ denotes the angular integration over the $N$-dimensional unit sphere $\Omega(N)$. The eigenvectors $e_i = \lambda_i / r$ of norm unity span $\Omega(N)$ and no longer depend on the radius. Collecting all powers of $r$ in the numerator and comparing to the leading power of the denominator $d\gamma$ at large $r \gg 1$, the integral only converges if the following inequality holds:

$$\frac{\beta}{2} N(N+\nu) - 1 - \gamma d \; < \; -1 \tag{B.0.2}$$

which is exactly eq. (4.2.2).

Next we compute the partition function $\mathcal{Z}(\xi)$, where for the rest of this appendix we restrict ourselves to the potential $V(\lambda) = \lambda$. The same steps can be taken for a purely monic potential $V(\lambda) = \lambda^d$ as well.

In principle we could repeat the same calculation in terms of eigenvalues as above, but it will be more instructive to start directly from the matrix elements:

$$\begin{aligned}
\mathcal{Z}(\xi) &= \int d\mathcal{X} \exp\left[-\xi \frac{n\beta}{\gamma} \mathrm{Tr} \mathcal{X}^\dagger \mathcal{X}\right] \\
&= \int_{\Omega(\beta N(N+\nu))} da_{\beta N(N+\nu)} \int_0^\infty dr r^{\beta N(N+\nu)-1} \exp\left[-\xi \frac{n\beta}{\gamma} r^2\right] \\
&= \frac{1}{2} \left(\frac{\gamma}{\xi n \beta}\right)^{\frac{\beta}{2} N(N+\nu)} \Gamma\left(\frac{\beta}{2} N(N+\nu)\right) \int_{\Omega(\beta N(N+\nu))} da_{\beta N(N+\nu)}
\end{aligned} \tag{B.0.3}$$

Here we have used radial coordinates for the $\beta N(N+\nu)$ component vector of all independent matrix elements $\mathcal{X}_{ij}$, with squared norm $r^2 = \mathrm{Tr} \mathcal{X}^\dagger \mathcal{X}$. We do not need to compute the angular integral explicitly as it cancels out below.

If we insert the result eq. (B.0.3) into the relation (4.2.8) we immediately obtain

$$\begin{aligned}
\mathcal{Z}_\gamma &= \frac{1}{\Gamma(\gamma)} \int_0^\infty d\xi \; e^{-\xi} \; \xi^{\gamma-1} \mathcal{Z}(\xi) \\
&= \frac{1}{2\Gamma(\gamma)} \left(\frac{\gamma}{\beta n}\right)^{\frac{\beta}{2} N(N+\nu)} \Gamma\left(\gamma - \frac{\beta}{2} N(N+\nu)\right) \Gamma\left(\frac{\beta}{2} N(N+\nu)\right) \cdot \\
&\cdot \int_{\Omega(\beta N(N+\nu))} da_{\beta N(N+\nu)}
\end{aligned} \tag{B.0.4}$$

Combining the last two equations we arrive at

$$\frac{\mathcal{Z}(\xi)}{\Gamma(\gamma)\mathcal{Z}_\gamma} = \frac{\xi^{-\frac{\beta}{2}N(N+\nu)}}{\Gamma\left(\gamma - \frac{\beta}{2}N(N+\nu)\right)} \tag{B.0.5}$$

the ratio of the two Gaussian partition functions at finite values of $N$, $\nu$ and $\gamma$ valid for all three $\beta$.

In the last step of this appendix we compute the mean eigenvalue position in the Gaussian model. It can be either defined through the spectral density, see eq. (4.3.3), or in terms of the first moment, where we start with the standard WL ensembles:

$$\begin{aligned}
\langle\lambda(\xi)\rangle &= \frac{1}{\mathcal{Z}(\xi)}\int d\mathcal{X}\frac{1}{N}\mathrm{Tr}\left(\mathcal{X}^\dagger\mathcal{X}\right)\exp\left[-\xi\frac{n\beta}{\gamma}\mathrm{Tr}\mathcal{X}^\dagger\mathcal{X}\right] \\
&= \frac{1}{N\mathcal{Z}(\xi)}\int_{\Omega(\beta N(N+\nu))} da_{\beta N(N+\nu)}\int_0^\infty dr r^{\beta N(N+\nu)-1}r^2\exp\left[-\xi\frac{n\beta}{\gamma}r^2\right] \\
&= \frac{\gamma}{2n\xi}(N+\nu)
\end{aligned} \tag{B.0.6}$$

in agreement with section 2.4.2. Note that the $\beta$-dependence has cancelled out. We can immediately use this result to compute the same quantity for the generalised Gaussian model,

$$\begin{aligned}
\langle\lambda\rangle_\gamma &= \frac{1}{\mathcal{Z}_\gamma}\int d\mathcal{X}\frac{\frac{1}{N}\mathrm{Tr}\left(\mathcal{X}^\dagger\mathcal{X}\right)}{\left(1+\frac{n\beta}{\gamma}\mathrm{Tr}\mathcal{X}^\dagger\mathcal{X}\right)^\gamma} \\
&= \frac{1}{N\mathcal{Z}_\gamma\Gamma(\gamma)}\int_0^\infty d\xi\; e^{-\xi}\;\xi^{\gamma-1}\mathcal{Z}(\xi)\langle\lambda(\xi)\rangle \\
&= \frac{\gamma(N+\nu)}{2n\left(\gamma-\frac{\beta}{2}N(N+\nu)-1\right)}
\end{aligned} \tag{B.0.7}$$

This result is used in the rescaling of both large-$N$ limits. As a check it reduces to eq. (B.0.6) in the limit $\gamma\to\infty$, with a weight $\exp[-n\beta r^2]$.

# Appendix C

# Explicit $\beta = 2$-solution for all $k$-point densities at finite $N$ and $\gamma$

In this appendix we present all details for the solution of the generalized WL ensemble with unitary invariance $\beta = 2$ and confining potential $V(\lambda) = \lambda$. In this case the orthogonal polynomials of the WL ensemble are know to be Laguerre, allowing for an explicit solution at finite $N$ and finite $\gamma$.

The orthogonal polynomials in eq. (4.2.12) read for the weight function $\exp[-\xi\frac{2n}{\gamma}\lambda]$

$$P_k(\lambda) \;=\; (-)^k k! \left(\frac{\gamma}{2n\xi}\right)^k L_k^\nu\left(\frac{2n\xi}{\gamma}\lambda\right) \tag{C.0.1}$$

with norms

$$h_k \;=\; k!\,(k+\nu)!\left(\frac{\gamma}{2n\xi}\right)^{2k+\nu+1} \tag{C.0.2}$$

Here the Laguerre polynomials are defined as usual

$$L_k^\nu(z) \;=\; \sum_{j=0}^{k}(-1)^j\binom{k+\nu}{k-j}\frac{z^j}{j!} \quad , \quad \text{with} \quad L_k^\nu(z)' \;=\; -L_{k-1}^{\nu+1}(z) \tag{C.0.3}$$

Using eq. (4.2.17) we can immediately read off the WL partition function from the norms,

$$\mathcal{Z}(\xi) \;=\; \left(\frac{\gamma}{2n\xi}\right)^{N\nu+N^2}\prod_{k=0}^{N-1}(k+1)!\,(k+\nu)! \tag{C.0.4}$$

As the next step we can compute the partition function eq. (4.2.8) given by

$$\begin{aligned}\mathcal{Z}_\gamma &= \frac{1}{\Gamma(\gamma)}\int_0^\infty d\xi\; e^{-\xi}\;\xi^{\gamma-1}\;\left(\frac{\gamma}{2n\xi}\right)^{N\nu+N^2}\prod_{k=0}^{N-1}(k+1)!\,(k+\nu)! \\ &= \left(\frac{\gamma}{2n}\right)^{N\nu+N^2}\frac{\Gamma(\gamma-N(N+\nu))}{\Gamma(\gamma)}\prod_{k=0}^{N-1}(k+1)!\,(k+\nu)! \qquad \text{(C.0.5)}\end{aligned}$$

This leads to the following ratio needed for example inside the relation (4.2.10)

$$\frac{\mathcal{Z}(\xi)}{\Gamma(\gamma)\mathcal{Z}_\gamma} = \xi^{-N(N+\nu)}\frac{1}{\Gamma(\gamma-N(N+\nu))} \qquad \text{(C.0.6)}$$

It confirms independently part of the result from the previous appendix, eq. (B.0.5) for $\beta = 2$.

The spectral density for finite $N$ follows by inserting this ratio as well as the standard Laguerre density at finite-$N$,

$$R(\lambda;\xi) = \lambda^\nu\; e^{-\xi\frac{2n}{\gamma}\lambda}\sum_{k=0}^{N-1}\frac{k!}{(k+\nu)!}\left(\frac{2n\xi}{\gamma}\right)^{\nu+1}L_k^\nu\left(\frac{2n\xi}{\gamma}\lambda\right)^2 \qquad \text{(C.0.7)}$$

into (4.2.10):

$$R_\gamma(\lambda) = \frac{1}{\Gamma(\gamma-N(N+\nu))}\int_0^\infty d\xi\; e^{-\xi}\;\xi^{\gamma-1-N(N+\nu)}R(\lambda;\xi) \qquad \text{(C.0.8)}$$

With the help of eq. (C.0.3) we can derive and simplify the Christoffel-Darboux identity for Laguerre polynomials of equal arguments

$$\sum_{k=0}^{N-1}\frac{k!}{\Gamma(k+1+\nu)}L_k^\nu(y)^2 = \frac{N!}{\Gamma(N+\nu)}\left[L_{N-1}^\nu(y)L_{N-1}^{\nu+1}(y) - L_N^\nu(y)L_{N-2}^{\nu+1}(y)\right] \qquad \text{(C.0.9)}$$

We thus arrive at our final result for the generalized density at finite $N$ and $\gamma$:

$$\begin{aligned}R_\gamma(\lambda) = \frac{N!}{\Gamma(\gamma-N^2-N\nu)\Gamma(N+\nu)}\left(\frac{2n}{\gamma}\right)^{\nu+1}\lambda^\nu\int_0^\infty d\xi\; e^{-\xi\left(1+\frac{2n}{\gamma}\lambda\right)}\xi^{\gamma-N^2-N\nu+\nu} \\ \cdot\left[L_{N-1}^\nu\left(\frac{2n\xi}{\gamma}\lambda\right)L_{N-1}^{\nu+1}\left(\frac{2n\xi}{\gamma}\lambda\right) - L_N^\nu\left(\frac{2n\xi}{\gamma}\lambda\right)L_{N-2}^{\nu+1}\left(\frac{2n\xi}{\gamma}\lambda\right)\right] \qquad \text{(C.0.10)}\end{aligned}$$

This single integral over an exponential times polynomials can be performed explicitly, at the expense of a double sum. Since this equivalent result is not very illuminating or useful for the asymptotic we do not display it here.

Proceeding along the same lines as above we can write down the general result for the $k$-point density correlations functions as they follow from eq. (4.2.16)

$$R_\gamma(\lambda_1,\ldots,\lambda_k) = \frac{N!^k \left(\frac{n}{\gamma}\right)^{k\nu}}{\Gamma(\gamma - N^2 - N\nu)\Gamma(N+\nu)^k} \prod_{j=1}^{k} \lambda_j^\nu \int_0^\infty d\xi\ e^{-\xi\left(1+\frac{2n}{\gamma}\sum_{j=1}^k \lambda_j\right)} \cdot$$
$$\cdot\, \xi^{\gamma-1-N^2-(N-k)\nu} \det_{1\le i,j\le k} \left[ \frac{\left(L_N^\nu\left(\frac{2n\xi}{\gamma}\lambda_i\right) L_{N-1}^\nu\left(\frac{2n\xi}{\gamma}\lambda_j\right) - L_N^\nu\left(\frac{2n\xi}{\gamma}\lambda_j\right) L_{N-1}^\nu\left(\frac{2n\xi}{\gamma}\lambda_i\right)\right)}{\lambda_j - \lambda_i} \right] \tag{C.0.11}$$

In order to compare the finite-$N$ result (C.0.10) with the macroscopic $\gamma$- and $N$-independent density $\vartheta_{\hat\alpha}(x)$ eq. (4.3.13), we adopt the following procedure:

1. We rescale $R_\gamma(\lambda)$ with mean value $\langle\lambda\rangle_\gamma$ eq. (4.3.3) and normalize to 1: $\hat\rho_\gamma(x) \equiv N^{-1}\langle\lambda\rangle_\gamma R_\gamma\left(\langle\lambda\rangle_\gamma x\right)$.

2. Next, we express $\gamma$ as a function of $\hat\alpha$ and $N$, $\gamma = \hat\alpha + N(N+\nu) + 1$, and pass to squared variables: $\hat\vartheta_{\hat\alpha}(x) \equiv |x|\hat\rho_\gamma(x^2)$.

3. Then, we compare $\hat\vartheta_{\hat\alpha}(x)$ and $\vartheta_{\hat\alpha}(x)$ for $\nu = 0$ in Fig. C.1. The agreement is already very good for $N = 4$, apart from the region close to the origin.

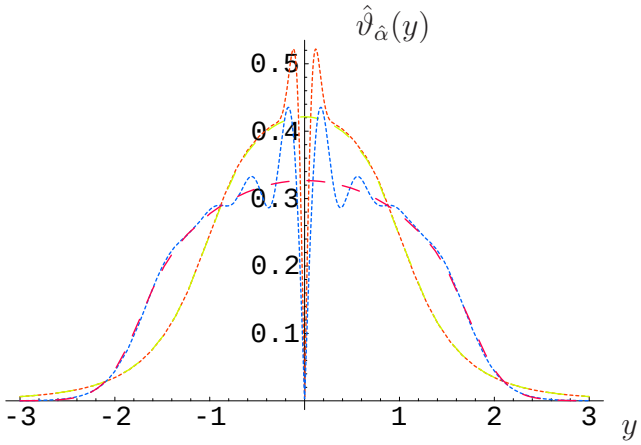


Figure C.1: The macroscopic generalized semi-circle density $\vartheta_{\hat{\alpha}}(x)$ eq. (4.3.13) for $\hat{\alpha} = 1.02$ and 14 (green and dashed red), compared with the finite $N = 4$ result $\hat{\vartheta}_{\hat{\alpha}}(x)$ (blue and dash-dotted orange).

# Appendix D

# Hypergeometric function of a matrix argument

Following Kaneko [140], we first report the definition of the constant $C_1$ appearing in (5.2.17):

$$C_1 := S_{n,0}(\ell_1 + m, \ell_2, \beta) \tag{D.0.1}$$

where:

$$S_{n,0}(y_1, y_2, z) := \prod_{i=1}^{n} \frac{\Gamma\left(i\frac{z}{2}+1\right)\Gamma\left(y_1+1+(i-1)\frac{z}{2}\right)\Gamma\left(y_2+1+(i-1)\frac{z}{2}\right)}{\Gamma\left(\frac{z}{2}+1\right)\Gamma\left(y_1+y_2+2+(n+i-2)\frac{z}{2}\right)} \tag{D.0.2}$$

The hypergeometric function of a matrix argument takes a symmetric matrix $(m \times m)$ $\mathbf{X}$ as input and provides a real number as output. It is defined as a series of Jack functions of parameter $\beta$, which generalize the Schur function, the zonal polynomial and the quaternion zonal polynomial to which they reduce for $\beta = 1, 2, 4$ respectively. Given a partition $\kappa$ of an integer $k$, i.e. a set of integers $\kappa_1 \geq \kappa_2 \geq \ldots \geq 0$ such that $|\kappa| = \kappa_1 + \kappa_2 + \ldots = k$, and a matrix $\mathbf{X}$, the Jack function $C_\kappa^{(\beta)}(\mathbf{X})$ is a symmetric and homogeneous polynomial of degree $|\kappa|$ in the eigenvalues $x_1, \ldots, x_m$ of $\mathbf{X}$.

The hypergeometric function is defined as:

$$ {}_pF_q^{(\beta)}(a_1,\ldots,a_p;b_1,\ldots,b_q;\mathbf{X}) := \sum_{k=0}^{\infty}\sum_{\kappa\vdash k}\frac{(a_1)_\kappa^{(\beta)}\ldots(a_p)_\kappa^{(\beta)}}{k!(b_1)_\kappa^{(\beta)}\ldots(b_q)_\kappa^{(\beta)}}C_\kappa^{(\beta)}(\mathbf{X}), \qquad \text{(D.0.3)} $$

where the symbol $\kappa \vdash k$ means that $\kappa$ is a partition of $k$ and $(a)_\kappa^{(\beta)} = \prod_{(i,j)\in\kappa}\left(a - \frac{i-1}{\beta} + j - 1\right)$ is a generalized Pochhammer symbol.

The series (D.0.3) converges for any $\mathbf{X}$ if $p \leq q$; it converges if $\max_i |x_i| < 1$ and $p = q + 1$; and diverges if $p > q + 1$, unless it terminates [132; 141].

# Appendix E

# The $\mu \to 0$ limit of the spectral density

In the case $N_1 = N_2 = N$ and $\beta = 2$, the average spectral density was computed exactly in [135] as:

$$R_2(\lambda; N_1 = N_2 = N) = \frac{N^2}{4\lambda(1-\lambda)}\{P_N^2(\alpha) - 2\alpha P_N(\alpha)P_{N-1}(\alpha) + P_{N-1}^2(\alpha)\} \tag{E.0.1}$$

where $\alpha = 2\lambda - 1$ and $P_N(x)$ is a Legendre polynomial.

This case corresponds to $\mu \to 0$ in eq. (5.2.14). In this appendix, we show explicitly how to get from (5.2.14) to (E.0.1).

First, we remark that the identity between Jacobi and Legendre polynomials $P_n^{(0,0)}(x) = P_n(x)$ holds [formula 22.5.35 in [155]]. Hence, in the case $\mu \to 0$ we have from (5.2.14):

$$R_2(\lambda; N_1 = N_2 = N) = \sum_{n=0}^{N-1}(2n+1)\{P_n(1-2\lambda)\}^2 \tag{E.0.2}$$

Next, we use the Christoffel-Darboux formula for Legendre polynomials [see formula 22.12.1 in [155]] at equal arguments $x = y = 1 - 2\lambda$:

$$\sum_{n=0}^{N-1}(2n+1)P_n^2(y) = N[P_N'(y)P_{N-1}(y) - P_{N-1}'(y)P_N(y)] \tag{E.0.3}$$

Then, we exploit the differential relation [22.8.5 in [155]]:

$$(1-y^2)P_n'(y) = -nyP_n(y) + nP_{n-1}(y) \tag{E.0.4}$$

to get:

$$R_2(\lambda; N_1 = N_2 = N) = \frac{N}{1-y^2}[NP_{N-1}^2(y) - yP_N(y)P_{N-1}(y) - (N-1)\cdot \\ \cdot P_N(y)P_{N-2}(y)]\Big|_{y=1-2\lambda} \tag{E.0.5}$$

Thanks to the recurrence relation [22.7.10 in [155]], we obtain the following identity for $P_{N-2}(y)$:

$$P_{N-2}(y) = \frac{1}{N-1}[(2N-1)yP_{N-1}(y) - NP_N(y)] \tag{E.0.6}$$

which is then substituted into (E.0.5). Eventually, given that $y = 1-2\lambda$ and the Legendre polynomials have the same parity of their index, we obtain:

$$R_2(\lambda; N_1 = N_2 = N) = \frac{N^2}{4\lambda(1-\lambda)}[P_N^2(2\lambda-1) - 2(2\lambda-1)P_N(2\lambda-1)\cdot \\ \cdot P_{N-1}(2\lambda-1) + P_{N-1}^2(2\lambda-1)] \tag{E.0.7}$$

in complete agreement with (E.0.1).

# References


[1] E.P. Wigner, Proc. Cambridge Philos. Soc. **47**, 790 (1951). 1

[2] F.J. Dyson, J. Math. Phys. **3**, 140 (1962). 1, 11, 18, 83

[3] F.J. Dyson, J. Math. Phys. **3**, 1199 (1962). 1, 3

[4] J. Wishart, Biometrika **20**, 32 (1928). 1, 23

[5] P.L. Hsu, Ann. Eugenics **9**, 250 (1939). 1

[6] J. P. Keating and N. C. Snaith, J. Phys. A: Math. Gen. **36**, 2859 (2003). 2

[7] P. Diaconis, *Group Representations in Probability and Statistics* (Institute of Mathematical Statistics, Hayward, California, 1998). 2

[8] I. Goulden and D.M. Jackson, Canadian J. Math. **49**, 865 (1997). 2

[9] P.J. Hanlon, R.P. Stanley and J.R. Stembridge, Contemp. Math. **138**, 151 (1992). 2

[10] E.V. Shuryak and J.J.M. Verbaarschot, Nucl. Phys. A **560**, 306 (1993); J.J.M. Verbaarschot, Phys. Rev. Lett. **72**, 2531 (1994). 2, 23

[11] C.W.J. Beenakker, Rev. Mod. Phys. **69**, 731 (1997). 2, 82, 84, 85, 86, 95

[12] B.D. McKay, Lin. Alg. Appl. **40**, 203 (1981). 2

[13] G.J. Rodgers and A.J. Bray, Phys. Rev. B **37**, 3557 (1988). 2, 5

[14] A.L. Andrew, *Choosing test matrices for numerical software*, in W.L. Hogarth and B.J. Nege, editors, Computational Techniques and Applications Conference: CTAC-89, pages 561-567 (1990). 2

[15] J. Demmel, Math. of Comp. **50**, 449 (1988). 2

[16] K.B. Efetov, *Random Matrices and Supersymmetry in Disordered Systems*, in *Applications of Random Matrices in Physics*, NATO Science Series vol. 221, ed. by E. Brézin, V. Kazakov, D. Serban, P. Wiegmann and A. Zabrodin (Springer Netherlands, 2006). 2

[17] M.B. Eisen, P.T. Spellman, P.O. Brown and D. Botstein, Proc. Natl. Acad. Sci. **95**, 14863 (1998). 2

[18] S.N. Majumdar, O. Bohigas and A. Lakshminarayan, J. Stat. Phys. **131**, 33 (2008). 2, 23, 24

[19] J. Ambjørn, L. Chekhov, C.F. Kristjansen and Yu. Makeenko, Nucl.Phys. B **404**, 127 (1993) and Erratum *ibid* B **449**, 681 (1995). 2

[20] S. Heusler, S. Müller, A. Altland, P. Braun and F. Haake, Phys. Rev. Lett. **98**, 044103 (2007) (and references therein). 2

[21] A.G. Constantine, Ann. Math. Statist. **34**, 1270 (1963). 2, 26

[22] A.T. James, Ann. Math. Statist. **35**, 475 (1964). 2

[23] R.J. Muirhead. *Aspects of Multivariate Statistical Theory* (John Wiley and Sons, New York, 1982). 2, 25

[24] E. Telatar, European Transactions on Telecommunications **10**(6), 585 (1999). 2, 23

[25] P. Viswanath, D. Tse and V. Anantharam, IEEE Transactions on Information Theory **47**(1), 241 (2001). 2

[26] Y.V. Fyodorov, [math-ph/0412017] (2004). 2, 12, 15, 16

[27] T. Guhr, A. Müller-Groeling and H.A. Weidenmüller, Phys. Rept. **299**, 189 (1998); T. Papenbrock and H.A. Weidenmüller, Rev. Mod. Phys. **79**, 997 (2007); M.A. Stephanov, J.J.M. Verbaarschot and T. Wettig, [arXiv:hep-ph/0509286] (2005); M. Dieng and C.A. Tracy, [arXiv:math.PR/0603543] (2006). 2

[28] A. Altland and M. Zirnbauer, Phys. Rev. Lett. **76**, 3420 (1996) and Phys. Rev. B **55**, 1142 (1997); M. Zirnbauer, J. Math. Phys. **37**, 4986 (1996); M. Caselle, [cond-mat/9610017] (1996). 3

[29] D. Bernard and A. LeClair, *A classification of non-hermitian random matrices*, contribution to the proceedings of the NATO Advanced Research Workshop on Statistical Field Theories, Como 18-23 June 2001, [cond-mat/0110649v1] (2001). 3

[30] U. Magnea, J. Phys. A: Math. Theor. **41**, 045203 (2008). 3

[31] P. Cizeau and J.-P. Bouchaud, Phys. Rev. E **50**, 1810 (1994). 3

[32] J. Ginibre, J. Math. Phys. **6**, 440 (1965). 5

[33] K. Rajan and L.F. Abbott, Phys. Rev. Lett. **97**, 188104 (2006). 5

[34] G. Akemann, Phys. Rev. Lett. **89**, 072002 (2002); J.C. Osborn, Phys. Rev. Lett. **93**, 222001 (2004). 5

[35] V.L. Girko, Theory Probab. Appl. **29**, 694 (1984). 6

[36] G. Akemann, G.M. Cicuta, L. Molinari and G. Vernizzi, Phys. Rev. E **59**, 1489 (1999) and Phys. Rev. E **60**, 5287 (1999). 6, 21, 53, 54, 63, 127

[37] A.C. Bertuola, O. Bohigas and M.P. Pato, Phys. Rev. E **70**, 065102 (2004); A.Y. Abul-Magd, Phys. Rev. E **71**, 066207 (2005); F. Toscano, R.O. Vallejos and C. Tsallis, Phys. Rev. E **69**, 066131 (2004). 6, 13, 52, 54, 58, 60, 61, 78

[38] A.Y. Abul-Magd, Phys. Rev. E **72**, 066114 (2005) and Physica A **361**, 41 (2006). 6, 121

[39] V.E. Kravtsov and K.A. Muttalib, Phys. Rev. Lett. **79**, 1913 (1997); K.A. Muttalib and M.E.H. Ismail, Phys. Rev. E **76**, 051105 (2007). 6

[40] D.S. Dean and S.N. Majumdar, Phys. Rev. Lett. **97**, 160201 (2006) and Phys. Rev. E **77**, 041108 (2008). 7, 30, 31, 34, 35, 96, 101, 120

[41] K. Johansson, Comm. Math. Phys. **209**, 437 (2000). 7, 23, 29, 30, 33, 40, 120

[42] P. Vivo, S.N. Majumdar and O. Bohigas, J. Phys. A: Math. Theor. **40**, 4317 (2007). 7, 31, 32

[43] G. Akemann and P. Vivo, to appear in *JSTAT* [arXiv:0806.1861] (2008). 8, 52

[44] P. Vivo and E. Vivo, J. Phys. A: Math. Theor. **41**, 122004 (2008). 8, 84

[45] C.M. Bender and S. Boettcher, Phys. Rev. Lett. **80**, 5243 (1998); C.M. Bender, D.C. Brody and H.F. Jones, Phys. Rev. Lett. **89**, 270401 (2002). 11

[46] M.L. Mehta, *Random Matrices* (3rd Edition, Elsevier-Academic Press, 2004). 11, 14, 15, 19, 21, 55, 56, 57, 85, 87

[47] I. Dumitriu and A. Edelman, J. Math. Phys. **43**, 5830 (2002). 12, 22, 45

[48] P. Vivo and S.N. Majumdar, Physica A **387**, 4839 (2008). 12

[49] G. Akemann and E. Kanzieper, J. Stat. Phys. **129**, 1159 (2007). 16

[50] G. Akemann and L. Shifrin, J. Phys. A: Math. Theor. **40**, F785 (2007). 16

[51] F.J. Dyson. Comm. Math. Phys. **19**, 235 (1970). 16

[52] F.G. Tricomi, *Integral Equations*, (Pure Appl. Math. V, Interscience, London, 1957). 19, 38

[53] C.A. Tracy and H. Widom, Comm. Math. Phys. **163**, 33 (1994). 22, 28

[54] M. Dieng, Int. Math. Res. Notices **37**, 2263 (2005). 22

[55] S.S. Wilks, *Mathematical Statistics* (John Wiley & Sons, New York, 1962). 22, 23

[56] K. Fukunaga, *Introduction to Statistical Pattern Recognition* (Elsevier, New York, 1990). 22

[57] L.I. Smith, *A tutorial on Principal Components Analysis*, online at www.cs.otago.ac.nz/cosc453/student_tutorials/principal_components.pdf (2002). 22, 23

[58] R.W. Preisendorfer, *Principal Component Analysis in Meteorology and Oceanography* (Elsevier, New York, 1988). 22

[59] I.M. Johnstone, Ann. Statist. **29**, 295 (2001). 23, 30

[60] S. Maslov and Y.C. Zhang, Phys. Rev. Lett. **87**, 248701 (2001). 23

[61] Y.K. Yu and Y.C. Zhang, Physica A **312**, 1 (2002). 23

[62] R.A. Janik and M.A. Nowak, J. Phys. A: Math. Gen. **36**, 3629 (2003). 23

[63] V.A. Marčenko and L.A. Pastur, Math. USSR-Sb, **1**, 457 (1967). 24

[64] F.J. Dyson, Rev. Mex. Fis. **20**, 231 (1971). 24

[65] O. Bohigas and J. Flores, Rev. Mex. Fis. **20**, 217 (1971). 24

[66] K. Życzkowski and H-J. Sommers, J. Phys. A: Math. Gen. **34**, 7111 (2001). 24

[67] N.S. Witte, P.J. Forrester and C.M. Cosgrove, Nonlinearity **13**, 1439 (2000). 25, 26

[68] A. Edelman, online at web.mit.edu/18.338/www/handouts/handout3.pdf. 25, 26

[69] I. Dumitriu and P. Koev, SIAM J. Matrix Anal. Appl. **30**, 1 (2008). 26

[70] C. Tracy and H. Widom, Comm. Math. Phys. **159**, 151 (1994); *ibid* **177**, 727 (1996). 28

[71] A. Edelman and P.-O. Persson, *Numerical methods for random matrices.*, Technical report, Massachussets Institute of Technology, [arXiv:math-ph/0501068] (2002). 29

[72] S. Kotz and S. Nadarajah, *Extreme Value Distributions: Theory and Applications* (World Scientific Publishing Limited, London, 2000). 29

[73] S.N. Majumdar, *Les Houches lecture notes on 'Complex Systems', 2006* ed. by J.-P. Bouchaud, M. Mézard and J. Dalibard [arXiv: cond-mat/0701193] (2007). 29

[74] J. Baik, P. Deift and K. Johansson, J. Am. Math. Soc. **12**, 1119 (1999). 29

[75] J. Baik and E.M. Rains, J. Stat. Phys. **100**, 523 (2000). 29

[76] M. Prähofer and H. Spohn, Phys. Rev. Lett. **84**, 4882 (2000); J. Gravner, C.A. Tracy and H. Widom, J. Stat. Phys. **102**, 1085 (2001); S.N. Majumdar and S. Nechaev, Phys. Rev. E **69**, 011103 (2004); T. Imamura and T. Sasamoto, Nucl. Phys. B **699**, 503 (2004). 29

[77] S.N. Majumdar and S. Nechaev, Phys. Rev. E **72**, 020901(R) (2005). 29

[78] M.G. Vavilov, P.W. Brouwer, V. Ambegaokar and C.W.J. Beenakker, Phys. Rev. Lett. **86**, 874 (2001); A. Lamacraft and B.D. Simons, Phys. Rev. B **64**, 014514 (2001); P.M. Ostrovsky, M.A. Skvortsov and M.V. Feigelman, Phys. Rev. Lett. **87**, 027002 (2001); J.S. Meyer and B.D. Simons, Phys. Rev. B **64**, 134516 (2001); A. Silva and L.B. Ioffe, Phys. Rev. B **71**, 104502 (2005); A. Silva, Phys. Rev. B **72**, 224505 (2005). 29

[79] G. Biroli, J-P. Bouchaud and M. Potters, Europhys. Lett. **78**, 10001 (2007). 29

[80] H. Touchette, [arXiv:0804.0327] (2008). 30

[81] A. Aazami and R. Easther, J. Cosmol. Astropart. Phys. JCAP03 013 (2006). 31

[82] J.-P. Dedieu and G. Malajovic, [arXiv:math/0702360] (2007). 31

[83] A. Cavagna, J.P. Garrahan and I. Giardina, Phys. Rev. B **61**, 3960 (2000). 31

[84] Y.V. Fyodorov, H-J. Sommers and I. Williams, JETP Letters **85**, 261 (2007). 31

[85] A.J. Bray and D.S. Dean, Phys. Rev. Lett. **98**, 150201 (2007). 31

[86] Y.V. Fyodorov and I. Williams, J. Stat. Phys. **129**, 1081 (2007). 31

[87] P. Deift, A. Its and I. Krasovsky, Comm. Math. Phys. **278**, 643 (2008). 32

[88] Y. Chen and S.M. Manning, J. Phys. A: Math. Gen. **29**, 7561 (1996); *ibid* **27**, 3615 (1994). 32, 125, 126

[89] K.A. Muttalib and J.R. Klauder, Phys. Rev. E **71**, 055101 (2005). 52

[90] L. Laloux, P. Cizeau, J.-P. Bouchaud and M. Potters, Phys. Rev. Lett. **83**, 1467 (1999). 51

[91] J.-P. Bouchaud and M. Potters, *Theory of Financial Risks* (Cambridge University Press, Cambridge, 2001). 51

[92] Z. Burda and J. Jurkiewicz, Physica A **344**, 67 (2004); Z. Burda, J. Jurkiewicz and B. Waclaw, Acta Phys. Pol. B **36**, 2641 (2005) and references therein. 51

[93] T. Guhr and B. Kälber, J. Phys. A: Math. Gen. **36**, 3009 (2003). 51

[94] J. Kwapień, S. Drożdż and P. Oświęcimka, Physica A **359**, 589 (2006). 51

[95] G. Biroli, J.-P. Bouchaud and M. Potters, Acta Phys. Pol. **38**, 4009 (2007). 51, 54

[96] A.C.R. Martins, Physica A **383**, 527 (2007). 51

[97] Z. Burda, A.T. Görlich and B. Wacław, Phys. Rev. E **74**, 041129 (2006). 51, 52, 54, 65, 120

[98] T. Nagao and T. Tanaka, J. Phys. A: Math. Theor. **40**, 4973 (2007). 51

[99] A.M. García-García and J.J.M. Verbaarschot, Nucl. Phys. B **586**, 668 (2000); A.M. García-García, Phys. Rev. E **64**, 066121 (2001) 066121. 52, 71

[100] J.J.M. Verbaarschot, Nucl. Phys. B **426**, 559 (1994). 57, 70

[101] T. Nagao and P.J. Forrester, Nucl. Phys. B **435**, 401 (1995). 57, 70, 71

[102] T. Nagao and K. Slevin, J. Math. Phys. **34**, 2075 (1993); *ibid* **34**, 2317 (1993). 58

[103] J. Ambjørn, C.F. Kristjansen and Yu. Makeenko, Mod. Phys. Lett. A **7**, 3187 (1992); G. Akemann, Nucl. Phys. B **507**, 475 (1997). 62, 63

[104] J. Ambjørn, Yu. Makeenko and C.F. Kristjansen, Phys. Rev. D **50**, 5193 (1994). 63

[105] I.S. Gradshteyn and I.M. Ryzhik, *Table of Integrals, Series, and Products* (6th Edition, Academic Press, London, 2000). 65, 93

[106] G. Akemann, P.H. Damgaard, U. Magnea and S. Nishigaki, Nucl. Phys. B **487**, 721 (1997); E. Kanzieper and V. Freilikher, Philos. Magazine **77**, 1161 (1998); A.B.J. Kuijlaars and M. Vanlessen, Comm. Math. Phys. **243**, 163 (2003). 68, 69

[107] M.K. Sener and J.J.M. Verbaarschot, Phys. Rev. Lett. **81**, 248 (1998); B. Klein and J.J.M. Verbaarschot, Nucl. Phys. B **588**, 483 (2000). 70, 71

[108] P.J. Forrester, T. Nagao and G. Honner, Nucl. Phys. B **553**, 601 (1999). 70

[109] M.E. Berbenni-Bitsch, A.D. Jackson, S. Meyer, A. Schäfer, J.J.M. Verbaarschot and T. Wettig, Nucl. Phys. Proc. Suppl. **63**, 820 (1998); J.-Z. Ma, T. Guhr and T. Wettig, Eur. Phys. J. A **2**, 87 (1998) and Erratum *ibid* **2**, 425 (1998). 70

[110] P.H. Damgaard and S.M. Nishigaki, Phys. Rev. D **63**, 045012 (2001). 71, 72, 74, 75, 76

[111] P.J. Forrester, Nucl. Phys. B **402**, 709 (1993). 72, 75

[112] T. Wilke, T. Guhr and T. Wettig, Phys. Rev. D **57**, 6486 (1998). 72

[113] S.M. Nishigaki, P.H. Damgaard and T. Wettig, Phys. Rev. D **58**, 087704 (1998). 72, 74

[114] I. Dumitriu, *Eigenvalue statistics for the Beta-ensembles*, Ph.D. thesis, Massachusetts Institute of Technology (2003). 72

[115] A. Edelman, SIAM J. Matrix Anal. Appl. **9**, 543 (1988). 72

[116] G. Akemann, J. Fischmann and P. Vivo, unpublished. xi, 81

[117] R. Landauer, IBM J. Res. Dev. **1**, 223 (1957) and Phil. Mag. **21**, 863 (1970); D.S. Fisher and P. A. Lee, Phys. Rev. B **23**, 6851 (1981). 83

[118] Ya.M. Blanter and M. Büttiker, Phys. Rep. **336**, 1 (2000). 83

[119] R. Balian, Nuovo Cim. **57**, 183 (1958). 83

[120] K.A. Muttalib, J.L. Pichard and A.D. Stone, Phys. Rev. Lett. **59**, 2475 (1987). 83

[121] M. Büttiker, Phys. Rev. Lett. **65**, 2901 (1990). 84

[122] V.A. Khlus, Soviet Physics - JETP **66**, 1243 (1987). 84

[123] G.B. Lesovik, JETP Lett. **49**, 592 (1989). 84

[124] H. Schanz, M. Puhlmann and T. Geisel, Phys. Rev. Lett. **91**, 134101 (2003). 84

[125] R.S. Whitney and Ph. Jacquod, Phys. Rev. Lett. **96**, 206804 (2006). 84

[126] M.H. Pedersen, S.A. van Langen and M. Büttiker, Phys. Rev. B **57**, 1838 (1998). 84, 95

[127] J.E.F. Araújo and A.M.S. Macêdo, Phys. Rev. B **58**, R13379 (1998). 84, 86, 92

[128] P. Braun, S. Heusler, S. Müller and F. Haake, J. Phys. A: Math. Gen. **39**, L159 (2006). 84, 91, 93

[129] D.V. Savin and H.-J. Sommers, Phys. Rev. B **73**, 081307(R) (2006). 84, 85, 86, 91, 93

[130] E.N. Bulgakov, V.A. Gopar, P.A. Mello and I. Rotter, Phys. Rev. B **73**, 155302 (2006). 84

[131] P.J. Forrester, J. Phys. A: Math. Gen. **39**, 6861 (2006). 85

[132] P.J. Forrester, *Log-gases and random matrices*, online at http://www.ms.unimelb.edu.au/~matpjf/matpjf.html (2008). 85, 135

[133] L.S. Levitov and G.B. Lesovik, JETP Lett. **58**, 230 (1993); H. Lee, L.S. Levitov and A.Yu. Yakovets, Phys. Rev. B **51**, 4079 (1995). 86

[134] D.V. Savin, H.-J. Sommers and W. Wieczorek, Phys. Rev. B **77**, 125332 (2008). 86, 92, 93

[135] H.U. Baranger and P.A. Mello, Phys. Rev. Lett. **73**, 142 (1994). 86, 87, 88, 94, 95, 136

[136] R.A. Jalabert, J.-L. Pichard and C.W.J. Beenakker, Europhys. Lett. **27**, 255 (1994). 86, 87, 95

[137] P.W. Brouwer and C.W.J. Beenakker, J. Math. Phys. **37**, 4904 (1996). 86, 92, 95

[138] T. Nagao and M. Wadati, Journal of the Physical Society of Japan **60**, 3298 (1991). 87

[139] S. Ghosh, [arXiv:0711.4432] (2007). 87

[140] J. Kaneko, SIAM J. Math. Anal. **24**, 1086 (1993). 88, 89, 134

[141] P. Koev and A. Edelman, Math. of Comp. **75**, 833 (2006). 91, 135

[142] M. Novaes, Phys. Rev. B **75**, 073304 (2007). 92, 93, 94, 95, 100, 117

[143] G. Berkolaiko, J.M. Harrison and M. Novaes, [cond-mat/0703803] (2007). 92

[144] M. Novaes, [arXiv:0805.4590] (2008). 94, 117

[145] C.W.J. Beenakker, Phys. Rev. Lett. **70**, 1155 (1993). 95

[146] A. García-Martín and J.J. Sáenz, Phys. Rev. Lett. **87**, 116603 (2001). 95

[147] H.-J. Sommers, W. Wieczorek and D.V. Savin, Acta Phys. Pol. A **112**, 691 (2007). 95, 108

[148] V.Al. Osipov and E. Kanzieper, [arXiv:0806.2784] (2008). 96

[149] E. Kanzieper, Phys. Rev. Lett. **89**, 250201 (2002). 96, 121

[150] S. Hemmady, J. Hart, X. Zheng, T.M. Antonsen, E. Ott and S.M. Anlage, Phys. Rev. B **74**, 195326 (2006). 96

[151] P. Facchi, U. Marzolino, G. Parisi, S. Pascazio and A. Scardicchio, [arXiv:0712.0015] (2007). 97

[152] P. Vivo, S.N. Majumdar and O. Bohigas, in preparation. 99

[153] Z. Burda, R.A. Janik, J. Jurkiewicz, M.A. Nowak, G. Papp and I. Zahed, Phys. Rev. E **65**, 021106 (2002). 121

[154] C. Beck and E.G.D. Cohen, Physica A **322**, 267 (2003). 121

[155] M. Abramowitz and I.A. Stegun, *Handbook of Mathematical Functions* (Dover, New York, 1972). 125, 136, 137